Modelling of cavitation in nozzles for diesel injection applications

by

Kaushik Saha

A thesis
presented to the University of Waterloo
in fulfillment of the
thesis requirement for the degree of
Doctor of Philiosophy
in
Mechanical Engineering

Waterloo, Ontario, Canada, 2014

Author's Declaration

I hereby declare that I am the sole author of this thesis. This is a true copy of the thesis, including any required final revisions, as accepted by my examiners.

I understand that my thesis may be made electronically available to the public.

Abstract

Extreme low pressure regions develop in the high pressure direct injection fuel flow inside the fuel injector holes, compelling the liquid fuel to transform to vapour phase in the form of vapour cavities or bubbles, a phenomenon known as cavitation. The cavitation phenomenon determines the quality of primary atomization and hence affects the performance of direct injection diesel or gasoline engines. A cavitation model, coupled with the mixture multiphase approach and RNG $k - \epsilon$ turbulence model, has been developed and implemented in this study for analysing cavitation. The cavitation model has been implemented in ANSYS Fluent platform. The model predictions have been compared with results from experimental works available in the literature. A good agreement of the model predictions has been observed. Comparisons of the model with other cavitation models (Schnerr & Sauer and Zwart-Gerber-Belamri) available in ANSYS Fluent have been carried out with both mixture and Eulerian-Eulerian multiphase approaches. The overall performance of the proposed model in comparison with other models has been observed to be more effective.

The model has been further applied to diesel vs. biodiesel cavitation as biofuels are the greener alternatives of conventional fossil fuels in recent times. Additionally effects of property differences between diesel and biodiesel, inlet pressure fluctuations have been investigated. Liquid phase viscosity has been observed to be the determining parameter amongst all the properties for cavitation characteristics. The present study has also assessed the relevance of following factors for the case of cavitation in diesel injectors : a) compressibility, b) stress of a flowing liquid, c) wall roughness and d) turbulence. The two phase flow passes through the nozzle at very high velocities and hence can no longer be considered incompressible. Stress can affect the inception of cavitation as the liquid under considerable stress can fail and then rupture to form cavities. In the real nozzles at microscopic levels there are always some non-uniformities or crevices that can aggravate cavitation and hence its importance should be assessed. The flow passage inside the injector is small enough to have high enough Reynolds number to get a turbulent flow. Moreover the turbulent fluctuations can cause drastic drop in the local pressure, even though the mean thermodynamic pressure is higher than the saturation pressure, causing unexpected cavitation. Parametric studies indicate that the compressibility becomes important at high pressure differences and effects of stress and turbulent pressure fluctuations are not significant for cavitation in diesel injectors. The effect of the inlet pressure fluctuation has also been assessed for diesel and biodiesel. Diesel appears to be more susceptible to pressure fluctuations compared to biodiesel due to the difference in the viscosity.

The developed cavitation model has been finally implemented to simulate cavitation

in the complex geometry of a real fuel injector along with needle movements. Diesel vs. biodiesel cavitation has also been studied in the complex geometry to understand the effects of needle movements.

Acknowledgements

I would like to express my deepest gratitude to my supervisor, Dr. Xianguo Li, for his invaluable guidance, steady encouragement, inspiration and support throughout my PhD. I would also like to thank my committee members, Dr. Chao Zhang, Dr. Fue-Sang Lien, Dr. Zhongchao Tan and Dr. Boxin Zhao for taking the time to scrutinize my thesis. Their comments are highly appreciated.

I would like to thank all my past and present group members, especially Dr. Ghobad Amini, Dr. Ehab Abu-Ramadan, Dr. Ibrahim E. Alaefour, Dr. Saher Al Shakhshir, Aaron Pereira, Queenie So and Abbas Ghasemi. Without their help, encouragement and fruitful discussions throughout the course of my PhD., I would not have been able to put together this important publication.

I would like to acknowledge Dr. Sibendu Som at Argonne National Laboratory for sharing his experience on cavitation modelling and his support for cavitation simulations with needle movements. I would also like to express my gratitude to Dr. Michele Battistoni at University of Perugia, Italy for sharing his experience on cavitation modelling and treatment of bubble dynamics in multi-dimensional cavitation simulations.

The financial supports by Ontario Research Fund-Research Excellence (ORF-RE) Program, and Green Auto Power Train are greatly appreciated.

The experience of graduate school would not be the same without good friends. My thanks go to my friends Sudipto, Syamantak, Arijit, Ravindra, Mukto, Sharad, Raja, Pradeep, Arpan, William, Nancy, Crystal, Eugene, Katie and many others. I would always value your support and encouragement. My friends during my Masters and Undergraduate Studies especially Swetaprovo, Arnab, Surya, Ritobrata, Ganesh and Soham have provided me the strength to pursue PhD. Their contribution will never be forgotten.

Dedication

This is dedicated to my father Mr. Monoranjan Saha and mother Mrs. Dalia Saha. Their unconditional support despite being in ill-health and continuous encouragement to fulfil my dreams have paved the way of this journey.

Table of Contents

List of Tables

List of Figures

NOMENCLATURE

B Bulk Modulus, Pa

c, c_o Speed of sound in liquid, m/s

CN Cavitation Number

C_c Contraction coefficient

C_d Drag coefficient

C_D Discharge coefficient

d Diameter or width of the nozzle

D Diameter or width of the extended domains upstream and downstream of the nozzle

f_v, f_l Mass fraction of gaseous phase and liquid phase respectively

K Cavitation Parameter

k Turbulent kinetic energy, m^2/s^2

L Length of the nozzle, m

N''', $\hat{n}_0$ Bubble number density, $1/m^3$

p Local static pressure, Pa

$p_B(t)$ Instantaneous pressure inside the bubble, Pa

p_{eff} Effective pressure including turbulent fluctuation and stress, Pa

p_{sat} Saturated vapour pressure (Threshold Pressure), Pa

p' Fluctuating pressure, Pa

p_{ref} Reference pressure, Pa

P_{in} Inlet pressure, Pa

P_{out} Outlet pressure, Pa

ΔP Difference between inlet and outlet pressure, Pa

R Bubble radius, m

R_e Vapour formation rate, $kg/(m^3 \cdot s)$

R_c Liquid formation rate, $kg/(m^3 \cdot s)$

R_P Phase change rate, $kg/(m^3 \cdot s)$

Re Reynolds number of the nozzle flow

Re_{rel} Relative Reynolds number for Eulerian-Eulerian simulations

S_{11} Principal strain rate, 1/s

t Time, s

u_i Advected velocity, m/s

u_j Advecting velocity, m/s

u' Fluctuating velocity, m/s

Greek

α^* Damping coefficient for turbulent viscosity

α_v, α_l, α_g Volume fraction of vapour, liquid and non-condensable gas, respectively

σ Surface tension, N/m

ϵ Turbulent dissipation rate, m^2/s^3

ρ, ρ_v, ρ_l, ρ_g Density of mixture, vapour, liquid and non-condensable gas, respectively

μ Mixture viscosity, Pa·s

μ_t Turbulent viscosity, Pa·s

ω Specific turbulent dissipation rate, 1/s

ω_0 Initial droplet oscillation frequency, 1/s

Chapter 1

Introduction

Over the last several decades there has been a tremendous increase in the world energy consumption especially in case of oil: from 2 Terawatts (TW) in 1965 to over 5 Terawatts (TW) in 2009 [1]. The reason behind such increasing demand is attributed to the increase in world population and growing demand of automobiles and public transport. Consequently there is a growing need for better environment protection and air quality which poses a stiff challenge for engineers to design vehicles with higher power output yet better fuel economy and less pollutant formation. Direct injection (DI) diesel and gasoline engines have become an important area of research as it achieves higher compression ratio compared to conventional spark ignition engine and thus it serves the purpose of better fuel economy and better thermal efficiency [2]. The permissible limits of pollutants for both gasoline and diesel engines have been reduced drastically [3] to cope up with the dual crisis of energy consumption and air pollution. However the fossil fuel reserves are fast depleting and this crisis paved the way for use of alternative fuels such as biodiesel or bioethanol. As a result the significance of fundamental understanding of the correlation between the internal flow in the fuel injector and spray formation in the combustion chamber is still there and is becoming more meaningful in the recent times because of emergence of alternative fuels. Further understanding of cavitating flow and its connection with spray formation will provide better insight in achieving better performance of internal combustion engines. As a consequence cavitation inside fuel injectors, is garnering immense interest among the scientific community.

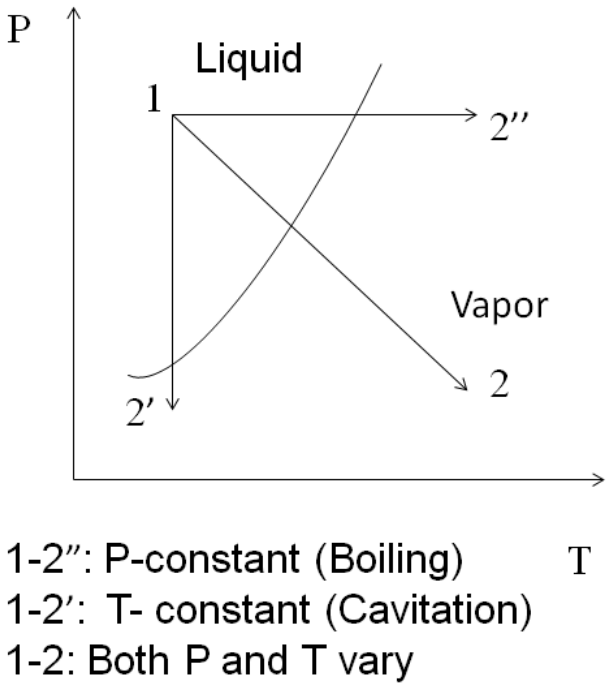

Figure 1.1: Difference between cavitation and boiling shown in a Pressure (P) vs. Temperature (T) diagram.

1.1 Cavitation and Spray Behavior

1.1.1 Cavitation Fundamentals

In a flowing liquid whenever the local pressure in certain regions drop below the vapour pressure of the fuel concerned then vapour cavities or bubbles appear and the phenomenon is known as "cavitation". The flow inside the fuel injector thus becomes complicated to study as in most cases it is a high speed two-phase flow in a small passage. Though cavitation seems similar to boiling in terms of formation of vapour bubbles there is a fundamental difference. Both the processes are illustrated in Fig.1.1. Boiling happens when the thermodynamic state changes from liquid to vapour phase at constant pressure and by increasing the temperature. Cavitation is a thermodynamic process where the state is changed at constant temperature by lowering the pressure. "Cavitation" a word coined by Froude was first envisaged as a physical phenomenon by Parson in the period (1895-1906) [4]. Cavitation is generally a design concern for fluid machinery as the cavitation

bubbles collapse followed by release of tremendous energy manifested in the form of pressure waves [4–6]. On the contrary in case of fuel injector the phenomenon of cavitation is generally known to be useful as cavitation decreases contact of liquid phase with nozzle wall and hence increases the effective exit velocity of the liquid fuel which becomes helpful for primary atomization of the fuel jet once it comes out of the fuel injector.

The cavitation bubble in a liquid goes through mainly four stages: a) nucleation, b) growth, c) collapse and d) rebound [4]. The type of phase transition that involves nucleation is called first-order phase transition [7,8]. This involves thermodynamic state change from one phase to another with intermediate metastable stages. When the local pressure is below vapour pressure then nucleation of vapour bubbles occur at that location. The liquid thus moves towards a more stable lower free energy state. If the bubble pressure is greater than the local liquid pressure then it will grow and if the pressure is less than the local ambient pressure it will shrink/collapse. If the bubble is not fully collapsed then there is another stage when the bubble tends to re-grow in size known as "rebound". Following this bubble go through "collapse" again. The "collapse" rate is so fast that a pressure wave propagates from the bubble wall to its center and then gets reflected back from bubble center to bubble wall and some energy gets refracted to the liquid medium as shock wave [6]. In cases of cavitation there are innumerable bubbles and apart from the four above-mentioned phenomena, the bubbles can coalesce or breakup depending on the level of interaction between the bubbles and surrounding liquid flow. However, phenomenon of nucleation is complicated to model and in cavitation modelling, typically a specific number density of very small bubbles are assumed to be existing and only growth and shrink/collapse of vapour bubbles or cavities are modelled.

Types of Cavitation

The phenomenon of cavitation can be classified based on different aspects. According to Knapp [6] cavitation can be broadly classified based on the combined criteria of principal physical characteristics and the conditions at which cavitation is taking place in the following way,

1. **Travelling cavitation**: This type of cavitation involves formation of bubbles or cavities followed by their movement along with the liquid flow. It is a kind of transient cavitation where the bubbles grow, shrink or collapse as they travel with the flow.

2. **Fixed cavitation**: After "cavitation inception" or start of cavitation, liquid drifts away from the solid boundary to allow the vapour cavity to grow. This is known

as "fixed" cavitation. The fixed cavity may grow or shrink and may collapse by entraining liquid in to the cavity. The liquid adjacent to the vapour cavity often contains innumerable travelling cavities/bubbles. This means "fixed" cavitation can be accompanied by "traveling" cavitation.

3. **Vortex cavitation**: "Vortex" cavitation generally happens on the blade tips of ship propellers, which is why it is often regarded as "tip" cavitation. The core of the vortex is a zone of high shear and as a result vapour cavities are formed.

4. **Vibratory cavitation**: "Vibratory" cavitation occurs when a specific liquid element passes through cavitating zone more than once. The reason for this phenomenon can be attributed to the presence of the high amplitude and high frequency pressure pulse caused by the movement of any solid body or parts within the fluid machinery such as the needle movement in high pressure diesel injector.

Parameters Affecting Cavitation

It is generally known that the local thermodynamic pressure of the liquid has to drop below the saturation pressure for cavitation inception to occur. According to classical definition saturation pressure therefore becomes the cavitation threshold. In reality this information does not provide the full insight behind the cavitation formation. To get an elaborate understanding of cavitation inception or cavitation phenomenon in general the following factors should be taken into account [4].

1. **Liquid Temperature and Saturation Pressure**: The liquid temperature is important as it determines the saturation pressure of the liquid which is the cavitation threshold in the classical case. However, isothermal modelling approach is typically adopted in the literature.

2. **Turbulence**: If Reynolds number is high enough (typically when greater than 2000), then the flow is generally turbulent and turbulence has been known to affect cavitation on several occasions [4]. In the analysis of cavitation in fuel injectors turbulence have been considered in most of the studies in the literature. Additionally turbulent pressure fluctuation can cause drop in instantaneous local pressure leading to cavitation.

3. **Viscous Stress**: The viscous effects are important in case of cavitation inception. Researchers have observed in a flow the cavitation inception may occur even before

the local pressure drops below the saturation pressure [4]. A liquid element under shear stress caused by the flow can rupture to give rise to cavity and thus the knowledge of static pressure is not enough to predict the occurrence of cavitation.

4. **Quality of Solid Boundary**: Cavitation occurring in a flow passage will depend on the quality of the wall surface. Small crevices or pits on the walls may act as nucleation sites or may lead to early transition to turbulence and thus may cause earlier onset of cavitation.

5. **Compressibility**: Vapour phase is generally considered compressible. While liquid compressibility is typically not perceived as a major factor, but is important for bubble dynamics or cavitation studies. During the collapse of the bubble, the bubble surface moves at a very high velocity causing the liquid to act as compressible fluid. In case of flow through fuel injectors the liquid moves at very high speed and thus the overall mixture also becomes compressible. The needle movements in fuel injectors will cause fluctuations in the flow-field and liquid phase compressibility will be vital in the analysis.

Cavitation in Fuel Injectors

The cavitation in a spray nozzle has been an extensive topic of research since late 1950's. Correlations were envisaged between spray formation and flow inside the nozzle [9]. If the nozzle inlet is sharp and the flow enters the nozzle from a larger cross-section to a smaller cross-section in the nozzle then the streamlines cannot exactly follow the solid boundary and squeeze towards the centerline of the nozzle causing a flow separation near the inlet which is known as vena-contracta. As a result there is a sharp increase in the liquid velocity inside the nozzle in that region. There can be reattachment of the flow depending on the flow variables and dimensions of the nozzle. The cavitation thus determines the nature of the internal flow and the internal flow influences the spray breakup of the liquid jet. The spray breakup affects the combustion characteristics of the fuel inside the combustion chamber and the sequence is illustrated in Fig.1.2. It is important to point out that performing experiments to study two phase flow inside an actual fuel injector is very difficult. As a result majority of the experimental studies have been carried out in simple geometry nozzles with circular or rectangular cross-sections. For similar reasons many modelling studies, concentrating on fundamental understanding, are carried out in simple geometries.

In direct injection fuel injector a vapour cavity is formed at cavitation inception [9]. Further increase in the pressure difference results in the elongation of the vapour cavity

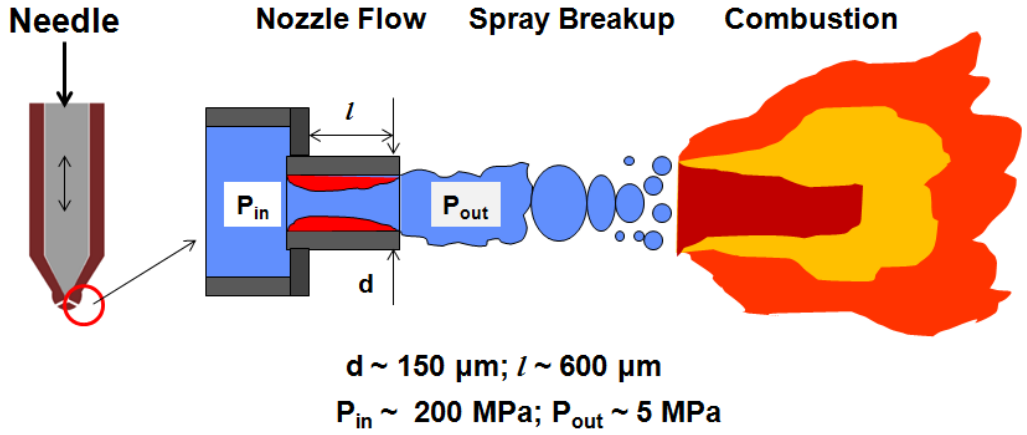

Figure 1.2: Illustration of a cavitating nozzle and cavitation affecting spray breakup and combustion

along with the appearance of foamy or bubbly mixture at the end of the cavity. The classifications presented in the preceding section indicate that in diesel injector the cavitation phenomenon can be a combination of "fixed" and "travelling" cavitation. The two important non-dimensional numbers that are used to characterize cavitating flows are cavitation parameter, K and cavitation number CN. For a diesel injector with an inlet pressure of P_{in}, and a liquid of saturation pressure (for the given liquid temperature) P_{sat}, the cavitation parameter, K is expressed as [6] ,

$$K = \frac{P_{\text{in}} - P_{\text{sat}}}{P_{\text{in}} - P_{\text{out}}} \tag{1.1}$$

The cavitation number CN is expressed in terms of inlet pressure P_{in}, back pressure P_{out}, and saturation pressure of the liquid fuel used P_{sat} [9].

$$CN = \frac{P_{\text{in}} - P_{\text{out}}}{P_{\text{out}} - P_{\text{sat}}} \tag{1.2}$$

The two important non-dimensional numbers that helps to characterize the nozzle flow are Discharge Coefficient (C_D) and Reynolds number (Re). Discharge coefficient is expressed as

$$C_D = \frac{\dot{m}_{\text{actual}}}{\dot{m}_{\text{theoretical}}} = C_c\sqrt{K} \tag{1.3}$$

where, C_c is contraction coefficient. Schmidt [9] indicated that when injection pressure is very high with respect to the back pressure K tends to become unity and $C_D \approx C_c$ and therefore, discharge coefficient at high injection pressure represents the ratio of effective area of the liquid jet emanating from the nozzle to the actual exit area of the nozzle. Derivation of C_D is elaborated in Literature Review chapter. For cavitation analysis Re is mathematically represented as

$$Re = \frac{\rho_l V_{\text{exit}} d}{\mu_l} \tag{1.4}$$

where, d is exit diameter of the nozzle, V_{exit} is the average exit velocity of the nozzle.

Apart from "cavitation" there are two other terms commonly used for fuel injectors, "supercavitation" and "hydraulic flip". "Supercavitation" means the vapour region extends to the outlet of the nozzle . It is considered to be beneficial for primary atomization as there is no shear resistance on the liquid jet from the wall of the injector and hence the liquid jet can manage to exit the nozzle at higher velocity. "Hydraulic flip is a phenomenon which is generally characteristic to spray injector nozzles [9]. In this case the liquid flow completely separates from the wall of the injector and downstream gas enters into the nozzle and occupies the space. It has been observed that under realistic operating conditions hydraulic flip does not occur in case of diesel injector nozzles [9]. Hydraulic flip is generally considered undesirable in case of spray injector nozzles as it results in poor quality of atomization.

Conicity is another important terminology, used for describing the hole pattern (straight or converging or diverging) in a fuel injector and is defined as

$$k \text{ or } C \;=\; \frac{D_{\text{in}} - D_{\text{out}}}{10} \tag{1.5}$$

It is also important to know different types of fuel-injector sac and needle combinations. There are three main types, a)valve covered orifice (VCO), b) mini-sac and c) micro-sac [10]. An illustration is shown in Fig. 1.3. VCO nozzles are good in fuel injection timing and controlling of injected fuel amount, but fuel distribution to the different holes is very sensitive to needle concentricity in the injector, leading to uncertainties in spray formation. For mini-sac nozzles fuel spray is relatively less sensitive to misalignment of needle. However, due to nature of the injector geometry, fuel might get injected even after needle is closed, which is not desirable for precise operations. Micro-sac nozzles are more recent and their unique designs mitigate the problems that can arise in other two-type of nozzles and hence is fast becoming the preferred choice of researchers.

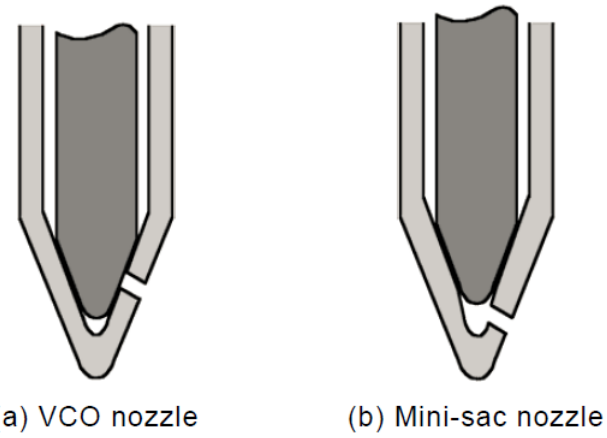

Figure 1.3: Diagrams of (a) VCO and (b) mini-sac nozzles [10].

1.1.2 Effect of Cavitation on Spray Breakup

After the fuel jet issues out of the injector hole, it is subjected to breakup and atomization. Generally the jet first disintegrates into large filaments or blobs or drops, a phenomenon known as "primary breakup". In case of high pressure diesel injection cavitation and turbulence originating from inside the nozzle or fuel injector hole are the driving mechanisms for primary breakup [11]. After the primary breakup, the blobs or drops undergo further breaking up into small and smaller droplets, which is known as "secondary breakup" or "atomization". In case of very high exit velocity from the nozzle, the fuel jet might readily undergo atomization without going through primary breakup. Therefore, the complete spray pattern is determined by the relative magnitudes of inertia, surface tension and aerodynamic drag.

Generally cavitation is relevant for only primary breakup. As a result discussion will be limited to the primary breakup process. Basic processes affecting primary breakup are illustrated in Fig.1.4. Turbulence inside the nozzle flow induces small surface waves of the liquid jet emerging out of the nozzle and these small disturbances can amplify the aerodynamic shear forces and thus cause splitting of the liquid jet. However this process of breaking up due to amplified disturbance has a time-scale larger than the actual time-scale of breakup process as the primary breakup happens almost immediately. Consequently aerodynamic effects are considered secondary causes for primary breakup [11]. Turbulence initiating inside the nozzle is rather a more influential factor for primary breakup. The radial perturbation in the exiting jet induced by in-nozzle turbulence can be strong enough

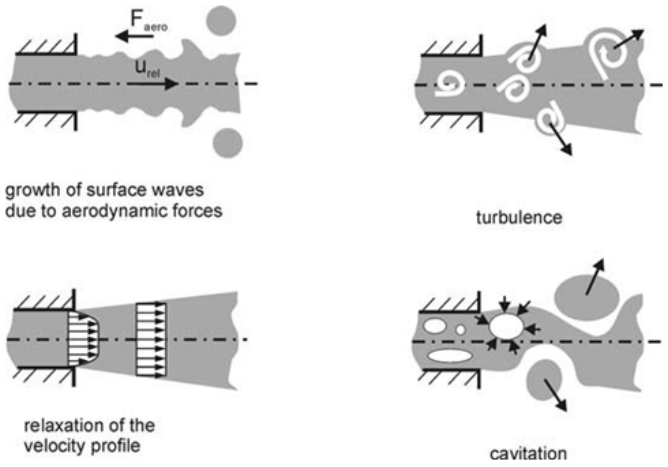

Figure 1.4: Schematic illustration of mechanisms of primary breakup [11].

to overcome surface tension forces leading to formation of primary drops [12]. Turbulence occurring inside the nozzle is considered as one of the determining causes for primary breakup. Another possible factor is velocity relaxation of fuel jet. The fuel jet is no longer bounded by walls immediately after exiting the nozzle and free shear boundary condition is experienced by the outer edge of the fuel jet. If the flow inside the nozzle happens to be fully developed (large L/D ratio) then the velocity at near wall region would be lesser than that at the core of the flow. However after exiting the nozzle the outer edges of the jet experience a rise in velocity due to free shear at the outer edge and viscous shear from the core of the jet. As a result there is a flat velocity profile in the core of the jet and acceleration in the outer edges can potentially cause strong enough disturbances to cause breakup. Nevertheless in high pressure direct injection, flow is generally not fully developed (small L/D ratio) inside the nozzle and cavitation is most likely to occur. Consequently evolution of velocity inside the nozzle to a block profile in the jet is less feasible for high pressure injection [11]. Cavitation is considered as another dominating factor for primary breakup. Cavitation bubbles residing in the core of the flow may implode once the internal flow turns in to an external free jet imparting strong disturbances for causing primary breakup. Experimental studies indicate that transformation of single-phase turbulent flow to two-phase cavitating turbulent flow leads to larger spray angle and smaller penetration length [13–18]. Higher radial momentum and lower axial momentum of the fuel jet in the near nozzle region due to cavitation induced disturbance could be a possible reason for this change in the spray pattern. Implosion of cavitation bubbles induces further turbulence and hence cavitation and turbulence together are believed to be the driving agents for

primary breakup process for high pressure direct injection.

Cavitation increases the hydraulic resistance of the nozzle, and hence reduces the injected fuel mass in an unpredictable manner. Cavitation may cause poor fuel/air mixture formation in the engine, unstable combustion and higher emissions or can enhance the efficiency of atomization processes resulting in smaller droplets i.e. lower sauter-mean diamater (SMD). SMD (d_{32}) is a measure of average droplet size in a spray. In addition, cavitation can prevent nozzles from coking, which is a growing challenge in the context of decreasing hole diameters and increasing usage of the bio-fuels. The relation between local nozzle flow and spray development in the combustion chamber is still challenging and an on-going research topic from both experimental and numerical aspects. Numerical investigation of cavitation, till date, is still relevant and difficult as the density and viscosity ratios between the phases are huge and at high pressure injection obtaining reliable experimental data is a daunting task.

1.2 Thesis Objectives and Outline

The objective of this work is to develop a cavitation model for diesel injectors that could provide a reasonable estimate of the boundary condition at nozzle hole outlet for better prediction of spray breakup models with justifiable approximations and at low computational cost. There is scope of detailed modelling of cavitating two-phase flow in diesel injectors, considering nucleation, coalescence, breakup, growth and collapse of bubbles, which would require significant computational resources. However keeping in mind about the primary motivation of the cavitation modelling, it is worthwhile to invest efforts in developing a relatively simpler model that would address the key factors of cavitation. Therefore, the aim of the present study is to focus on specifically

- To develop an "accurate" (engineering point of view) cavitation model with reasonable computational cost
- To validate the present model with available experimental data
- To compare its performance with some commonly used models in the literature
- To investigate the difference between cavitation characteristics of diesel and biodiesel
- To provide an insight of needle movement effects on cavitation in a typical multi-hole fuel injector

The present cavitation model developed in this study has been coupled with the mixture multiphase approach and implemented in ANSYS Fluent platform.

There are several assumptions adopted by different cavitation models in the literature, which are not explained or justified in the cavitation literature. Efforts have been made to highlight the basis of some of these assumptions to provide a clear picture of the intricacies and challenges involved in cavitation modelling and the necessities for such approximations. The model predictions have been compared with qualitative and quantitative information from experimental data in the literature. The underlying assumptions, approximations, limitations and utilities of the present model are discussed elaborately. The performance of the present cavitation model has been also assessed with existing cavitation models in ANSYS Fluent, which are also commonly adopted by the researchers.

In this chapter an introduction to the cavitation and spray breakup phenomenon, background information of diesel injector and relevant non-dimensional numbers has been given. Literature review is presented in chapter two covering experimental and numerical works on cavitation. In chapter three the formulations of the modelling work are given including governing equations of mixture and Eulerian-Eulerian multiphase approaches, turbulence models and cavitation models along with material properties and solution procedure. Comparison of the predictions of the present model with those of commonly used cavitation models and experimental results are provided in chapter four. Two existing cavitation models in ANSYS Fluent (Schnerr-Sauer and Zwart-Gerber-Belmari) have also been assessed by coupling with Eulerian-Eulerian multiphase approach and the results are shown in chapter four as well. Chapter five provides comparative assessment of cavitation of diesel and biodiesel in an axisymmetric nozzle at different pressure differentials (between inlet and outlet), effects of turbulence modelling, liquid compressibility, fuel physical properties and wall roughness, variation in initial amplitude parameter as well as cavitation variations under the influence of inlet pressure fluctuations. Needle movement effects on cavitation are presented in chapter six. Finally the thesis is concluded with discussion of summary of present study and recommendations for future work in chapter seven.

Chapter 2

Literature Review

The onus of discovering the existence of cavitation phenomenon was on Reynolds when he had to explain the strange behaviour of ship propellers at high rotational speed [19]. However Reynolds failed to realize the possibility of phase transformations and he rather speculated the chance of air entrainment in the wakes of the propellers. The first success to the best of the knowledge of the author was achieved by Parsons [20] in 1906. Since then it became another field of extensive research in the field of multiphase fluid mechanics. The earliest work in the area of cavitating nozzles dates back to 1950s, when Ranz tried to connect the internal flow of the nozzle with the spray formation outside the nozzle [21]. Plethora of research has taken place in the field of cavitation and bubble dynamics. Experimental works are less common in the literature compared to modelling or numerical works because of limitation imposed by the length scale and time scale of this phenomenon. For fuel injector nozzles the flow goes at very high speed and through a very small passage. As a result, experiments have been done for mostly nozzles with scaled up dimensions, which still manage to throw some light on the fundamental understanding of the cavitation phenomenon.

2.1 Experiments on Cavitation

For the last few decades several researchers have carried out experimental studies on cavitation in injector nozzles, which have contributed to the understanding of the cavitation phenomenon in fuel injectors. In actual direct injection fuel injectors the engines operate at very high injection pressure in the order of 200 MPa [22]. The actual geometry is very complicated with multiple holes and a moving needle inside controlling the fuel flow rate

through the holes. The total time span of the operations is in the order of few milliseconds. It is very difficult to execute experimental studies at exactly same operating conditions and same geometry. As a result most of the studies have been done with scaled up simple nozzle geometries for lower pressure differences. Most of the works provide images that give an estimate of the extent of the cavitating regions or the regions where cavitation is most likely happening. Shadowgraph techniques have been employed using high speed photography with charge-coupled device (CCD) cameras for these studies. Some researchers have also recorded X-ray computed tomography (CT) images, which after proper post processing could provide quantitative information about two-phase flow composition. Laser based techniques have also been adopted providing qualitative and/or quantitative information. Discharge coefficient and mass flow rate variations with change in pressure differences are obtained in most of the experimental studies. Moreover the quantitative information of the flow variables that are reported are either global (e.g. mass flow rate) or local (e.g. velocity at a specific location in the nozzle). Overall a broad classification can be made regarding the experimental works: Qualitative and Quantitative.

2.1.1 Qualitative Studies

Optically accessible nozzles or fuel injectors are used for imaging purposes. In the studies resorting to shadowgraph techniques the images are taken with high-speed CCD camera on one side of the flow and light source on the other side. The resultant images have an aggregation effect as the light penetrates through the entire domain and the transmitted light is captured by the camera. Owing to the difference in the optical density of two phases there is a variation of contrast in each image which provides an impression about the location and extent of cavitating regions. [16, 23–36].

For experimental studies of cavitation the pioneering work was done by Bergwerk [23]. The importance of cavitation for direct fuel injection was first realized because of his landmark work. He conducted experiments with transparent nozzles of relatively large dimensions compared to the actual fuel injector nozzles. He observed the phenomena "cavitation" and "hydraulic flip". He succeeded in drawing some useful conclusions such as : a) chance of hydraulic flip decreases with decrease in the size of the nozzle, b) the relative effect of geometry imperfections in small scale nozzles are much more compared to large ones. Nurick [25] carried out his experiments in scaled-up transparent nozzles (d≈8 mm) and observed both cavitating flow and hydraulic flip in the transparent nozzles. His main contribution was developing a correlation between coefficient of discharge and cavitation parameter of injector nozzles by varying upstream and downstream pressures and the length to diameter ratios of the nozzles. His analysis proved to be more useful for

a limiting case of axisymmetric nozzles. Specifics related to his correlation will be provided in the "One-dimensional Analysis" sub-section. Chaves et al. (d≈0.2 mm) [26] extended the study of cavitation to show "supercavitation" which is different from hydraulic flip. He used rounded nozzles with insufficient ground surface inside the nozzle. It is believed that nozzles with sharp inlet are more prone to cavitate and therefore, nozzles with rounded inlets are not going to cavitate as much as the sharper ones. However in his study it was shown that surface irregularities are enough to cause cavitation and hence cavitation occurs also in rounded inlet nozzles with rough walls. He also did some analysis of scale effects for nozzles by comparing available results for large scale and his own results for real scale nozzles and concluded that cavitation is a phenomenon which does not scale with the geometry of the nozzle. In small nozzles cavities were observed while in larger ones, large bubbles could be seen which helped him to conclude that bubbles or cavities have their own length scales which do not depend on the length scale of the nozzle. Soteriou et al. [16] carried out experiments with large scale nozzles and he also observed cavitation and hydraulic flip. In his study he observed bubbly flows unlike the observations of Chaves et al. [26] in real scale nozzles. Arcoumanis et al. [29,30] performed a comparative study of real-scale and large-scale multi-hole injectors. For large-scale injectors foamy bubbles were seen while for real-scale injectors distinct voids were observed as illustrated by Arcoumanis et al. [29] and presented in a schematic form in Fig. 2.1. However some researchers are apprehensive about the true form of cavitation inside the diesel injector [9]. As pointed out by Schmidt and Corradini [9] the large voids due to scattering of light might appear as a bubbly mixture in large scale injectors or nozzles. Overall consensus is that in real scale nozzles or injector holes, near the inlet the vapour is in the form of wall-attached cavity and near the nozzle exit it is predominantly foamy or bubbly mixture. Moreover due to pressure fluctuations and needle movements the cavity length may vacillate. Overall cavitation scenario becomes a mixed phenomena comprising of travelling, fixed, vortex and even vibratory cavitation.

Genge and Roosen [28] and Winklhofer et al. [31] used planar nozzles i.e. nozzles with square or rectangular cross-sections for their cavitation experiments. In both the studies the dimensions were comparable as well as close to size of real scale fuel injector holes. Nozzle heights were in the range of 0.2-0.3 mm, the nozzle widths were close to 0.3 mm and the nozzle lengths were 1 mm in both cases. Genge and Roosen [28] used water while Winklhofer et al. [31] worked with European diesel fuel. Their operating conditions were comparable and the qualitative observations of cavitation also turned out to be similar. Cavitation inception and "supercavitation" were observed at almost same pressure differences (inlet and outlet pressures), around 6 MPa and 7 MPa respectively. Winklhofer et al. [31] used 3 types of nozzles: 1 straight and 2 converging nozzles. Except the images by

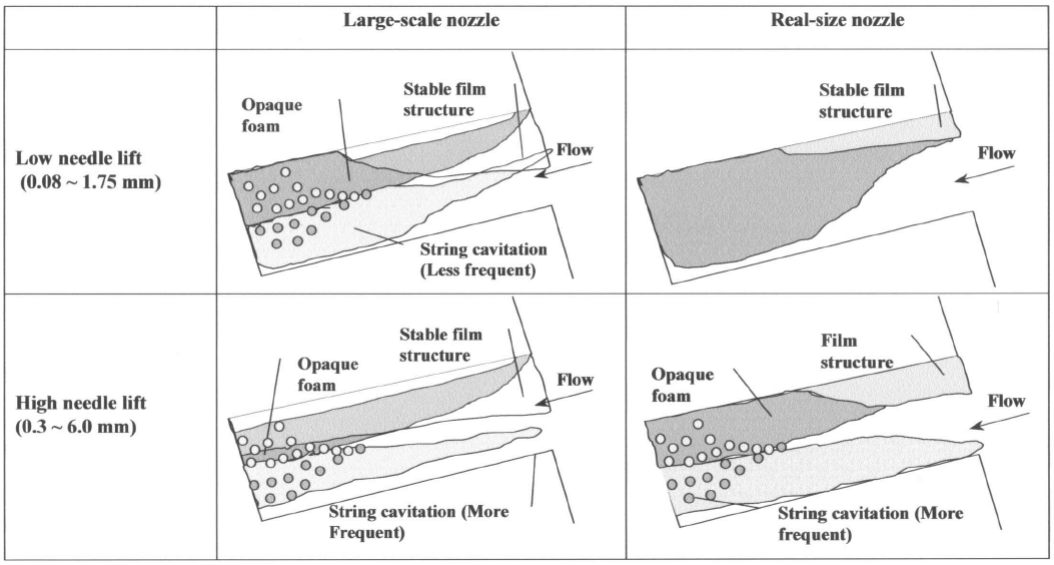

Figure 2.1: Illustration of cavitation patterns in large and real scale nozzles envisaged by Arcoumanis et al. [29].

Winklhofer et al. [31] none of the studies have done extensive post-processing for conveniently characterizing the nature of the flow. Winklhofer et al. took 20-30 backscattered images of the two-phase flow for each operating conditions and performed an ensemble avaerage on them to generate representative images. They used colour schemes to distinguish cavitating, non-cavitating and foamy (both liquid and vapour) regions with blue, red and greenish yellow respectively. For cavitation images poor quality is a concern and creates inconvenience for the readers and the model assessment studies. A study has been done by Lockett et al. [37] devoted to the image acquisition and image processing of two phase flow images. Transparent acrylic assembly of multiple holes were designed and fitted to the lower part of a multi-hole injector in their study. Detailed procedure of obtaining ensemble averaged images and method of background intensity subtraction to achieve high quality images were documented in their study as shown in Fig. 2.2.

Suh et al. [34, 35] carried out experiments to assess the effects of dimensions of nozzle and fuel properties (diesel vs. biodiesel) on cavitation. Their key observation was that diesel cavitation inception occurs sooner than biodiesel, presumably due to lower viscosity of diesel. They also reported cavitation was suppressed considerably by tapering of nozzles. Erosion in fuel injectors due to cavitation is not frequently reported in the literature unlike the case of cavitation in pumps or other hydraulic devices [38–40]. Improper design

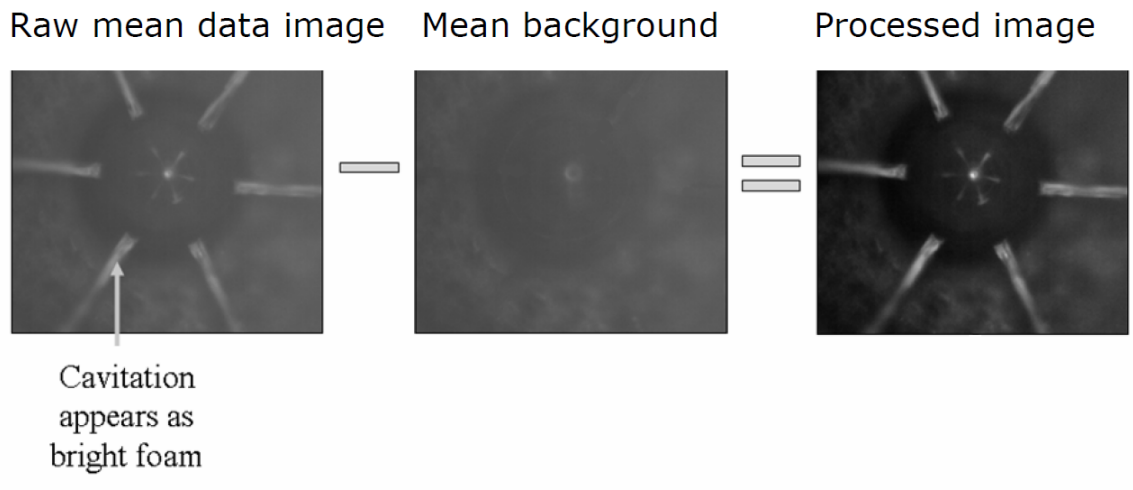

Figure 2.2: Sample procedure of image processing for understanding cavitation shown by Lockett et al. [37].

of needle and injector holes may lead to cavitation damages when subjected to collapse of bubbles. Design optimization has revealed that tapered or converging holes and specially manufactured needles can prevent cavitation damage as well as result in low exhaust emissions [40]. It is worthwhile to mention here that under certain scenarios where cavitation bubbles are subjected to rapid collapse or implosion, luminescence occurs [38, 41]. To the best of the knowledge of the author luminescence has not been reported to be occurring inside fuel injector holes. This indicates that intense bubble collapse may not occur inside a modern fuel injector.

Badock et al. [27] performed experiments with both laser sheet illumination and shadowgraph technique. They realized that compared to the images taken by the shadowgraph, laser illuminated images reveal the same length of cavitation inside the injector hole. Additionally, laser based technique enables a view of the liquid core which is shrouded by cavitation films which is otherwise not visible with shadowgraph. Soteriou et al. [42] used a laser sheet to illuminate a plane through a cavitating flow and images were captured under different operating conditions. Not many studies have been executed with laser sheet illumination method. More studies with both shadowgraph technique and laser sheet illumination are needed for real scale nozzles or injectors under realistic operating pressures with different kind of fuels e.g. diesel, biodiesel or diesel-biodiesel blends.

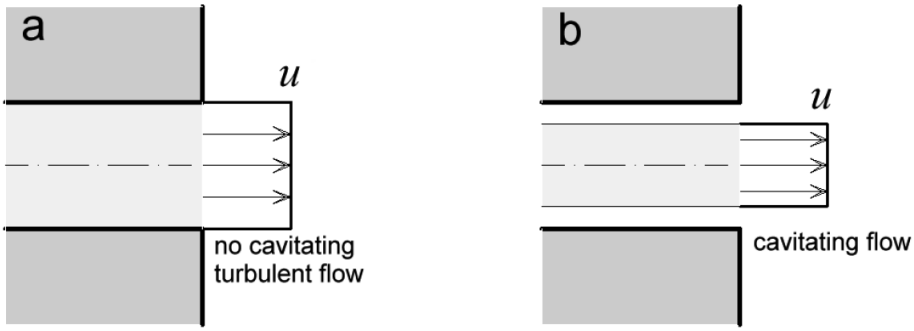

Figure 2.3: Illustration of area reduction of cavitating flow at nozzle exit provided by Desantes et al. [47].

2.1.2 Quantitative Studies

To develop complete understanding of the cavitating flow, quantitative information is undoubtedly crucial. Variation of mass flow rates and discharge coefficients with pressure difference across the nozzle are generally widely reported in the experimental studies [14, 16, 23, 25, 26, 29, 31, 34, 35, 43–52]. In cases of considerable cavitation the effective mass flow rate is significantly lower than the theoretical estimate based on single-phase inviscid flow. Since the liquid core remains shrouded with vapour films or cavities the effective area of the exit flow reduces and mass flow rate turns out to be considerably low. This concept has been extensively discussed in the review article by Schmidt et al. [9, 47] and can be understood from the illustration adopted from the work by Desantes et al. [47] in Fig. 2.3. Therefore, mass flow rates and discharge coefficients provide an assessment of the flow efficiency of the nozzle under cavitating conditions.

Bergwerk et al. [23] observed that discharge coefficient goes down to close to 0.60 at very high pressure difference compared to high values such as 0.75-0.80 for low pressure difference and is not strongly dependant on Reynolds number. As mentioned before the bubbles or cavities have their own length scale which makes it hard to perform dimensional analysis of cavitation inception. However inception of cavitation could be estimated as the combined observation of the researchers [16, 23, 25, 26, 29], where they concluded that the ratio of downstream pressure to the pressure difference across the nozzle can become a constant value at cavitation inception if the vapour pressure of the liquid concerned is small enough with respect to both inlet and back pressures of the nozzle and thus becomes weakly dependent of the geometry. Bergwerk [23] found that this ratio to be approximately two-thirds for his analysis. Winklhofer et al. [31] carried out quantitative analysis with straight and converging nozzles. The inlet pressure was fixed at 10 MPa and the outlet pressure was

varied. Winklhofer et al. [31] observed very important features of the cavitation in all three types of nozzles. They noted that the mass flow rate values in all three types of nozzles at cavitation inception and choked flow conditions were almost equal even though pressure differentials (inlet and outlet pressures) required to achieve these states were very different for choked flow conditions. Choked flow conditions occurred after cavitation inception had already taken place. Choked flow conditions have also been observed or inferred by other researchers [16, 26, 53, 54]. Discharge coefficient C_D, generally tends to decrease with decrease in cavitation parameter K, which means increase in pressure difference or increase in cavitation [9, 47]. The limiting value of C_D turns out to be around 0.61 where the hydraulic flip occurs. When the flow is non-cavitating generally C_D has a tendency to slight increments with decrease in K. This indicates then flow is non-cavitating increase in pressure difference causes the flow to overcome the viscous losses, but the once the flow cavitates there is dip in the flow efficiency or C_D due to vapour formation and shrinkage in effective area [9, 47, 49]. This loss can be referred as "cavitation loss" for the nozzle. While the flow is cavitating generally it is seen that C_D varation with K closely follows Nurick's correlation which will be elaborated in the "One-dimensional Analysis" section as mentioned before.

Quantitative information about vapour concentration is rare to come across. X-ray based computed tomography (CT) scans have been employed in the literature to estimate the vapour void (volume) fraction in scaled up nozzles [55–58]. Two-dimensional slices of a cross-section at specific axial locations in a nozzle are obtained using X-ray tube, collimator and an array of detectors. These two-dimensional images can be combined into a three-dimensional representation of the flow. Calibrations are achieved by scanning sections of nozzle filled with air and water so that concentrations of vapour in cavitating flows can be assessed. Sample scanned images are shown in Fig. 2.4.

Neutron radiography is another technique that has been used in the literature for detection of phase (liquid or vapour) concentrations in engineering devices e.g. fuel cells, fuel injectors [59–63]. Neutron radiography is based on the principle that neutrons interact with the nucleus of the atom, rather than the electrons. Neutron radiations are attenuated by some low atomic number elements, such as hydrogen, boron etc., but transmit through heavy materials such as titanium or lead [62]. Once the neutron beam penetrates through the test object it is converted to visible light and then photographic films or CCD sensors are exposed to the visible light to provide images. Takenaka et al. [61] captured neutron radiography images of cavitating flow. Figure 2.5 by Takenaka et al. demonstrates that in the hole region there are not enough signals to suggest presence of liquid fuel to prove that the nozzle is cavitating. However they did not present any image of non-cavitating case for comparison. They did not carry out any quantitative assessment with neutron

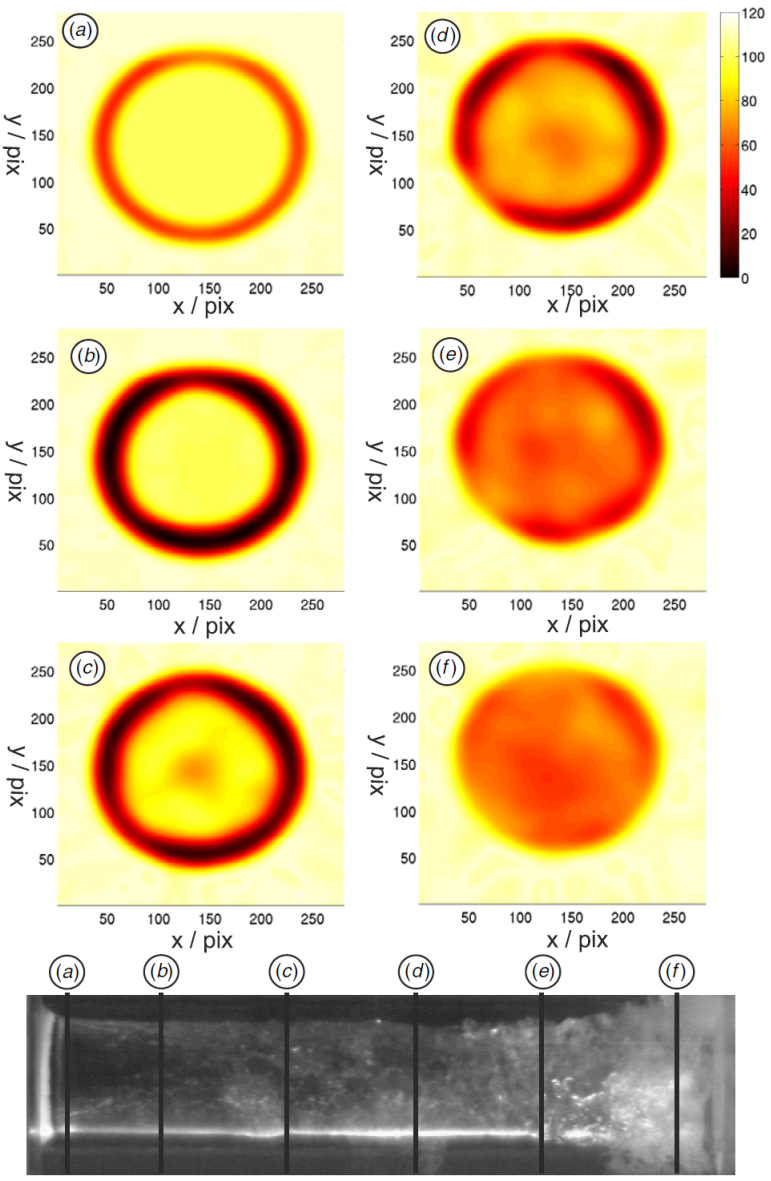

Figure 2.4: Cross-sectional CT images at different axial positions shown by Bauer et al. [58].

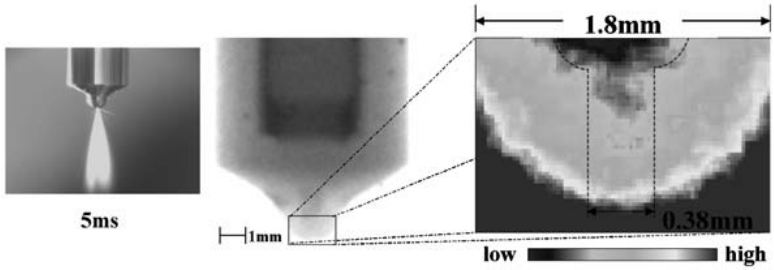

Figure 2.5: Visualization of fuel cavitation in the nozzle hole 360 rpm at 5 ms from start of injection using neutron radiography, performed by Takenaka et al. [61] .

radiography. Estimating void fraction in cavitating flows with neutron radiography has not been done yet in the literature, to the best of my knowledge. Nonetheless there are cases where neutron radiography have been used for void fraction assessment of two-phase non-cavitating flow such as Kureta et al. [60]. Despite the fact that the work of Kureta et al. did not involve cavitation, it was worthwhile to mention their work here to justify that neutron radiography could be valid for vapour concentration estimation of cavitating flows.

Obtaining velocity distributions inside a cavitating nozzle is important for understanding flow patterns in two-phase flow. Winklhofer et al. [31] measured velocity profiles with a fluorescence tracing method. A laser light pulse (248 nm, 30 ns) irradiated a narrow area of the fluid. Images captured at constant time intervals after the laser pulse illumination show the displacement and thus provide the velocity profile. However they were unsure about the measurement accuracies in the near wall regions. Laser Doppler Velocimetry (LDV) is used for non-intrusive, time-resolved measurements of local fluid velocities and their fluctuations [64]. Velocity measurements using LDV in a cavitating flow has also been undertaken [32, 65]. In both the papers LDV measurements were performed in large scale injectors with a design similar to real scale multi-hole fuel injectors at different axial locations in the injector holes.

Particle Image Velocimetry (PIV) is a technique for measuring the instantaneous velocities in the entire domain of interest and hence is not a point measurement technique unlike LDV. Carrying out PIV in a cavitating flow is not common. To the best of the knowledge of the author the only study of cavitation in a fuel injector involving PIV is by Aleiferis et al. [66]. They investigated flow patterns in 3 locations in a commercial fuel injector, all in upstream of the nozzle holes, in 20× optical acrylic models to facilitate PIV measurements. PIV study of cavitation in fuel injector holes could not be found in the literature even in scaled up setups.

2.2 Modelling of Cavitation Phenomena

Modelling of cavitation phenomena can be broadly classified as "one-dimensional" and "multi-dimensional multiphase" models. One-dimensional model generally makes necessary assumptions to treat a multi-dimensional problem as a one-dimensional one. It estimates the discharge coefficient of a nozzle operating under a range of operating conditions. However one-dimensional model cannot provide extensive details of the two-phase flow and that is where multi-dimensional multiphase models become useful.

Classification of existing multiphase models is not easy and can be approached in more than one way. The models can be broadly divided as a) bubble-based and b) thermodynamic models. Bubble based models use the concept of individual bubble growth to estimate the evolution of the two-phase flow composition. While thermodynamic models rely on the equilibrium principles to evaluate the thermodynamic states and hence the concentration of vapour. On the other hand it can be also be categorized on the basis of multiphase approach, such as a) Eulerian-Lagrangian, b)Eulerian-Eulerian, c) Mixture and d)Volume Of Fluid (VOF) [67]. For VOF and Mixture approaches there is only one set of transport equations, mass and momentum along with vapour fraction conservation equation. As a result these two approaches can be clubbed together as "single-fluid" model. While Eulerian-Eulerian and Eulerian-Lagrangian approach involves effectively two different fluids in the form of liquid and vapour for cavitation analysis. In Eulerian-Eulerian both liquid and vapour are continuum phases and in Eulerian-Lagrangian liquid is continuous and vapour is dispersed phase. Both Eulerian-Eulerian and Eulerian-Lagrangian approaches can be considered as "two-fluid" model. In the Eulerian-Eulerian approach mass and momentum conservation equations of each phase are required. In the Eulerian-Lagrangian approach, the force balance equation is needed for the dispersed phase. Since bubbles constitute the dispersed phase, additional equations may be needed for capturing the essence of bubble size change, bubble coalescence, bubble breakup and population balance. Typically most of the existing models require a source term formulation for the mass and/or momentum balance of the two-phase fluid flow, especially while resorting to mixture, VOF and Eulerian-Eulerian multiphase approaches. Eulerian-Lagrangian approach uses bubble dynamics to assess individual bubble size change and correlate that with overall alteration of volume fraction of vapour. A thermodynamic model, for example Homogeneous Equilibrium Model (HEM) for cavitation [68, 69], does not require source term formulation even though their analysis is based on effectively mixture multiphase approach. There are few models that have been coupled with more than one multiphase approaches. As a result the multiphase approaches are briefly discussed at first.

Bubble dynamics is definitely the key to bubble-based cavitation models. Compre-

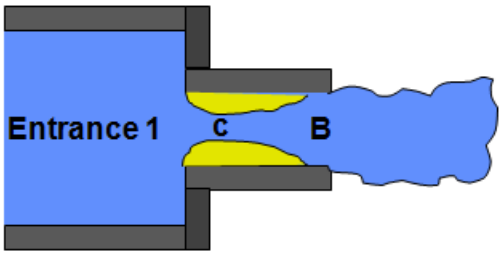

Figure 2.6: Flow in a sharp-edged nozzle.

hending state-of-the-art bubble dynamics equations is essential for understanding different perspectives of cavitation modelling. Additionally turbulence modelling is needed for analysing the constitutive equations for turbulent two-phase flow. Finally models for cavitation treatment are presented. For each of the cavitation treatment models, associated multiphase approach and turbulence models are mentioned as adopted in the literature. Energy equations are generally not accounted for cavitation modelling purposes barring few exceptions which require enthalpy estimation of the two-phase flow. Schmidt and Corradini [9] in their review article carried out an order of magnitude analysis to infer that it in not feasible for the bubbles to attain sizes where heat transfer effects would be considerable for growth. Som et al. [70] stated that temperature difference across the length of nozzle is small enough ($\approx$ 10 K) to ignore effect of temperature variations. This section is organized as: One-dimensional Analysis; Multi-dimensional Multiphase Analysis; Bubble Dynamics; Turbulence Models; Treatment of Cavitation.

2.2.1 One-dimensional Analysis

In 1976 Nurick [25] carried out experimental and theoretical analyses of cavitating flow in sharp-edged orifices or nozzles. His main contribution is his one-dimensional theoretical model for predicting discharge coefficient. His theoretical analysis is still germane to cavitation study to the present day with advanced numerical models, powerful computational resources and sophisticated experimental techniques. His theoretical model has been revisited in the literature for its pertinence [9, 47] to cavitation studies. Figure 2.6 presents the typical flow pattern in a sharp-edged nozzle. The entrance region has been denoted as 1, "c" is the core of the flow at the location of the minimum cross-section in the flow separation region, while B is the exit location after the flow is reattached.

According to Nurick [25] P_c tends towards the saturation pressure P_{sat} of the concerned fluid with increment in the flow rate and remains the same until "hydarulic flip" occurs.

Thus under cavitating conditions he got,

$$\left(\frac{P_1 - P_{\text{sat}}}{P_1 - P_B}\right)_{crit} = \left(\frac{C_D}{C_c}\right)^2 \tag{2.1}$$

The left hand side of the equation is effectively cavitation parameter K. The resultant expression thus becomes $C_D = C_c\sqrt{K}$. In the experiment the pressure values and the flow rates were measured. As a result Eq. 2.1 can be used for comparison with experimental values of C_D for cavitating conditions. Weisbach [71, 72] measured variation of C_c which is expressed by the following correlation.

$$C_c = 0.63 + 0.37\left(\frac{A_B}{A_1}\right)^3 \tag{2.2}$$

The contribution of the second part becomes negligible as soon as $\frac{A_B}{A_1}$ starts going down. In the actual data of Weisbach [71] as $\frac{A_B}{A_1} \rightarrow 0$, $C_c \rightarrow 0.61$ which is known as a limiting value of sharp-edged nozzle beyond which "hydraulic flip" is likely to occur. It turns out that under cavitating conditions the variation of C_D with K is linear with a slope of one-half [9]. For non-cavitating conditions naturally Eq. 2.1 is not applicable. According to Schmidt and Corradini [9] C_D remains constant at 0.84 based on the assumption that flow past the contraction zone expands to fill the nozzle. Schmidt and Corradini [9] assembled data from different experimental studies and plotted them along with Nurick's theoretical predictions. In the this thesis results from few more studies have been included along with the ones presented by Schmidt and Corradini in Fig.2.7. Most of the data are consistent with the theoretical one-dimensional model especially under cavitating conditions. The general trend is increase in C_D with increase in K under cavitating conditions and then a gentle decrease in C_D under non-cavitating conditions with further increase in K. Gelalles' [43], Bergwerk's [23] and Soteriou's [16] data follow the theoretical curve relatively well. The straight nozzle used by Winklhofer et al. had been denoted as "J" nozzle [31]. "J" nozzle had rectangular cross-section and rounded inlet. Despite the fact that Winklhofer's "J" nozzle is not a sharp-edged circular one, the data from their study confirms to the theoretical curve quite well. Nurick et al. [25] in his study did point out that C_c of both circular and rectangular nozzles can tend towards 0.61 when subjected to high pressure differences. The experimental data which are not following the theory well are by Chaves et al. [26], Hiroyasu et al. [14], Reitz [44], Payri et al. [48, 49]. Back pressure in Chaves' study was atmospheric. Hence K values were always much closer to 1 and not 2. However the qualitative trend was similar to other studies. Similar argument could be applied for Payri et al. [49], denoted as "Payri" in Fig. 2.7. Data of Hiroyasu et al. [14] laid completely below Nurick's curve. Another set of data from Payri et al. [48] denoted as "Payri 2", also did

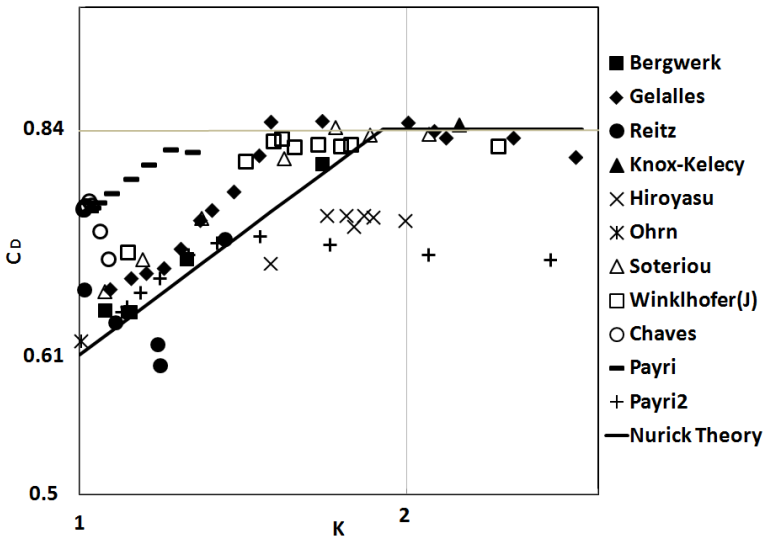

Figure 2.7: Comparison of Nurick's theory [25] with experimental studies [14, 16, 23, 26, 31, 43–46, 48, 49] : first seven are from Schmidt et al. [9] review and last four sets of experiments are included by the author.

not entirely match the theoretical prediction. The predictions worked well for cavitating conditions, but deviated a lot for non-cavitating conditions. Factors such as scale and geometry of the nozzle can be determining factors behind such deviations. Reitz's [44] study was not done in optically accessible nozzle, but based on Nurick's observations [25] it can be inferred that "hydraulic flip" was the reason behind sudden dip in C_D values. Success of Nurick's theory especially under cavitating conditions inspired Schmidt and Corradini [9, 73] to derive exit velocity following the footsteps of Nurick [25].

Increase in C_D with increase in K means decrease in C_D with increment in pressure difference. This behaviour can be explained with more clarity in conjunction with choked flow under supercavitating conditions. Choked flow implies approximately constant mass flow rate irrespective of change in pressure difference. Under these conditions numerator of C_D is going to remain constant while denominator will keep increasing leading to consistent drop in C_D.

2.2.2 Multi-dimensional Multiphase Analysis

One-dimensional analysis, though does a decent job in predicting discharge coefficient for various experiments, it can never unravel the details of internal two-phase flow. Moreover modelling primary breakup for spray and atomization requires the boundary condition at the hole or nozzle exit. Extensive multi-dimensional numerical models is a viable way to fulfil that need. Experimental characterization of real scale fuel injector with complex needle movement is and always will be challenging to execute. A properly validated CFD model is a powerful and economic design optimization tool. However numerical study of cavitating flows even in a simple geometry has always been extremely challenging as there is $10^4 - 10^5$ orders of magnitude difference between the densities of the two phases. Despite the adversities involved in numerically simulating such a phenomenon several models have been proposed over the last three decades to address the problem of cavitation in a fuel injector. Attempt has been made to provide a complete depiction of the present state of the cavitation modelling.

Single-Fluid Models

The governing equations for both mixture and VOF models are similar. Mixture multiphase models when coupled with cavitation models are considered as "single-fluid" models. However as specified before both Mixture and VOF are placed under the type of "single-fluid" because of similarity in the associated partial differential equations (PDEs).

The mixture multiphase models consist of one set of governing equations taking into account both the phases simultaneously and mostly consider zero relative velocity between the two phases. These models generally have one vapour fraction conservation equation which takes into account the phase change processes. Consequently, single-fluid models are computationally efficient but less accurate because of the inherent simplifications adopted in these approaches.

The VOF method is a numerical technique that helps to simulate the interaction between two immiscible fluids by tracking the interface in each computational cell spread over the domain. This method involves solving an auxiliary equation of volume fraction, apart from the Navier-Stokes equations and turbulence model equations (if applicable). Sum of volume fractions of the two phases must equate to unity and hence continuity gets satisfied automatically [67]. VOF method has been adopted in the literature for solving cavitation problems by some of the researchers. The underlying approximation of implementing VOF is that the cavitation region can be represented by large scale interface contrary to

the idea of two-phase regions of vapour cavities and dispersed bubbles as perceived in experiments [9, 29, 57].

Two-Fluid Models

The "two-fluid" models adopted in the literature are the Eulerian-Eulerian approach and Eulerian-Lagrangian approach. In the Eulerian-Eulerian approach the two phases are treated separately which means that there are two sets of conservation equations with mass and momentum exchange coefficients to account for the interactions between the two phases. This approach is commonly referred to as "two-fluid" model in the cavitation modelling literature. Therefore, mass and momentum conservation equations are solved for both liquid and vapour phases. The pressure p is shared by both phases.

Eulerian-Lagrangian multiphase approach is desired generally when one of the two phases has low volumetric concentration, or in other words dilute or dispersed in nature. The phase which serves as continuum is regarded as "primary phase" and the other phase is denoted as "discrete phase". For the cavitation modelling liquid is used as "primary phase" and vapour as "discrete phase" manifested in the form of vapour cavities and bubbles.

2.2.3 Bubble Dynamics

The growth and collapse of a bubble without the influence of thermal effects is known to be in the "inertia controlled" regime. Different governing equations have been derived by various researchers based on distinct sets of assumptions. The most commonly adopted one is by Rayleigh [74] and Plesset [75]. Two other equations were suggested, one by Gilmore [76] and other by Herring [77] and Trilling [78].

Rayleigh-Plesset Equation

Rayleigh-Plesset is the most commonly adopted equation for bubble dynamics and cavitation studies. This equation has been either used as it is or modified while executing cavitation modelling. The assumptions behind the Rayleigh-Plesset equation will be stated followed by the bubble dynamics equation derived by them.

Assumptions:

1. No relative velocity between bubble and liquid phase.

2. Liquid is incompressible.

3. Uniform bubble temperature, T_B, and uniform bubble pressure, P_B.

4. Uniform liquid viscosity.

5. Uniform ambient temperature T_∞ and uniform ambient pressure P_∞ .

The second order ordinary differential equation that is used as governing equation for bubble dynamics is given below,

$$\frac{P_B\left(t\right) - P_\infty(t)}{\rho_L} = R\frac{d^2R}{dt^2} + \frac{3}{2}\left(\frac{dR}{dt}\right)^2 + \frac{4\vartheta_L}{R}\frac{dR}{dt} + \frac{2\sigma}{\rho_L R} \tag{2.3}$$

Where P_B(t) is bubble pressure and P_∞(t) is ambient pressure at time instant "t". R is the instantaneous bubble radius. ρ_L and υ_L are liquid density and kinematic viscosity respectively. σ is the surface tension of the gaseous phase with the liquid phase. The solution of Eq. 2.3 gives the instantaneous growth rate and the instantaneous bubble radius at each time instant provided the initial radius at time t = 0 is known and the growth rate $\frac{dR}{dt}$ = 0 at time t = 0. The above equation without the viscous and surface tension effects was first developed by Rayleigh in 1917 [74]. Later in 1949 Plesset [75] included the terms that were missing in the equation and since then the equation is venerated as the Rayleigh-Plesset bubble dynamics equation.

A simplified form of Rayleigh-Plesset equation,

$$\dot{R} = \sqrt{\frac{2}{3}\frac{|p_{\text{sat}} - p^*_\infty|}{\rho_L}}$$

has been widely adopted in cavitation modelling studies specially when mixture, VOF or Eulerian-Eulerian multiphase approaches are used. Details of this simplified form, known as "Linear Rayleigh Equation" are elaborated in the Chapters "Model Details" and "Model Validation".

Gilmore Equation

In 1952 Gilmore used Kirkwood-Bethe hypothesis [79] for deriving his bubble dynamics equation. According to Kirkwood-Bethe hypothesis it is assumed that when the liquid

phase velocity is a considerable fraction of the sonic velocity then a spherical wave propagates within the liquid at a speed of (u + c) where u is the velocity of the liquid and c is the velocity of the sound in the liquid. The Gilmore equation is given below,

$$R\frac{d^2R}{dt^2}\left(1-\frac{dR/dt}{c}\right)+\frac{3(dR/dt)^2}{2}\left(1-\frac{dR/dt}{3c}\right)=H\left(1+\frac{dR/dt}{c}\right)+\frac{R}{c}\left(1-\frac{dR/dt}{c}\right)\frac{dH}{dt} \quad (2.4)$$

The Gilmore equation thus does not consider the effect of liquid viscosity and surface tension. Here c stands for speed of sound in liquid and H stands for the liquid enthalpy.

Herring and Trilling Equation

The equation was derived originally from generalized Bernoulli equation. A relation between enthalpy and pressure was employed in this derivation. It was assumed that speed of sound is constant, equal to "c_o". The equation is given below.

$$R\frac{d^2R}{dt^2}\left(1-\frac{2(dR/dt)}{c_o}\right)+\frac{3(dR/dt)^2}{2}\left(1-\frac{4(dR/dt)}{3c_o}\right)=\frac{R}{\rho_o c_o}\frac{dP}{dt}+\frac{P-p_o}{\rho_o} \quad (2.5)$$

P is the pressure at a particular time instant t. p_o and ρ_o are the reference pressure and density respectively. Similar to Gilmore equation Herring and Trilling equation does not consider the viscous and surface tension effects in bubble collapse but do consider liquid compressibility.

Among these bubble dynamics equations Rayleigh-Plesset equation is less complex and hence it is relatively convenient to incorporate in cavitation modelling compared to the Gilmore or Herring and Trilling equations. Moreover Rayleigh-Plesset considers effects of surface tension and viscosity unlike other two equations. As a result except few studies a simplified form of Rayleigh-Plesset equation is used in cavitation modelling.

2.2.4 Turbulence Models

Turbulence models that have been employed for cavitation modelling in the literature can be broadly classified to two types, Reynolds Averaged Navier-Stokes (RANS) and Large Eddy Simulation (LES). The two approaches differ based on the treatment of Navier-Stokes equations. RANS resort to ensemble or time averaging of the flow variables such as velocity, pressure etc. and then decomposing Navier-Stokes equations into mean and fluctuating components. RANS equations provides estimate of the mean flow which is vital for practical engineering applications.

LES has been less frequently used for cavitation modelling compared to RANS models. LES is not based on time averaging unlike RANS. Cavitating flow is transient in nature and RANS model results are going to blur out the fluctuations, which can be prevented by adopting LES. Motivation behind LES is that momentum, mass, energy, and other scalars are influenced mostly by large eddies [67]. LES relies on the concept that large scale eddies are geometry dependant while small scale eddies are universal in nature as inferred by Kolmogorov in 1941 [80, 81]. LES involves a filtering approach based on spatial averaging, where larger flow structures are simulated directly and the smaller ones are modelled. The modelling of small scale unresolved eddies is known as "subgrid-scale modelling". Therefore, LES decomposes Navier-Stokes equations by dividing the flow variables into two parts: resolved and subgrid-scale (SGS).

2.2.5 Treatment of Cavitation

Treatment of cavitation is the key component of numerical analysis of cavitation in diesel injectors. Majority of the models will be reviewed here and their distinct features will be highlighted. Some of the cavitation models have been coupled with more than one multiphase approaches. While some cavitation models have been tested with different turbulence models. As a result relevant information about associated multiphase approaches and turbulence models will be provided while discussing the different cavitation models. Majority of the models have been coupled with single-fluid or precisely mixture multiphase approach. These models require an additional equation apart from the Navier-Stokes equation for closure of the equations as density is an additional variable. Flow does not have to be compressible to make density variable as density is a function of void fraction in mixture approach. The additional equation turns out to be thermodynamics based relation between void fraction and flow variables or equation of state of the mixture or a volume fraction conservation equation with a source term based on bubble dynamics.

Barotropic Model

Different versions of barotropic models have been adopted in the literature. Barotropic flow means that change in fluid density is solely dependant on pressure variation i.e. $\rho = \rho(p)$. This means in case of two-phase bubbly flow for an infinitesimal change in pressure the bubbles will undergo an instantaneous change in volume. As pointed out by Brennen [4] this criterion is not necessarily fulfilled all the time as that would require the typical frequencies in the flow affecting the bubbles to be always less than the natural frequency of the bubbles.

The first barotropic model was introduced by Delannoy and Kueny [82]. They solved one set of mass balance and Euler equations (i.e. Navier-Stokes without viscous diffusion terms). They carried out two-dimensional simulations for water flow in a venturi tube. They resorted to single-fluid (mixture) approach assuming that the homogeneous equilibrium assumption is valid for the cavitating flow. The underlying assumption of homogeneous equilibrium model (HEM) is that all the phases are in thermodynamic equilibrium at all times [4]. They considered three possible regimes: liquid, vapour and intermediate medium comprising of liquid and vapour. In the intermediate region the density was varied with pressure following a sine law, thus providing an equation of state for the two-phase mixture. According to Delannoy and Kueny compressibility is only a concern at the moment of bubble collapse and therefore, the places where liquid and vapour phases are away from the interface could be safely considered incompressible flow [82]. Their model was further extended to include viscous and turbulence modelling effects by Coutier-Delgosha et al. [83] . Similar two-dimensional simulations were also carried out by Avva et al. [84] for cavitation analysis using enthalpy formulation and based on thermal equilibrium assumption. They could not simulate high speed flows due to stability issues caused by order of magnitude difference in density of the two phases, in spite of achieving good agreement with Nurick's correlation.

The most widely adopted barotropic model for cavitation analysis was by Schmidt et al. [68, 69, 85]. They modelled the cavitating flow as two-phase compressible flow using a sound speed estimated based on the homogeneous equilibrium model (HEM) proposed by Wallis [86]. The criteria of HEM are average values of velocity, temperature to be almost same as the values for each phase. The main governing equations for their HEM cavitation analysis are mass conservation, momentum conservation along two axes and algebraic equation of state for closure of hydrodynamic equations. The algebraic equation originates from a differential equation relating pressure to density ($\frac{D\rho}{Dt} = \frac{1}{a^2}\frac{Dp}{Dt}$) for isothermal or isentropic conditions. Their model was applicable for both cartesian and polar co-ordinates and is basically a single-fluid or precisely a mixture approach with no separate governing

equation for phase volume fraction conservation. Pressure to density mapping yielded the composition of the cavitating flow. The sonic speed (a) of flow was estimated using formula provided by Wallis [86] consisting of densities of and sonic speeds in individual phases as well as void fraction values as follows

$$a = \frac{1}{\sqrt{(\alpha \cdot \rho_v + (1-\alpha)\rho_l) \cdot \left(\frac{\alpha}{\rho_v \cdot a_v^2} + \frac{1-\alpha}{\rho_l \cdot a_l^2}\right)}} \tag{2.6}$$

where α is void or vapour volume fraction and a is the sonic speed in the mixture, while subscripts v and l stand for vapour and liquid phases respectively. Schmidt et al. [9, 69] also stressed on the fact that liquid Mach number itself can go beyond 0.4 and hence the overall flow will be definitely compressible. It is well known that even if individual phases are incompressible, sonic speed of a two-phase flow is very low resulting in an overall compressible flow [4]. Schmidt et al. [68] partially validated their model by comparing the model predictions of collapse rate of bubble with experimental findings of Ohl et al. [87]. The main drawback for their work was that turbulence was not taken into account. Additionally allowance of gradual density changes in cases of gradual pressure changes impair the applicability of their model for low speed large scale cavitating flows characterised by gradual variation in pressure yet steep density gradients.

Schmidt's barotropic HEM has been adopted by other researchers. HEM was extended to three dimensional analysis by Dumont and his research group [88, 89]. A cavitation model, very similar to the one by Schmidt et al. has been implemented in OpenFOAM® [90] and has been utilized for cavitation analysis by Salvador et al. [91,92]. In the OpenFOAM® model used by Salvador et al. mixture compressibility is a linear function of vapour and liquid compressibilities, unlike the original model of Schmidt et al.

$$\Psi = \alpha\Psi_v + (1-\alpha)\Psi_l$$

The compressibility was represented as inverse of square of the sonic speed($\Psi = \frac{1}{a^2}$). Interestingly both Schmidt et al. and Salvador et al. ignored turbulence stating that length scales being quite small cavitation effects will supersede impacts of turbulence. Reitz and his research group implemented HEM in KIVA-3V [93] coupled with spray and atomization models [94,95]. They included turbulence with HEM and showed that inclusion of turbulence modelling yields C_D predictions closer to measured values compared to the HEM predictions ignoring turbulence.

Homogeneous Relaxation Model

Apart from barotropic models another cavitation model based on thermodynamic principles is the Homogeneous Relaxation Model (HRM). HRM, based on the homogeneous mixture multiphase approach, was originally implemented as a flash boiling model by Schmidt's group [96, 97] in OpenFOAM [90]. It uses the difference between the instantaneous and the equilibrium composition of the flow at each location along with an empirical time-scale correlation to estimate the time required to reach equilibrium between the two phases. A smaller value of the time-scale in comparison to the flow time-scale through the nozzle represents a case that is close to thermal equilibrium. The HRM for flash boiling was extended to simulate cavitation also by Schmidt's group using a mixture multiphase approach [98]. Since the thermal non-equilibrium effects are much more significant in flash boiling flows compared to cavitating flows, it is expected that the model would need smaller time scales in cavitation simulations [98]. This is because phase change phenomena is expected to occur very fast in case of cavitation accompanied with instantaneous heat transfer [4]. In Schmidt's HRM, the mass conservation and momentum equations are combined to derive a pressure equation consisting of material derivative of quality as the source term.

The estimation of the source term is achieved through HRM [99],

$$\frac{Dx}{Dt} = \frac{x - \bar{x}}{\Theta} \tag{2.7}$$

Exponential relaxation of the quality, x to the equilibrium value $\bar{x}$, over a timescale $\Theta = \Theta_0 \alpha^a \psi^b$. Equilibrium quality,

$$\bar{x} = \frac{h - h_l}{h_v - h_l}$$

Quality,$x = \frac{\alpha \rho_v}{\rho}$ and void fraction ($\equiv$ vapour volume fraction) $\alpha = \frac{\rho_l - \rho}{\rho_l - \rho_v}$. Therefore, there are 4 unknowns: ρ, U, p, x and 4 equations: mass balance, momentum balance, pressure, and HRM equations.

The parameters for diesel cavitation cases and gasoline flash boiling ($P_{\text{in}} > 1$ MPa), $\Theta_0 = 3.84 \times 10^{-7}\,[s]$, $a = -0.54$, $b = -1.76$ and $\psi = \left|\frac{p_{sat} - p}{p_{crit} - p_{sat}}\right|$ while for gasoline flash boiling ($P_{\text{in}} \leq 1$ MPa) the parameters are, $\Theta_0 = 6.51 \times 10^{-4}\,[s]$, $a = -0.257$, $b = -2.24$ and $\psi = \left|\frac{p_{sat} - p}{p_{sat}}\right|$

Recently HRM has also been implemented with a VOF approach by CONVERGE [100] and researchers at Argonne National Laboratory [101]. In their model liquid and vapour are treated as two different species. The governing equations were mass, momentum and

species conservation equations to evaluate the flow field variables as well as the composition. The source term in the species conservation equation is estimated by HRM. To avoid numerical diffusion, artificial sharpening of interface, high-resolution interface capturing (HRIC) scheme has been used in their study. Both HRM models in OpenFOAM and CONVERGE have been validated with data from Winklhofer et al. [31].

Bubble Pressure Difference

Bulk of the existing cavitation models are based on bubble pressure difference. The underlying assumption of sole dependence of rate of bubble radius change on pressure difference across bubble surface, governs the evolution of two-phase flow composition. The approach can be criticized to be overly simplified as it misses out on the effects of surface tension and other parameters such as liquid viscosity and non-condensable gases. Models based on Linear Rayleigh equation belong to a special type of bubble pressure difference based cavitation models. Despite the simplification, cavitation models based on bubble pressure difference, specifically Linear Rayleigh Equation have achieved considerable success in cavitation modelling. There are substantial differences amongst the models based on bubble pressure difference and those will be elaborated here.

- Kubota et al.: One of the earliest cavitation models was by Kubota et al. [102, 103]. Their model was applied to hydrofoils and not fuel injectors or nozzles. Their model is generally denoted as "bubble two-phase flow" or BTF. They assumed a compressible viscous fluid whose density varies considerably for cavitation analysis which effectively indicates adoption of a single-fluid mixture approach. They used a modified Rayleigh equation ignoring surface tension and viscous damping to relate the local void fraction with the macroscopic flow field. Bubble breakup and coalescence were not considered and a constant bubble number density was assumed. The effect of surrounding bubbles on the evolution of an individual bubble was considered, but they inferred that in the bubble dynamics equation effect of neighbouring bubbles fazes out with grid size, similar to the pattern that the Smagorinsky model [104] shows for LES studies. They did not explicitly adopted Linear Rayleigh Equation for their analysis. However their assumptions and weak numerical influence of surrounding bubbles on a single bubble's growth or decay lead to the scenario of Linear Rayleigh Approximation. Schmidt et al. in his review article indicated that this model would be reasonable for large scale, low Mach number flows, but most likely will not be desirable for small scale, high Mach number flows in diesel injectors.

- Heister and his co-authors: Heister and his research group [105–110] came up with cavitation models using mixture multiphase approach. They conceptualized a pseudo-density much as Kubota et al. and formulated differential equation to relate density variation with pressure difference across the bubble surface $(p - p_B)$ where p_B is the bubble pressure which they assumed to be equal to saturation pressure p_{sat}. Change of density is related to change of void fraction and hence change of bubble radius. Therefore, Linear Rayleigh gets implemented in their approach implicitly. They claimed that bubble dynamics based pressure density relations are better than 1 to 1 mapping of pressure and density in barotropic approaches. They argued that equation of state of a two-phase bubbly fluid is not meaningful as it misses out on temporal fluctuations due to bubble dynamics. They solved non-dimensional mass and momentum conservation along with their own density relations for closure of the governing equations. In one of their earlier works Chen and Heister [105] used a relation with void fraction and pressure difference $(p - p_v)$ which was

$$\alpha_{i+1}^{n} = \alpha_i^n + C(p - p_{\text{sat}}) \tag{2.8}$$

Here i is the grid point under consideration, n is the iteration number, p is the local pressure and C is an arbitrary constant with a very small value to ensure numerical stability as well as prevent violation of the physics of the flow. They also came up with two types of constitutive relations; one simple and one more complicated. The initial density relation with pressure proposed by Chen et al. [106] was

$$\frac{D\rho}{Dt} = C_0(p - p_{\text{sat}}) \tag{2.9}$$

where ρ is the dimensionless pseudo-density varying between zero and unity, C_0 is a very large arbitrary constant to secure the true nature of the bubbly flow as well as provide numerical stability. A large value of C_0 results in considerable variation in ρ with small change in $p - p_v$ which is the reality in case of cavitating flow. A more complex form was later proposed by Heister's research group [107–110].

$$\begin{aligned}\frac{D^2\rho}{Dt^2} = {} & \frac{6\alpha'(1+\alpha'+\alpha'^2)^2}{L_0^2(2+\alpha')(1-\alpha'^3)^{1/3}}(p - p_{\text{sat}}) \\ & + \left[\frac{11\alpha'^3 - \alpha'^2 - \alpha' - 1}{6\alpha'^3(1-\alpha'^3)} - \frac{1 + 4\alpha' + \alpha'^2}{6\alpha'^2(2+\alpha')(1+\alpha'+\alpha'^2)}\right]\left(\frac{D\rho}{Dt}\right)^2\end{aligned} \tag{2.10}$$

where $\alpha' = \sqrt[3]{1-\rho}$, $L_0 = \left(\frac{3}{4\pi n_o}\right)^{\frac{1}{3}}$, $n_o = \hat{n}_0\hat{D}^3$, $\hat{n}_0$ is the bubble number density and $\hat{D}$ is the characteristic length of the flow passage. They improvized by introducing

the concept of fixed number of bubble nuclei per unit mass of mixture, instead of constant bubble number density which has been used by Kubota et al. [103]. The bubble number density (number of bubbles per unit volume of the mixture) decrease with increase of void fraction as the bubble size should increase with increment in void fraction. The results of Heister and his group, and Kubota et al. converge for low void fraction but differ for high void fraction considerably because of this fundamental difference. Heister and his co-authors ignored turbulence because of promising results from their unsteady laminar cavitation analysis and lack of appropriate turbulence model for two phase flow. They carried out validation for only large nozzles ($D \approx 1$ mm, approximately 10 times larger) [109] and thus their models have not been proven to be reliable for real scale nozzles.

- Alajbegovic and his co-authors Alajbegovic and his co-authors adopted the Eulerian-Eulerian approach (commonly referred as two-fluid model in the literature) for cavitation analysis with mass transfer terms, estimated based on Linear Rayleigh equations. Mass, momentum conservation and turbulence equations were solved for each phase. In their earlier work [111] they assumed constant bubble number density, but later they modified their model [112–116] by using a heuristic methodology of varying the bubble number density with vapour volume fraction. The mass transfer terms for liquid to vapour and vice versa used by them are

$$\dot{m}_{lv} = \rho_l N''' 4\pi R^2 \frac{\partial R}{\partial t} = -\dot{m}_{vl} \tag{2.11}$$

  The average bubble radius is supposed to be changing and therefore, the bubble number density should change as well. Consequently their heuristic correlation is relevant to cavitation modelling.

- Battistoni et al.: Battistoni and his research group [117, 118] adopted an approach implemented in AVL Fire® [119]. Their cavitation model was very similar to that of Alajbegovic as they adopted the Eulerian-Eulerian multiphase approach. They made progress in treatment of bubble density as they adopted two different approaches for treatment of bubble number density, a) mono-disperse - all the bubbles are of same size and b) poly-disperse - bubbles are of various sizes. Estimating $\dot{R}$ is always vital. Both linear ($= \sqrt{\frac{2}{3}\frac{|\Delta p|}{\rho_l}}$) and non-linear ($= \sqrt{\frac{2}{3}|\frac{\Delta p}{\rho_l} - R\ddot{R}|}$) estimates of $\dot{R}$ were attempted. In the mono-disperse cases the variation of bubble density was achieved by the correlation of Alajbegovic [115]. The initial N_0''' was set to 10^{12} m^{-3}. The

mass exchange coefficients used for their cavitation modelling are provided here

$$R_P = \frac{1}{C_R} 3.95 \frac{\rho_v}{\sqrt{\rho_l}} sign(\Delta p)(N''')^{1/3}(\alpha_2)^{2/3}\sqrt{|\Delta p|} \quad linear \tag{2.12}$$

$$R_P = \frac{N'''}{C_R}\rho_v 4\pi R^2 sign(\Delta p)\sqrt{\frac{2}{3}|\frac{\Delta p}{\rho_l} - R\ddot{R}|} \quad non-linear \tag{2.13}$$

where $\Delta p = p_{\text{sat}} - p + C_E\frac{2}{3}\rho_l k_l$. The Egler coefficient (C_E) [120] is taken as 1.2 and the term with C_E helps to account for turbulent fluctuations. The tuning parameter C_R is 1 for cavitation and 5 for condensation [118]. Battistoni et al. indicated that considering value of the tuning parameter greater than unity for condensation ensures existence of subcooled vapour in fast transients and serves the purpose especially when modelling studies of vapour condensation or vapour bubble collapse are insufficient to facilitate cavitation simulations. The positive aspect of the values, is that they are of the order of unity which is not the case for tuning parameters in many other models in the literature. For the poly-disperse approach a probability distribution function for bubble radius was used. They solved two additional equations for bubble population with the bubble number density (N''') and the interfacial area density (A''') in order to take into account bubble breakup and coalescence for the poly-disperse approach. They inferred that using mono-disperse approach is better, as it reduces computational cost without noticeable compromise in accuracy. However they also pointed out that adopting poly-disperse approach would be suitable from the perspective of bubble collapse especially for cases of cavitation erosion caused by small bubbles. They utilized a recently developed (2004) $k-\zeta-f$ turbulence model [121] for closure of the modelling equations.

- Kunz et al.: Kunz et al. [122–124] proposed a unique approach for cavitation treatment. They adopted a radically different set of governing equations based on pseudo-compressibility or artificial compressibility method, originally envisaged by Chorin [125]. They had a volume conservation equation instead of mass conservation and had source terms $\dot{m}^-$ and $\dot{m}^+$ representing vapour and liquid formations respectively. Existence of non-condensable gases was considered. This unique approach achieves diagonal dominance, resulting in fast convergence. Turbulence modelling was considered by adopting high Reynolds number $k-\epsilon$ model. Individual phases were treated as incompressible. In case of cavitation treatment the vaporization and condensation

model equations were,

$$\dot{m}^- = \frac{C_{\text{dest}}\rho_v\alpha_l min[0, p - p_{\text{sat}}]}{(1/2\rho_l U_\infty^2)t_\infty} \tag{2.14}$$

$$\dot{m}^+ = \frac{C_{\text{prod}}\rho_v(\alpha_l - \alpha_g)^2(1 - \alpha_l - \alpha_g)}{t_\infty} \tag{2.15}$$

where $0.2 \leq C_{\text{dest}} = C_{\text{prod}} \leq 10^5$ and $t_\infty = d/U_\infty$ is the mean flow time scale. The vaporization model is again dependent on only bubble pressure difference $p - p_{\text{sat}}$ and not on surface tension, viscosity or non-condensable gas pressure inside the bubbles. The condensation model was however established on the simplified form of Ginzburg-Landau potential [122, 126]. However we have been unable to trace the procedure from the works of Hohenberg and Halperin [126] to the simplified version proposed by Kunz et al. [122]. The main drawback of their model is the wide variation of the tuning parameters depending on type of applications. The two positive features of their work are consideration of turbulence and including existence of non-condensable gases.

- Singhal et al. and Som et al. The Singhal approach is based on Equal Velocity Equal Temperature (EVET) and is referred in the literature as "Full Cavitation Model". They considered presence of non-condensable gases. Singhal et al. arrived at the following equation by combining liquid, vapour and overall mass conservation equations,

$$\frac{\partial(\rho_v\alpha)}{\partial t} + \frac{\partial(u_j\rho_v\alpha)}{\partial x_j} = \dot{m}_v = \frac{\rho_v\rho_l}{\rho}\frac{D\alpha}{Dt} \tag{2.16}$$

The derivation of the source term on right hand side of Eq.2.16 is elaborated in Appendix B.

From the source term they arrived at phase change rate equations for vapour formation and liquid formation with respective tuning parameters. Singhal et al. [127] used standard $k - \varepsilon$ model for his analysis. They used constant density for both liquid and vapour phases and he validated his model with Nurick's correlation [25]. Their model has been the most commonly adopted model in the past decade because their approach is computationally less expensive and have provided reasonable predictions from engineering perspective. Nonetheless there were quite a few concerns about the model development as some of the assumptions and approximations adopted were quite *adhoc* and will be discussed in Chapter "Model Details".

Som et al. implemented Singhal et al. model [70,128] and used realizable $k-\varepsilon$ model for modelling turbulence. They proposed a modified criterion for cavitation inception

based on the works by D.D. Joseph [129, 130], Winer and Bair [131] including the effect of viscous stresses. Som et al. [70] successfully validated their model with experimental results of Winklhofer et al. [31].

- Schnerr et al.; Margot et al.: Schnerr and Sauer did not consider non-condensable gases. Hence α denotes α_v only in Schnerr and Sauer model. Schnerr and Sauer [132] expressed α as

$$\alpha = \frac{\frac{4}{3}\pi R^3 N'''}{1+\frac{4}{3}\pi R^3 N'''}$$

The the time derivative of α was combined with the vapour and liquid mass conservation equations. Their cavitation model originates from the same Eq.2.16 as in the case of Singhal et al. [127] and more discussion is provided in Chapter "Model Details".

Another cavitation model based on "Linear Rayleigh Equation" was implemented by Sauer and Schnerr [133], and Schnerr and Sauer [132], using VOF approach. Yuan, Schnerr and Sauer [134, 135] adopted $k-\omega$ model to conclude inclusion of RANS turbulence models lead to time-invariant steady state solution. Yuan and Schnerr [136] considered non-condensable gases, vapour and liquid in their model and expressed vapour volume fraction as $\alpha_v = \alpha_l N''' \frac{4}{3}\pi R^3$. They adopted the CICSAM (compressive interface capturing scheme for arbitrary meshes) method for interface capturing, which is known to work well for problems with high viscosity ratio between the two phases [67].

Another cavitation model, that is similar to Schnerr's models, is the one implemented in Star CD ® [137] and adopted by Margot et al. [138–141]. Their source term of volume fraction equation ($Sa_v\rho \equiv R_P$) was

$$Sa_v = \frac{4\pi R^2 N'''}{1+\frac{4}{3}\pi R^3 N'''} sign(p_{\text{sat}} - p)\sqrt{\frac{2|p_{\text{sat}} - p|}{3\rho_l}} \tag{2.17}$$

They assessed their model predictions by comparing with the data of J type nozzle by Winklhofer et al. [31] and carried out CFD simulations of cavitation in fuel injector with moving needle.

- Zwart-Gerber-Belamri: Zwart, Gerber and Belamri [142] made the assumption of a constant bubble size to calculate the total interphase mass transfer rate per unit volume, R_P. They did not consider existence of non-condensable gases and their model was also based on "Linear Rayleigh Equation". This model is also discussed in details in Chapter "Model Details".

Discrete Bubble Model

Discrete Bubble Model (DBM) is the most detailed cavitation model among all the variations of cavitation treatments. This is typically coupled with Eulerian-Lagrangian multiphase approach, where liquid is the continuous phase and cluster of bubbles is the dispersed or discrete phase as elaborated before in the "two-fluid" subsection.

Giannadakis et al. [57] attempted to cover almost all possible features of bubble evolutions and interactions in a cavitating flow in diesel injector nozzle. A bubble population balance equation was additionally solved to consider bubble breakup, coalescence and nucleation. At each time step the instantaneous bubble sizes are assembled to estimate the vapour volume fraction at different locations of the flow field. Eventually estimate of liquid volume fraction was obtained and plugged back to the governing equations for obtaining the solution at that time step. The relevant information associated with different aspects of their model are briefly covered here.

They stressed on the fact that in DBM they were capturing the non-linear inertial effects which were not covered by models adopting simplified Linear Rayleigh Approach. The detailed bubble dynamics equation is solved including the effects of non-condensable gases, surface tension, viscosity and sometimes also adjacent bubbles.

$$\frac{p_{\text{sat}} - p_\infty(t)}{\rho_L} + \frac{p_{G0}}{\rho_L}\left(\frac{R_0}{R}\right)^{3k} = R\ddot{R} + \frac{3}{2}\left(\dot{R}\right)^2 + \frac{4\vartheta_L}{R}\frac{dR}{dt} + \frac{2\sigma}{\rho_L R} + 2\pi\Delta r^2(\dot{n}^*_{\text{bub}}\dot{R}R^2 + \dot{n}^*_{\text{bub}}\ddot{R}R^2 + 2\dot{n}^*_{\text{bub}}R\dot{R}^2) \tag{2.18}$$

where p_∞ denotes the far-field pressure in the liquid, p_{G0} is the partial pressure of non-condensable gases, Δr is the assumed radius of the spherical cluster of bubble interaction and $\dot{n}^*_{\text{bub}}$ is the number of bubbles in the parcel divided by the corresponding host cell volume. The exponent k is the index for process type; $k = 1$ is for isothermal process and $k = \frac{C_p}{C_v}$ is for adiabatic process. The initial partial pressure p_G is estimated assuming mechanical equilibrium, $p_{G0} = p_{\infty,t=0} - p_{\text{sat}} + \frac{2\sigma_L}{R_0}$. To consider the effect of turbulent fluctuations and relative velocity between bubble and surrounding liquid an effective far-field pressure was estimated, $p_{\infty,effective}(t) = p_{\infty,aver}(t) - C_E\frac{2}{3}\rho_L k_L - \frac{1}{4}\rho_L|\mathbf{u}_L - \mathbf{u}_B|^2$, with $C_E = 1.2$ as the Egler coefficient and k_L as the liquid phase turbulent kinetic energy. The initial bubble radii ranged from 0.01 to 2 μm. The bubble dynamics equation was numerically integrated using the explicit fifth-order Runge-Kutta-Fehlberg nethod.

Dynaflow [143], a CFD consultancy company, developed user-defined codes to couple with Population Balance Module of ANSYS Fluent [67] in order to implement their own DBM [144–146]. They have utilized modified versions of Rayleigh-Plesset equation, Herring

and Trilling, and Gilmore equations. They added an extra term in the bubble dynamics equations to account for the relative velocity between the bubble and the surrounding liquid. They did not consider nucleation or coalescence in their studies. Their attempts were not directed towards fuel injectors but more towards marine applications. However their studies add to the overall understanding of the cavitation modelling.

2.3 Engine Combustion Network

In the last couple of years researchers from different universities and research laboratories are coming together for the advancement of scientific research in the field of spray and engine combustion, which is known as Engine Combustion Network (ECN). ECN is also working on cavitation experiments and modelling with complex needle movements. Mainly two types of nozzles have been tested, Spray A and Spray B. Spray A is non-cavitating. Spray B tends to mildly cavitate. The motivation is to standardize the numerical methodologies and input parameters for different models. The details of the progress of ECN can be obtained from Sandia National Laboratory website [147].

2.4 Summary

A large body of work exists in the literature regarding the cavitation phenomenon in fuel injector nozzles. From the experimental studies a lot has been learned but the confusion of the pattern of the two phase mixture still persists, current accepted notion is that in real scale injectors there is cavity or film of vapour and then a diffused mixture of bubbles and liquid. It has been concluded that the bubbles/cavities do not exactly scale with the geometry rather they have their own length scale depending on the flow field. It has been learned that converging nozzles are going to suppress the separation and hence the cavitation extension. Experimental works are also needed for providing a benchmark for the assessment of the cavitation models. Good quality qualitative and quantitative information are needed. It seems the work by Winklhofer et al. [31] satisfies the overall requirement, which is apparent from its utility for model validation in the literature such as Refs. [70, 98, 101].

Barring a few exceptions in most studies both phases have been assumed to be incompressible which is not correct as the Mach number of the liquid phase alone in real injectors can reach a value of around 0.4 [9]. The wall effects have been considered very recently [148]. Attempts have started to investigate the cavitation characteristics of biodiesel

Table 2.1: Summary of previous modelling works:(BPD - Bubble Pressure Difference; DBM - Discrete Bubble Model; NLR- Non-linear Rayleigh)

Multiphase Approach	**Turbulence**	**Compressible**	**Bubble Mechanism**
Eulerian-Lagrangian [57, 145]	Yes	No	DBM
VOF [149]	Yes	No	Linear Rayleigh
VOF [101]	Yes	No	N/A
Mixture [124]	Yes	No	BPD
Mixture [108]	No	No	BPD
Mixture [69]	No	Yes	N/A
Mixture [98]	Yes	No	N/A
Mixture [70, 127]	Yes	No	Linear Rayleigh
Mixture [132, 142]	Yes	Yes	Linear Rayleigh
Eulerian-Eulerian [115, 117]	Yes	No	Linear Rayleigh/NLR

fuel [117, 128]. Considering performance of numerical prediction, feasibility to implement and computational cost the work by Singhal et al. [127] appears to be one of the most commonly adopted cavitation models despite its limitations. The model by Singhal et al. [127] also happens to be one of the few cavitation models that have considered non-condensable gases. Under high pressure, liquid fuel is expected to have very small amount of dissolved gases. Therefore, in the present study a cavitation model is developed using the setup of Singhal et al. model and propose a modified approach to overcome some of the issues related to Singhal et al. model [127].

Most of the modelling study resort to Bubble Pressure Difference or in some cases precisely Linear Rayleigh Equation for bubble growth or shrink rate. A summary of all the previous studies is essential at this stage. Therefore, the most relevant previous studies have been presented in a concise form in Table 2.1.

Chapter 3

Model Formulation

This Chapter presents the details related to model assumptions, governing equations, closure equations of mass source term and turbulence models, followed by discussion on material properties, boundary and initial conditions, and solution procedure adopted in this study.

The physical problem of cavitation involves nucleation, growth, collapse, coalescence and break up of bubbles depending on the local pressure values as well as the interaction of the flow field with the large population of bubbles/cavities. Moreover the bubbles do not always remain perfectly spherical. Accurately modelling all these features for cavitation study is not only difficult but also computationally very expensive. As mentioned before only Giannadakis et al. [57] have been able to address all possible aspects of bubble behaviour but implementing this extensive model is very difficult for complex geometries of real injectors. Hence most of the works in the literature have been devoted to the development of two-fluid (Eulerian-Eulerian) or single-fluid (mixture or VOF) models, which is evident from the Literature Review.

In this study a cavitation model, coupled with mixture multiphase model, has been developed. The proposed model has been implemented in the framework of the cavitation model by Singhal et al. [127] with the help of sub-routines or user-defined functions (UDFs) in ANSYS Fluent software. Some of the limitations of Singhal et al. model have been overcome in the present cavitation model. The limitations will be discussed in this chapter. Additionally two other cavitation models, Schnerr-Sauer and Zwart-Gerber-Belamri models, available in ANSYS Fluent are assessed. Both mixture and Eulerian-Eulerian multiphase approaches have been used for the later two cavitation models. The present cavitation model, based on the framework of Singhal et al. model, could not be implemented with

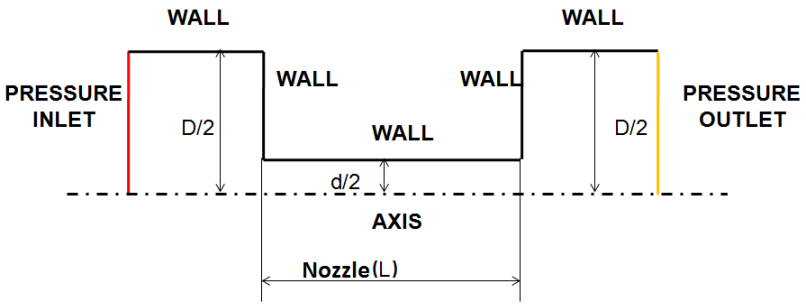

Figure 3.1: Computational Domain consisting of a section before the nozzle, the nozzle itself and a section after the nozzle. For rectangular cross section, d is the width of the nozzle and for circular cross section d is the diameter of the nozzle

the Eulerian-Eulerian approach as it is limited by the scope of the ANSYS Fluent platform which does not let Singhal et al. model to couple with Eulerian-Eulerian approach. The presence of non-condensable gases is important to be considered in cavitation models. In the ANSYS Fluent platform the option of including non-condensable gases is only available for the model by Singhal et al. [127]. As a result the model by Singhal et al. is used as framework for the cavitation model proposed in the present study.

The problem considered in this work is a cavitating two-phase flow in a nozzle. Three different computational domains have been used in this study.

1. For comparison of the models with the experimental study [31] a two-dimensional geometry has been used.
2. For comparison at high inlet pressure ($\geq$ 10 MPa) an axisymmetric nozzle geometry has been used.
3. For simulating cavitation with needle movements in a fuel injector a three-dimensional geometry has been used.

Figure 3.1 shows the schematic of a typical computational domain for two-dimensional and axisymmetric cases. The boundary condition at the nozzle exit cannot be estimated a priori always. As a result the boundary of the domain is often extended beyond the actual nozzle exit.

3.1 Assumptions

The following assumptions are adopted in this study of the cavitation in diesel injectors.

1. The two phase flow is isothermal.
2. When mixture multiphase approach is used, relative velocity between the two phases is assumed to be negligible with respect to the mean flow velocity.
3. The fluid consists of a mixture of liquid, vapour and a small proportion of non-condensable gases, such that
$$f_l + f_v = 1 \tag{3.1}$$
where f_v and f_l are the mass fractions of gaseous phase and liquid phase respectively. Existence of non-condensable gases is taken into account in the present model.
4. Both bubble growth (evaporation) and collapse (condensation) are considered. Phenomena such as, nucleation, collision and coalescence have not been included.
5. Linear Rayleigh equation stating, that the bubble size change is only dependent on the pressure difference across the bubble surface, is used to derive the phase change rate expressions [4].

The governing equations of mixture multiphase approach is provided here. The pertinent details about Eulerian-Eulerian multiphase approach are given in Appendix A.

3.2 Governing Equations

The governing equations for mixture approach, involves solving the standard Reynolds averaged Navier-Stokes equations and using any standard turbulence model, if required. For Singhal et al. model and the present cavitation model the fluid density is expressed as a function of gaseous mass fraction f_v, which is calculated by solving an additional transport equation coupled with the mass and momentum conservation equations. Non-condensable gases obey ideal gas law. The individual volume fractions can be expressed in terms of mass fractions.
$$\alpha_v = f_v \frac{\rho}{\rho_v};\ \alpha_l = f_l \frac{\rho}{\rho_l} \tag{3.2}$$

For the mixture multiphase model, the two-phase flow is governed by one set of conservation equations of mass and momentum as given below:

$$\frac{\partial \rho}{\partial t} + \frac{\partial (u_j \rho)}{\partial x_j} = 0 \tag{3.3}$$

$$\frac{\partial (\rho u_i)}{\partial t} + \frac{\partial (\rho u_i u_j)}{\partial x_j} = -\frac{\partial p}{\partial x_i} + \frac{\partial}{\partial x_j}\left[\mu_{\text{eff}}\left(\frac{\partial u_i}{\partial x_j} + \frac{\partial u_j}{\partial x_i} - \frac{2}{3}\frac{\partial u_i}{\partial x_i}\right)\right] \tag{3.4}$$

where the mixture density is calculated from

$$\frac{1}{\rho} = \frac{f_v}{\rho_v} + \frac{1 - f_v}{\rho_l} \tag{3.5}$$

where ρ, ρ_v and ρ_l are the mixture, gaseous phase and liquid phase densities, respectively. The gaseous mass fraction is determined from the transport equation:

$$\frac{\partial (\rho \alpha)}{\partial t} + \frac{\partial (u_j \rho \alpha)}{\partial x_j} = R_P \tag{3.6}$$

where R_P represents the source or sink term and the relevant details are provided later in this chapter. In case of the present cavitation model and the model by Singhal et al. gaseous phase consists of both vapour and non-condensable gases.

The effective viscosity in the momentum equation is expressed as $\mu_{\text{eff}} = \mu + \mu_t$ where μ is the molecular viscosity and μ_t is the turbulent viscosity which has to be modelled. For example,

$$\mu_t = C_\mu \rho \frac{k^2}{\epsilon} \tag{3.7}$$

for $k - \epsilon$ models and

$$\mu_t = \alpha^* \rho \frac{k}{\omega} \tag{3.8}$$

for $k - \omega$ models. The turbulence models are discussed in this chapter.

3.3 Model Closure Equations

The governing equations have two unknowns R_P and μ_t which need additional equations for closure of the model formulations. In this section the closure equations for estimation of mass source term and turbulence models are provided.

3.3.1 Mass Source Term

Four cavitation models have been investigated here: Schnerr and Sauer model, Zwart-Geber-Belamri model, Singhal et al. model and the present cavitation model. The source terms of the present cavitation model, proposed in this study, will be described here. Schnerr and Sauer model, Singhal et al. model and the present cavitation model starts with the same vapour mass conservation partial differential equation. The main difference is that Schnerr and Sauer model does not consider the existence of non-condensable gases.

$$\frac{\partial(\rho_v \alpha)}{\partial t} + \frac{\partial(u_j \rho_v \alpha)}{\partial x_j} = \frac{\rho_v \rho_l}{\rho} \frac{D\alpha}{Dt} \tag{3.9}$$

Vapour volume fraction is expressed in terms of bubble radius and bubble number density. Schnerr and Sauer model [132] considered 10^{13} $[1/m^3]$ as bubble number density, while the present cavitation model assumed 10^{12} $[1/m^3]$. From the literature it is found that a value in the range of $10^{11} - 10^{12}$ $[1/m^3]$ is reasonable for bubble number density [115, 117, 149] for small scale internal flows. Varying the bubble number density in the present model did not yield any noticeable difference as the average bubble radius varies as cube-root of the bubble number density for a given volume fraction. More details are available in the Chapter "Model Assessment". In reality bubble number density is not constant while the bubbles are growing or collapsing. Linear Rayleigh equation has been utilized in all the models investigated here. The derivation of Linear Rayleigh is provided before the description of the present cavitation model, since it is an integral part of the cavitation models studied here. The details of the other cavitation models, Singhal, Schnerr and Sauer, and Zwart-Gerber-Belamri models are provided in the Appendix B.

Linear Rayleigh Equation

The widely followed approach in cavitation modelling is to consider only the effect of pressure difference across the bubble surface, $p_{sat} - p_\infty$ for estimating rate of change bubble radius. This approximation is referred in the literature as "simplified Rayleigh" or "Linear Rayleigh" or "asymptotic law". Most cases the underlying reasons are either not explained in the literature or misinterpreted [127]. Derivation and associated approximations are covered here following the procedure of Brennen [4]. Ignoring thermal effects in bubble growth (inertia driven regime) and considering non-condensable gases, the Rayleigh-Plesset equation can be expressed as

$$\frac{p_{\text{sat}} - p_\infty(t)}{\rho_L} + \frac{p_{G0}}{\rho_L}\left(\frac{R_0}{R}\right)^{3k} = R\ddot{R} + \frac{3}{2}\left(\dot{R}\right)^2 + \frac{4\vartheta_L}{R}\frac{dR}{dt} + \frac{2\sigma}{\rho_L R} \tag{3.10}$$

It is assumed that the bubble has an initial size of R_0 when it is in mechanical equilibrium such that (Young-Laplace equation),

$$p_{G0} = p_{\infty,t=0} - p_{\text{sat}}(T_\infty) + \frac{2\sigma_L}{R_0}$$

For $p_{\infty,t>0} = p^*_\infty$ =constant, Eqn. 3.10 is analytically integrated after multiplying $2R^2\dot{R}$ both sides and forming time derivatives. The viscous term cannot be integrated and hence ignored, resulting in an inviscid case. Applying the initial condition $\dot{R}|_{t=0} = 0$ and assuming isothermal condition.

$$(\dot{R})^2 = \frac{2(p_{\text{sat}} - p^*_\infty)}{3\rho_L}\left[1 - \frac{R_0^3}{R^3}\right] + 2\frac{p_{G0}}{\rho_L}\frac{R_0^3}{R^3} ln\left(\frac{R}{R_0}\right) - \frac{2\sigma_L}{\rho_L R}\left[1 - \frac{R_0^2}{R^2}\right] \tag{3.11}$$

If a bubble experiences considerable pressure difference it will undergo explosive growth and soon it will be $R >> R_0$. Then Eq. 3.11 will give rise to

$$\dot{R} = \sqrt{\frac{2}{3}\frac{|p_{\text{sat}} - p^*_\infty|}{\rho_L}} \tag{3.12}$$

Present Cavitation Model

The present cavitation model based on the framework of Singhal et al. model considers non-condensable gases. The phase change rate expression of the present cavitation model is the base equation derived in Appendix B i.e. Eq. B.9.

$$R_P = \frac{3\alpha}{R}\frac{\rho_v\rho_l}{\rho}\frac{DR}{Dt} \tag{3.13}$$

and with Linear Rayleigh equation DR/Dt is

$$\frac{DR}{Dt} = (-1)^j\sqrt{\frac{2\left(|p_{\text{eff}} - p_{\text{sat}}|\right)}{3\rho_l}} \tag{3.14}$$

where

$$p_{\text{eff}} - p_{\text{sat}} \begin{cases} > 0 & j = 1 \quad \text{for vapour condensation} \\ < 0 & j = 2 \quad \text{for vapour formation} \end{cases}$$

in which p_{eff} is the mean affective local pressure, R is the effective bubble radius, α is the void fraction $(\alpha_v + \alpha_g)$, and R is expressed in terms of α and number density of bubbles ($N''' = 10^{12}[m^{-3}]$) [116]. The expression of α is

$$\alpha = \tfrac{4}{3}\pi R^3 N'''$$

The present cavitation model requires estimation of the local mean effective pressure. It is assumed that vapour formation or cavitation occurs when the local mean effective pressure is below the saturation pressure.

$$p_{\text{eff}} < p_{\text{sat}} \tag{3.15}$$

where the local mean effective pressure p_{eff} is related to the cumulative effect of local static pressure, turbulent pressure fluctuations [120] and stresses [70, 130] and is expressed as

$$p_{\text{eff}} = p - p' - (\mu + \mu_t)\, S_{11} \tag{3.16}$$

where p is the mean local static pressure, p' is the turbulent pressure fluctuation and is taken as $p' = 0.47\rho k$ if the turbulence is isotropic [120]. The effect of non-isotropic turbulence is taken care of by the last term in Eq. 3.16. S_{11} corresponds to the highest eigenvalue of the deviatoric strain tensor; to determine S_{11} first $det(S - \lambda I)$ is equated to zero, where S is the strain tensor and I is the identity matrix. Roots of λ are thus obtained and the highest value of λ is used to estimate S_{11}. For an axisymmetric flow in cylindrical co-ordinates, it becomes

$$S_{11} = \left(\frac{\partial u}{\partial x} + \frac{\partial v}{\partial r}\right) + \sqrt{\left(\frac{\partial u}{\partial x} - \frac{\partial v}{\partial r}\right)^2 + \left(\frac{\partial v}{\partial x} + \frac{\partial u}{\partial r}\right)^2} \tag{3.17}$$

and for a flow in two-dimensional cartesian co-ordinate system the expression is

$$S_{11} = \sqrt{\left(\frac{\partial u}{\partial x} - \frac{\partial v}{\partial y}\right)^2 + \left(\frac{\partial v}{\partial x} + \frac{\partial u}{\partial y}\right)^2} \tag{3.18}$$

In the present model most of the assumptions and approximations of Singhal et al. [127], which were quite *adhoc*, have been avoided. Since the present model works in the framework of Singhal et al. model in ANSYS Fluent, following adjustment is necessary as Singhal et al. model takes mass fraction as input.

$$\alpha = 1 - \frac{\rho}{\rho_l}\,(1 - f_v)$$

The expression used for pressure fluctuations due to turbulence is also different from the one by Singhal et al. [127]. Singhal et al. based their estimate on Batchelor's equation [120],

$$p' = 0.58\rho u'^2$$

while the present model relies on the expression recommended by Uberoi and Hinze [120].

$$p' = 0.7\rho u'^2$$

Here $k \approx \frac{3}{2}u'^2$, leading to $p' = 0.47\rho k$.It was inferred by Hinze [120] that the later expression performs better than the previous one. Other researchers in the literature [57, 117] suggested a different expression for turbulent fluctuations.

$$p' = C_E \frac{2}{3}\rho_l k_l$$

where C_E is known as Egler coefficient with a value of 1.2 and as a source of the Egler coefficient Ref. [120] was cited in the literature [57, 117]. Nevertheless no such coefficient could be found from the Ref. [120]. Recent study by Battistoni et al. [150] inferred that there is no authentic source that indicate utility of Egler coefficient for cavitating flows.

Synopsis of Cavitation Models

The three cavitation models, apart from the present model, have some serious concerns which are not consistent with the physics of two-phase flow. Schnerr-Sauer cavitation model does not consider non-condensable gases and defines bubble number density (N''') in terms of total liquid volume instead of the total mixture volume. The source term in Schnerr and Sauer cavitation model does not provide non-zero value at the start of cavitation with no vapour being initially present in the domain. Theoretically speaking Schnerr and Sauer cavitation model should not be predicting any cavitation under any circumstances. Internal adjustments in the ANSYS Fluent platform probably make the Schnerr-Sauer cavitation model work. Zwart-Geber-Belamri does not consider non-condensable gases and assumes constant bubble radius which is again not consistent with the physics of the problem. Singhal et al. model uses Weber number while it starts with zero relative velocity approximation. The present cavitation model does not have the above mentioned limitations of the other three models, which makes the formulation of the present cavitation model more consistent with the physics of the problem. The present cavitation model also considers effects of turbulent fluctuation and stress, which are generally known to affect cavitation [4]. Table 3.1 provides overview of the cavitation model equations.

3.3.2 Turbulence Models

The turbulent kinetic energy k and the turbulent dissipation rate ϵ are determined from the turbulence models. (RNG) $k - \epsilon$ turbulence model has been mostly used in this

Table 3.1: Overview of Cavitation Models (Param.-Parameters,Vap.-Vaporization,Cond.-Condensation;$\frac{DR}{Dt} = \sqrt{\frac{2|\Delta p|}{3\rho_l}}$)

Param.	**Schnerr et al.**	**Zwart et al.**	**Singhal et al.**	**Present**
Vap.	$\frac{3\alpha(1-\alpha)}{R}\frac{\rho_v\rho_l}{\rho}\frac{DR}{Dt}$	$F_v\frac{3\alpha_{nuc}(1-\alpha)\rho_v}{R}\frac{DR}{Dt}$	$C_e\frac{\sqrt{k}}{\sigma}\rho_l\rho_v\frac{DR}{Dt}f_l$	$\frac{3\alpha}{R}\frac{\rho_v\rho_l}{\rho}\frac{DR}{Dt}$
Cond.	$\frac{3\alpha(1-\alpha)}{R}\frac{\rho_v\rho_l}{\rho}\frac{DR}{Dt}$	$F_c\frac{3\alpha\rho_v}{R}\frac{DR}{Dt}$	$C_c\frac{\sqrt{k}}{\sigma}\rho_l\rho_l\frac{DR}{Dt}f_v$	$\frac{3\alpha}{R}\frac{\rho_v\rho_l}{\rho}\frac{DR}{Dt}$
Δp	$p_{\text{sat}} - p_{\text{eff}}$	$p_{\text{sat}} - p_{\text{eff}}$	$p_{\text{sat}} - p_{\text{eff}}$	$p_{\text{sat}} - p_{\text{eff}}$
p_{eff}	p	p	$p - p'$	$p - p' - S$
S	N/A	N/A	N/A	$\mu_{\text{eff}}S_{11}$
p'	N/A	N/A	$0.195\rho k$	$0.47\rho k$
Constants	N/A	$F_v = 50, F_c = 0.01$	$C_e = 0.02, C_c = 0.01$	N/A

study. Comparison has been done for some cases with three types of turbulence models, a)Re-Normalisation Group (RNG) $k-\epsilon$, b) Realizable $k-\epsilon$ and c) shear-stress transport (SST) $k-\omega$ models. RNG $k-\epsilon$ model attempts to consider effects of different flow-scales by adopting the production term [67] in contrary to standard $k-\epsilon$ model where eddy viscosity is estimated on the basis of a single turbulence length scale. Realizable $k-\epsilon$ model dynamically estimates C_μ to satisfy the physics of turbulent flows. It is known to be a good model for variety of applications ranging from separated flows, boundary-layer flows etc. [67]. SST $k-\omega$ model uses $k-\omega$ model in the boundary layer upto the viscous sub-layer and away from the wall uses $k-\epsilon$ approach to create a hybrid and versatile modelling option [67]. Reynolds stress model (RSM) has not been used for cavitation analysis in the literature. However options like RSM or LES should be explored in future. Turbulence modelling approaches adopted with Eulerian-Eulerian multiphase approach are also discussed here followed by discussion of near wall treatments.

RNG $k-\epsilon$

In the RNG $k-\epsilon$ model, the model equations are

$$\frac{\partial\rho k}{\partial t} + \frac{\partial(\rho u_j k)}{\partial x_j} = \frac{\partial}{\partial x_j}\left(\alpha_k\mu_{\text{eff}}\frac{\partial k}{\partial x_j}\right) + G_k - \rho\epsilon - Y_M \tag{3.19}$$

$$\frac{\partial\rho\epsilon}{\partial t} + \frac{\partial(\rho u_j \epsilon)}{\partial x_j} = \frac{\partial}{\partial x_j}\left(\alpha_\epsilon\mu_{\text{eff}}\frac{\partial\epsilon}{\partial x_j}\right) + C_{1\epsilon}\frac{\epsilon}{k}G_k - \rho C_{2\epsilon}\frac{\epsilon^2}{k} - R_\epsilon \tag{3.20}$$

where $G_k = \overline{u_i'u_j'}\frac{\partial u_j}{\partial x_i}$ corresponds to the production of turbulent kinetic energy due to mean velocity gradients, $Y_{\text{M}} = 2\rho\epsilon M_t^2$ is the contribution of the fluctuating dilatation in

compressible turbulence to the overall dissipation rate with $M_t = (k/a^2)$ and $a = \sqrt{\gamma RT}$. R_ϵ is a special term in this model which accounts for low, medium and high strain rates. The model constants for RNG $k-\epsilon$ model are

$$C_\mu = 0.0845;\ C_{1\epsilon} = 1.42;\ C_{2\epsilon} = 1.68$$

Realizable $k-\epsilon$

For the realizable $k-\epsilon$ model, k and ϵ are governed by,

$$\frac{\partial \rho k}{\partial t} + \frac{\partial (\rho u_j k)}{\partial x_j} = \frac{\partial}{\partial x_j}\left(\left(\mu + \frac{\mu_t}{\sigma_k}\right)\frac{\partial k}{\partial x_j}\right) + G_k - \rho\epsilon - Y_M \tag{3.21}$$

$$\frac{\partial \rho \epsilon}{\partial t} + \frac{\partial (\rho u_j \epsilon)}{\partial x_j} = \frac{\partial}{\partial x_j}\left(\left(\mu + \frac{\mu_t}{\sigma_\epsilon}\right)\frac{\partial \epsilon}{\partial x_j}\right) + \rho C_1 S\epsilon - \rho C_2 \frac{\epsilon^2}{k + \sqrt{\nu\epsilon}} \tag{3.22}$$

where $C_1 = max[0.43, \frac{\eta}{\eta+5}]$, $\eta = S\frac{k}{\epsilon}$, $S = \sqrt{2S_{ij}S_{ij}}$. S is the modulus of the mean rate of strain tensor. The model constants are,

$$C_2 = 1.9;\ \sigma_k = 1.0;\ \sigma_\epsilon = 1.2$$

SST $k-\omega$

For the shear-stress transport or SST $k-\omega$ model, the turbulent kinetic energy, k, and the specific turbulent dissipation rate, ω, are determined from,

$$\frac{\partial \rho k}{\partial t} + \frac{\partial (\rho u_j k)}{\partial x_j} = \frac{\partial}{\partial x_j}\left(\left(\mu + \frac{\mu_t}{\sigma_k}\right)\frac{\partial k}{\partial x_j}\right) + G_k - Y_k \tag{3.23}$$

$$\frac{\partial \rho \omega}{\partial t} + \frac{\partial (\rho u_j \omega)}{\partial x_j} = \frac{\partial}{\partial x_j}\left(\left(\mu + \frac{\mu_t}{\sigma_\omega}\right)\frac{\partial \omega}{\partial x_j}\right) + G_\omega - Y_\omega + D_\omega \tag{3.24}$$

where G_ω corresponds to the production of ω, Y_k and Y_ω represent the dissipation of k and ω due to turbulence and D_ω takes care about the cross-diffusion term that helps SST $k-\omega$ model to work well in the near wall regions as well as regions far away from the walls. The model constants are

$$\sigma_{k,1} = 1.176;\ \sigma_{\omega,1} = 2.0;\ \sigma_{k,2} = 1.0;\ \sigma_{\omega,2} = 1.168$$
$$a_1 = 0.31;\ \beta_{i,1} = 0.075;\ \beta_{i,2} = 0.0828$$

Near-Wall Treatments

For near-wall treatments, required for $k-\epsilon$ model, non-equilibrium wall function has been adopted as it has been recommended in the literature [70, 128] for cavitating flows. The other available options in ANSYS Fluent are standard wall function and enhanced wall treatment. Non-equilibrium wall functions are recommended for complex flows such as separation, reattachment or severe pressure gradient compared to standard wall functions [67]. Enhanced wall treatment, despite being a good option demands strict requirement of very fine mesh and thus might incur significantly more computational time especially for 3D simulations [67].

3.4 Material Properties

Material properties, as stated before, are vital for modelling the two-phase flows. Most of the models consider the liquid phase as incompressible and vapour phase as incompressible or compressible (ideal gas) [57,98,108,115,117,124,127,149]. In this study liquid compressibility effects have been included. Ideal gas has been used for analysing vapour densities. Once cavitation occurs the local static pressure of experienced by the vapour phase is either its saturation pressure at the given temperature or higher than that. Therefore, resorting to ideal gas law should serve the purpose. A liquid fuel cannot be 100 % pure. Hence it is reasonable to consider presence of very small amount ($\approx$ 1.5e-05 mass fraction) of non-condensable gases, which acts similar to the nucleation-sites for cavitation inception. This value has been considered in some of the modelling works in the literature [70, 127]. Air is used to represent non-condensable gases and ideal gas behaviour is assumed for equation of state of air. Recent findings also indicate that presence of non-condensable gases in the order of 2.0e-05 is reasonable [150].

In reality diesel and biodiesel, both are blends of several compounds. Diesel for example is a mixture of several hydrocarbons. Different hydrocarbons are characterized by different saturation pressures and hence this is a problem for the purpose of cavitation modelling. For numerical analysis of cavitation, saturation pressure at a given temperature has to be specified despite the wide range of variability. Therefore, a diesel surrogate needs to be chosen that will closely represent the physical behaviour of actual diesel fuels. For diesel surrogates decane, dodecane or even tetradecane can be the possible candidate. In this study tetradecane ($C_{14}H_{30}$) has been considered as the diesel surrogate. Finding a surrogate of biodiesel is more difficult as biofuels has a much wider range of variability depending on its origin and processing methodology. Biodiesels are typically transesterified

Table 3.2: Material Properties

Properties	**European Diesel**	**Diesel**	**Biodiesel**
Liquid phase density (kg/m^3)	835	822.7	877.2
Liquid phase viscosity ($Pa.s$)	0.0025	0.0025	0.00694
Vapour phase viscosity ($Pa.s$)	0.00004	0.00004	0.00007
Bulk modulus (GPa)	1.5	1.5	1.724
Saturation pressure (Pa)	1000	1000	1
Molecular weight ($g/mole$)	198	198	296
Surface tension (N/m)	0.02	0.02	0.00296

products of vegetable oils. They typically have higher densities and viscosities. Pure Fatty Acid Methyl Esters (FAMEs) contained in Soybean Methyl Ester are normally selected for biodiesel surrogate. In this study methyl ester of oleic acid, methyl oleate ($C_{19}H_{36}O_2$), a vital component of B100 [151], has been chosen as the biodiesel surrogate.

The properties of diesel and biodiesel fuels have been obtained from various sources available in the literature. Liquid phase densities and viscosities of diesel and biodiesel have been obtained from the work by Som et al. [70, 128] and Ra et al. [151]. It should be noted here that for liquid density variation reference density of diesel is taken as 822.7 kg/m^3 instead of 756 kg/m^3, which is the density of tetradecane. This is to better represent actual diesel characteristics at high pressure. Taking 756 kg/m^3 reference density does not yield the expected diesel density value at high pressure. The vapour phase viscosities of diesel and biodiesel have been obtained from the work by Ra et al. [151]. The bulk moduli of liquid phase diesel and biodiesel have been obtained from the work by Szybist et al. [152]. The values are summarized below in Table 3.2. For validation studies with Winklhofer [31] properties of "European Diesel" were used and for comparative study of diesel and biodiesel cavitation the properties of "Diesel" and "Biodiesel" were used. For the purpose of validation, effect of variation of liquid density was not considerable as the inlet pressure was 10 MPa. Consequently the validation studies have been typically carried out at constant liquid density.

The vapour phase density has been considered to be 0.01087 kg/m^3 [153] for Singhal et al. model. For liquid density variation Bulk modulus (B) is used which is defined as

$$B = \rho \frac{dp}{d\rho} \tag{3.25}$$

and assuming that the pressure and density differentials can be approximated as the difference between the two values of the reference condition and the other state in question,

an equation of state was derived [67],

$$\rho = \rho_{\text{ref}} \left[1 - \frac{p - p_{\text{ref}}}{B} \right]^{-1} \tag{3.26}$$

The thermodynamic state of liquid phase at high pressure in cavitating flow is in compressible liquid regime as the pressure is high ($\approx$ 200 MPa) and temperature is low ($\approx$ 300 K). The critical pressure and critical temperature of No. 2 diesel fuel are 2.46 MPa and 569.4 K respectively and those of biodiesel fuel are around 1.2 MPa and 770 K (varies depending on the composition of biodiesel) [154]. As a result the liquid phase of both diesel and biodiesel is at a a pressure higher than critical pressure and at a temperature lower than critical temperature. For variation of liquid phase density implementing Tait's equation of state has been recommended in the literature [5]. Validity of Tait's equation for water at high pressure ($\approx$ 2000-3000 atm.) and low temperature ($\approx$ 300 K) has been confirmed in the literature by comparing with experimental data [155]. The Tait's equation is given below,

$$\frac{p + B'}{p_o + B'} = \left(\frac{\rho}{\rho_o} \right)^n \tag{3.27}$$

The parameter "1/(nB′)" is the compressibility coefficient or "1/B" and the subscript "o" refers to standard conditions and in this case at atmospheric pressure and room temperature. The values of n and B′ for diesel and biodiesel are not available in the literature, to the best of the knowledge of the author. The values could be obtained only for water and hence the equation of density variation suggested in Fluent documentation [67] has been compared with Taits equation for prediction of density variation of liquid water with applied pressure in Fig. 3.2. In case of an applied pressure of 200 MPa the Fluent formulation overpredicts the density with respect to the Tait's equation by 2.4%. Below 200 MPa the deviation is even less. The sonic speed estimated in diesel fuel at high pressure injections is around 1400-1500 m/s and the flow velocity is in the order of 600 m/s resulting in an approximate liquid phase Mach number of 0.4 which is in agreement with observation of Schmidt et al. [69]. Therefore, for the operating conditions explored in this study the Fluent formulation has been considered to be good enough for estimating the densities of liquid phases of diesel and biodiesel in this study.

3.5 Boundary and Initial Conditions

Pressure is identified at the inlet and outlet of the nozzle, and no-slip boundary condition is considered at the walls. No-slip condition is also assumed at the interface of liquid

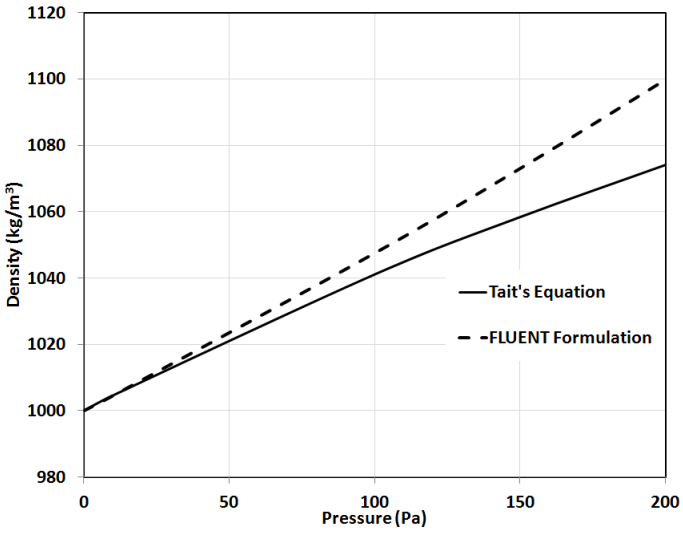

Figure 3.2: Comparison of predictions of liquid water density by Taits equation with FLUENT formulation [67], at pressures ranging from 0.1 MPa to 200 MPa.

and vapour for the mixture multiphase approach. Turbulence boundary conditions are specified by the turbulent intensity and hydraulic diameter at the inlet and the outlet. In order to incorporate the wall roughness effect, two inputs are provided, K_s, wall roughness height and C_s ($= 0.5$), roughness constant, in the wall boundary condition. The solution of the mixture multiphase model is used as the initial condition for running cases with the Eulerian-Eulerian multiphase model. Initializing Eulerian-Eulerian simulations with mixture multiphase solution incurred better numerical stability which is also claimed in the ANSYS Fluent documentation [67]. In pressure fluctuation cases UDFs are used to provide time-variant inlet boundary conditions.

Non-condensable gases help to initiate cavitation in the present and Singhal et al. models. The volume fraction of gaseous phase obtained from the present model include both vapour and non-condensable gases. Initially no vapour is present in the computational domain. However non-condensable gases are present in very small amount. Therefore $\alpha_{\text{initial}} = \alpha_0$ and in the present cavitation model estimate of α_0 is provided in terms of mass fraction of 1.5e-05. Literature indicates that mass fraction value in this order is reasonable to assume for cavitating flows [4,150]. It is reported that liquid under atmospheric pressure can contain around 15 ppm of non-condensable gases [4]. Even though cavitating flows occur under high pressures, it should be noted that once the non-condensable gases are dissolved in liquid fuel at atmospheric pressure like the case in automotive fuel tank,

there is no further exposure to non-condensable gases when the liquid fuel is pressurized. Additionally using Henry's law [156] it can be estimated that mass fraction of dissolved gases is in the order of 1.0e-05. Nitrogen and oxygen are the main constituents of air. With the help of Henry's law it can be calculated that at atmospheric pressure summation of mass fractions of nitrogen and oxygen in water at atmospheric pressure is approximately 2.3e-05 which is in the same order as the assumed initial mass fraction of non-condensable gases.

3.6 Numerical Implementation

The conservation equations and turbulence modelling equations are solved in ANSYS Fluent platform. ANSYS Fluent is finite volume based computational fluid dynamics (CFD) software widely used for solving fluid flow problems for engineering applications. Relevant details about numerical implementation are provided below.

The Pressure-based segregated algorithm is mostly utilized for solving the governing equations. The conservations equations are solved sequentially in segregated algorithm. Since the governing equations are non-linear and coupled, iterative solution is required to ensure convergence. Pressure-Based Coupled Algorithm has been found suitable for Eulerian-Eulerian simulations. Phase Coupled SIMPLE is a special type of SIMPLE method or segregated algorithm used in Eulerian-Eulerian simulations. Multiphase Coupled is a type of coupled algorithm meant for Eulerian-Eulerian simulations. The flow-chart shown in Fig. 3.3 elaborates the particulars of a typical pressure based segregated and coupled solvers. For cavitation modelling with mixture multiphase approach Semi-Implicit Pressure Linked Equations-Consistent (SIMPLEC) algorithm is used for pressure-velocity coupling. Pressure implicit with splitting of operator (PISO)are adopted for transient mixture multiphase simulations. PISO algorithm with neighbour correction is typically suggested for transient calculations [67]. PISO algorithm has the ability to maintain stable calculation even with large time step size.

Algebraic multigrid (AMG) method with a Gauss-Seidel type smoother is used. Second order discretization schemes are used for pressure, density, momentum, turbulent kinetic energy and dissipation rate. QUICK scheme is used for vapour phase transport equation. Multi-Phase Coupled (a type of Coupled solver) yielded better stability for Eulerian-Eulerian simulations. Under-relaxation factors (URF) are vital for cavitation simulations because order of magnitude difference in densities of the two phases and large pressure gradient cause numerical instability. Low to moderate values (between 0 to 0.5) are assigned for pressure, momentum and volume fraction URFs. For density, vaporization mass,

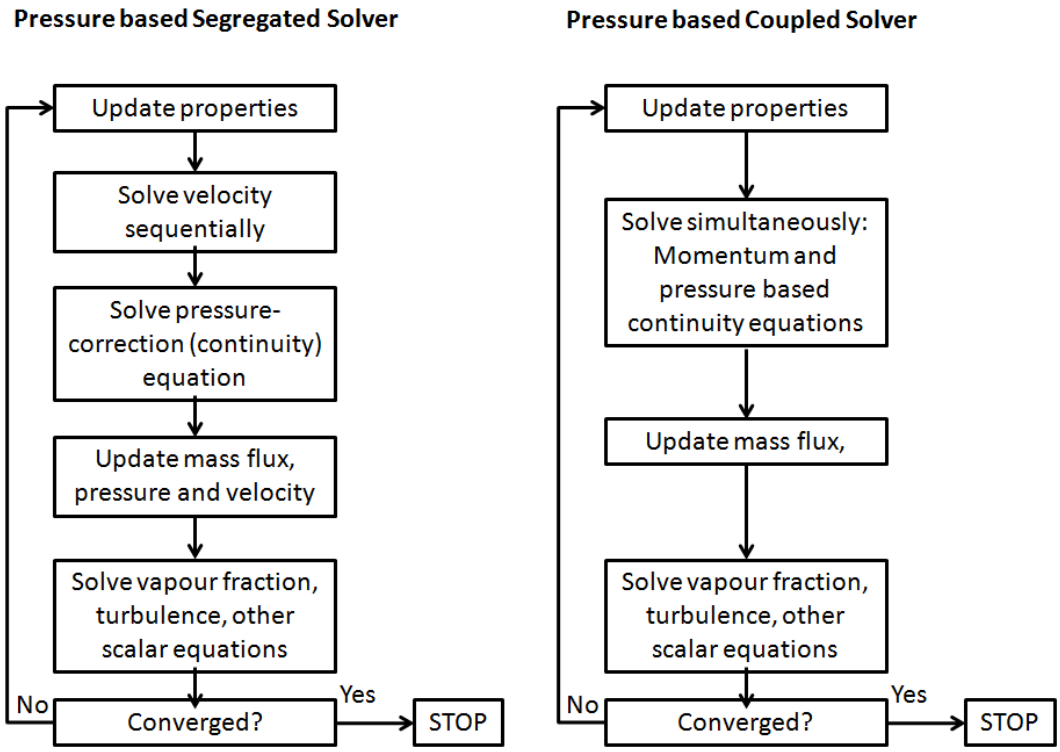

Figure 3.3: Flowchart for typical segregated and coupled solvers for analysing a generic flow problem [67].

turbulent kinetic energy, turbulent dissipation rate and turbulent viscosity average to high URFs work better.

The cavitation criterion including saturation pressure, turbulent pressure fluctuations and stress effects, and the source terms proposed in this study are implemented by incorporating user-defined function (UDF). Liquid compressibility effects as well as estimation of sonic speed in liquid are estimated with the help of user defined functions (UDFs). Sample codes are attached in Appendix C.

Chapter 4

Model Assessment

In this chapter the proposed model has been assessed with the experimental data in a rectangular cross-sectional nozzle from the work by Winklhofer et al. ($P_{\text{in}} = 10\ MPa$) and for an axisymmetric nozzle ($P_{\text{in}} = 100\ MPa$) in comparison to the performance of some of the existing cavitation models specifically the ones by Schnerr and Sauer [132], and Zwart, Gerber and Belamri [142]. Good quality data for cavitation at high injection pressure is still very rare. There are high inlet pressure studies such as, Soteriou et al. [16] and Chaves et al. [26]. However as elaborated in Literature Review Chapter that most of these studies do not provide enough information to successfully replicate the conditions for model validation. The image qualities of two-phase flows available for high pressure cases [16, 26] are extremely poor. Sometimes only discharge coefficient C_D variations are given as quantitative information. C_D is a fractional value and validating numerical predictions with C_D, cannot capture the subtle variations in the actual mass flow rates. Some high pressure data with complex geometry and intricate needle movements are available at Engine Combustion Network (ECN) website [147]. Nevertheless these nozzles are either non-cavitating (Spray A) or mildly cavitating (Spray B) and further experimental and numerical investigations are still going on [147].

The Eulerian-Eulerian multiphase approach has been only tested with Schnerr and Sauer and Zwart-Gerber-Belamri models. Three time step sizes 10^{-5} s, 10^{-6} s and 10^{-7} s have been tested in this study. It was observed that time step size of 10^{-6} s was reasonable in terms of computational time, stability and accuracy. As a result time step size of 10^{-6} is mainly used for Eulerian-Eulerian simulations. Eulerian-Eulerian results presented here are all at the instant of 0.5 ms i.e. after steady state is reached.

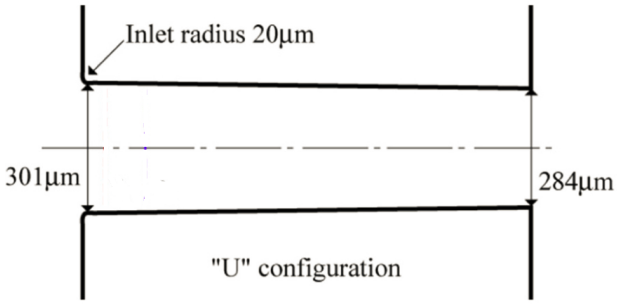

Figure 4.1: Schematic of the throttle geometry "U" in the study by Winklhofer et al. [31].

4.1 Comparison with the Experiment

The reliability of the developed model is assessed by comparing its predictions with the experimental observations of Winklhofer et al. [31]. The "U" nozzle used for comparison has a rectangular cross section with the depth of 0.3 mm, an inlet width of 0.301 mm, an outlet width of 0.284 mm and an inlet rounding radius of 0.02 mm. The nozzle length is 1 mm. Figure 4.1 displays the schematic illustration of the U nozzle. In the set-up of the experimental study [31], the inlet pressure was maintained at 10 MPa (100 bar), and the outlet pressure was varied from 1.5 to 8 MPa. The temperature was fixed at 300 K.

The computational domain is extended before the nozzle inlet and beyond the exit of the nozzle by 0.6 mm. Two-dimensional study has been carried out for the validation since it is the trend in the literature for the purpose of validation of cavitation models. However three-dimensional simulation has the potential for better prediction, but with significant increment in computational time. Additionally performing parametric studies is more feasible with two-dimensional cases. The throttle assembly depth is uniform along the length. Hence the contraction of the nozzle is only in terms of width. In the experiment the pressure was monitored a certain distance upstream of the nozzle inlet and downstream of the nozzle outlet. Volume fraction contours are presented in "Qualitative Comparison" subsection and other information obtained from modelling studies are documented in "Quantitative Comparison". Vapour volume fraction contours can only be assessed in terms of back-scattered images which are qualitative. Hence the need of a subsection titled "Qualitative Comparison".

Table 4.1: Comparison of predicted mass flow rates (g/s) from Grid I and Grid II with experiment [31].

$\Delta P(MPa)$	**Experiment**	**Grid I**	**Grid II**
6	7.18	7.60	7.30
7.5	7.81	8.14	8.07
8	7.80	8.14	8.08

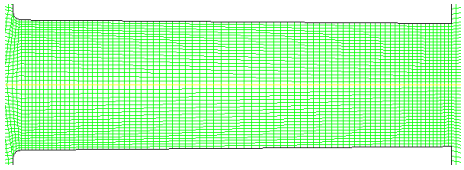

Figure 4.2: Nozzle section of Grid I used in validation study

4.1.1 Grid Independency

The nozzle section of the domain is subjected to a grid density of 90×20 (Grid I). In any numerical analysis it is imperative that effect of grid resolution will be tested to assess the reliability of the numerical results. To examine the effect of grid resolution, two different grid resolutions has been tested. In Grid II grid density of 140×30 is used in the nozzle block. Simulations were performed with both Grid I and Grid II. There were some improvements in the prediction of mass flow rates for different pressure difference (inlet and outlet) cases. The mass flow rate values are presented in Table 4.1 for three pressure differences 6, 7.5 and 8 MPa. The difference in the mass flow rate estimates from the two grids is high for low pressure (4%), but lower for high pressure difference cases. The predictions from Grid I are still reasonable from engineering point of view. Som et al. [70] carried out simulations in Winklhofer nozzle with same grid resolution as Grid I and found this resolution to be reliable. As a result the Grid I is considered reliable for the validation study and is shown in Fig. 4.2.

4.1.2 Qualitative Comparison

In the experiment [31] the nozzle was back illuminated and back scattered images were recorded. The vapour content was not quantitatively measured. However the predominantly vapour and liquid regions were identified. In the experimental images there is a greenish-yellow fuzzy region at the core of the flow which indicates that there is some

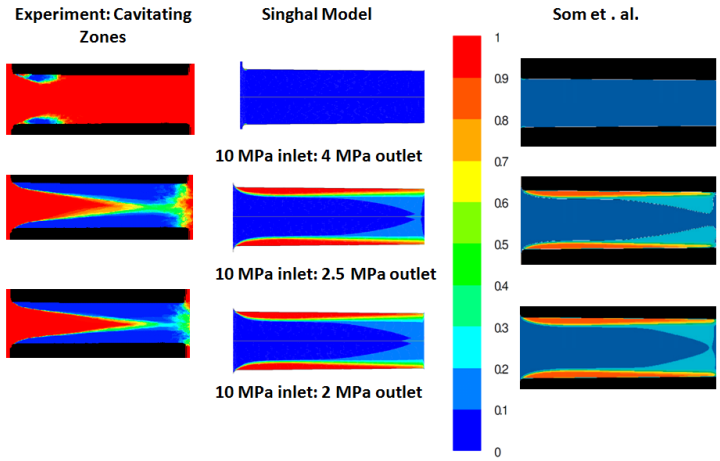

Figure 4.3: Comparison of model predictions of vapour volume fraction using Singhal et al. model and the results from Som et al. [70] with the experimental images from Winklhofer et al. [31](experiment: blue- cavitating,red-not cavitating).

chance of presence of vapour. The blue region, indicates presence of considerable vapour and red region denotes dominance of liquid. The experimental images are ensemble average of 20 snapshots taken for a given operating condition. As a result the fuzzy region is not always guaranteed to have cavitation. No scale or colormap was available for the experimental images.

In this subsection vapour volume fraction predictions from different cavitation models, when coupled with different multiphase approaches, are presented. At first Singhal et al. model is attempted and compared with experiment [31] and numerical results of Som et al. [70], for qualitative comparison. The vapour contour predictions are shown in Fig. 4.3. Realizable $k-\epsilon$ turbulence model has been adopted for the above result as the same was done by Som et al. The predictions from the present study, using Singhal et al. model, match very well with Som et al. predictions. The mass flow rates obtained using Singhal et al. model were similar to the ones obtained by Som et al. [70]. However there are discrepancies compared to the experimental images from Winklhofer et al. [31] as the back-scattered images have the depth-integrated effect. The colormap provided is only meant for numerical predictions.

Next the present cavitation model has been used for comparison using RNG $k-\epsilon$ turbulence model. Comparison of vapour contours with different turbulence models is presented later. Figure 4.4 presents a qualitative comparison of the present model results with the

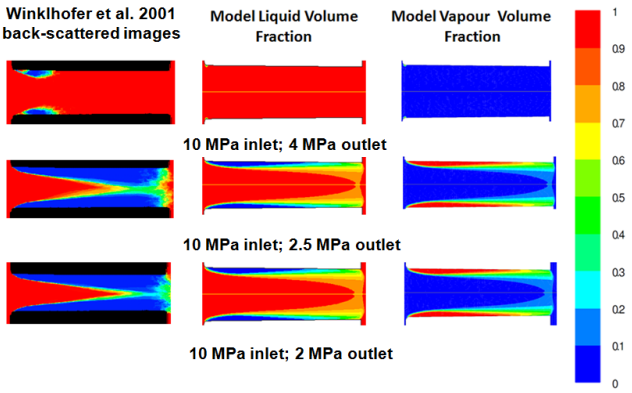

Figure 4.4: Qualitative comparison of modelling predictions of the present cavitation model with experimental images from the work of Winklhofer et al. [31] (experiment: blue-cavitating,red-not cavitating).

experimental images from [31]. In the experimental images, as mentioned before, a red region represents the non-cavitating region and the blue regions the cavitating regions and the light greenish region the fluctuations between liquid and vapour phases. The colormap provided is only meant for numerical predictions. It is seen that the model initially under-predicts the extent of cavitating zones, but performs better when the pressure difference between the inlet and the outlet is increased. For high pressure difference cases supercavitation is predicted as observed in the experiments. It is important to point out that the experimental images contain the integrated effect of the transmitted light through the two phase flow in the transparent nozzles, while the model contours belong to a single plane in the domain. Hence discrepancies in the qualitative comparison are expected. Neroorkar et al. [98] indicated that the intensity in the images from Winklhofer et al. [31] represent the probability of the local light transmittance. The voids created in the low pressure regions, cause the darkening of the observed flow area when observed with with back illumination. Therefore, information from the images cannot be used for quantitative comparison and considerable under-prediction of vapour content by the models with respect to the images is expected. Overall a decent qualitative agreement with the experimental results has been achieved. The above result has been published in a journal article [157].

Both realizable and RNG $k-\epsilon$ models have been tested for the validation case to compare their performances. For the case of 2 MPa outlet pressure i.e. pressure difference of $\Delta P = 8$ MPa the vapour contours are given in Fig. 4.5 using both RNG and Realizable k- models. The vapour contours look qualitatively similar with some differences in the

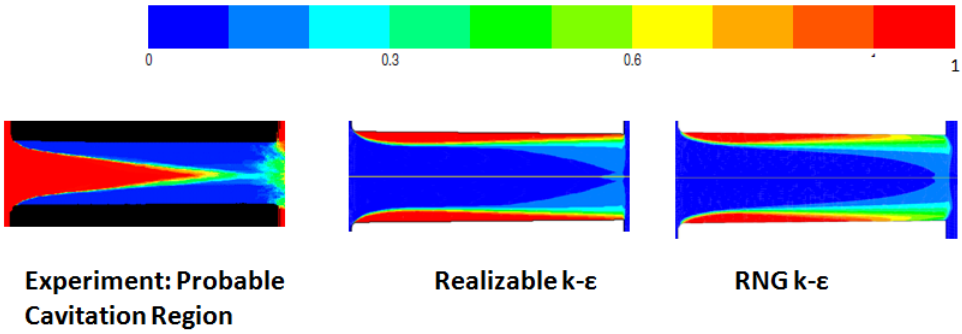

Figure 4.5: Qualitative comparison of vapour contours with Realizable $k-\epsilon$ and RNG $k-\epsilon$ turbulence models with the present cavitation model, with experimental image from Winklhofer et al. [31] for $\Delta P = P_{in} - P_{out} = 8.0$ MPa.

quantitative values of volume fraction of vapour in the cavitating regions. Convergence with realizable model was slower than RNG. The reason for this problem is because of the complicated calculation procedure of the realizable $k-\epsilon$ model as the parameter $C_{\mu t}$ used in modelling turbulent viscosity is not assumed to be constant and is varied depending on the flow field. The mass flow rate values predicted by both the turbulence models were almost same and were around 8.14 g/s. As a result it can be concluded that RNG $k-\epsilon$ model is good enough for the validation exercise. SST $k-\omega$ model is unstable for the high pressure difference cases. For pressure difference of 8.0 MPa supercavitation is not predicted by the SST $k-\omega$ model. For the low pressure difference cases noticeable difference is not observed.

The vapour contours obtained from Zwart-Gerber-Belamri, Schnerr-Sauer and the present cavitation models, coupled with mixture approach, are compared in Fig.4.6. The maximum vapour volume fraction values predicted by the three models are not only different, but also not of the same order. As a result the maximum values are stated above each contour and the minimum values (= 0.0) is stated below the color bar. Schnerr and Sauer and Zwart-Gerber-Belamri model results in this figure are from mixture multiphase approach. While all the models do not perform well in case of $P_{out} = 4.0$ MPa, only the predictions from the present model manage to achieve supercavitation (cavitation extending to the end of the nozzle section) for higher pressure differentials as seen in experiments. The present cavitation model manages to achieve reasonable qualitative agreement. The above result has been published in a conference [158].

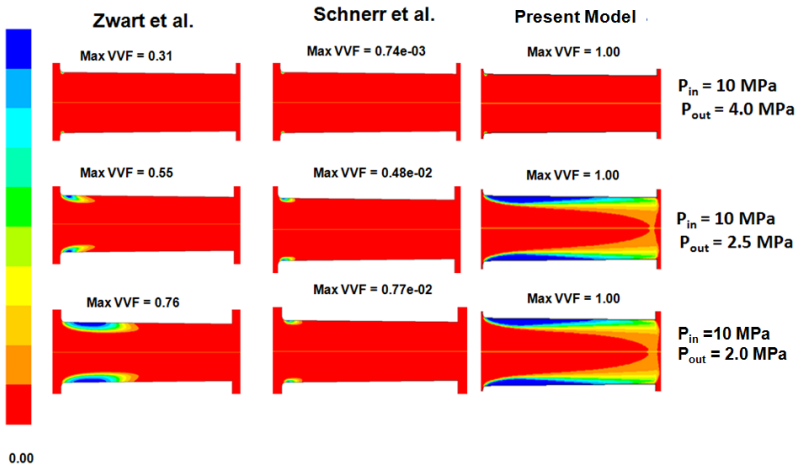

Figure 4.6: Comparison of vapour volume fraction contours for Zwart-Gerber-Belamri, Schnerr-Sauer and the present cavitation models, coupled with mixture approach, at three different pressure differentials ($\Delta P = P_{in} - P_{out}$): P_{in} = 10.0 MPa and P_{out} = 4.0 MPa, 2.5 MPa and 2.0 MPa at steady state (Maximum vapour volume fraction is abbreviated as Max VVF: Red- liquid, Blue - Vapour. Colour scheme has been changed to compare with the experimental images.).

The poor performance of Schnerr and Sauer model can be attributed to their methodology adopted for source term formulation. They defined bubble number density as number of bubbles present in unit volume of liquid instead of assuming it to be the number of bubbles present in the total control volume, which is done by most of the studies [116,117,149]. Moreover Schnerr and Sauer ignored the existence of non-condensable gases. Source terms used by the present model and Schnerr and Sauer although look very similar the above-mentioned differences cause significant differences in numerical prediction. Zwart-Gerber-Belamri model also ignored existence of non-condensable gases and they even considered constant bubble radius which is not realistic. They had tuning parameters which enabled them to provide relatively better performance. Therefore, it is seen that Schnerr and Sauer and Zwart-Gerber-Belamri models are not performing well for the nozzle, simulating the conditions of the experiment [31] when couple with mixture multiphase approach. Thus it can be inferred from the qualitative assessment that the present cavitation model performs better than Schnerr-Sauer and Zwart-Gerber-Belamri models when mixture multiphase approach is adopted.

Attempt has also been made to vary the F_{vap} parameter of Zwart-Gerber-Belamri model to seek better agreement with experiment when used with mixture multiphase approach.

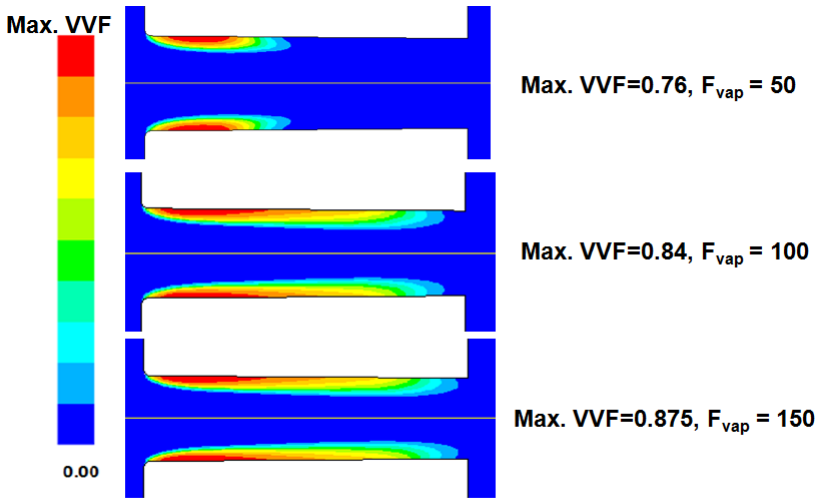

Figure 4.7: Comparison of vapour volume fraction contours when F_{vap} is varied when Zwart-Gerber-Belamri model is coupled with mixture multiphase approach, at (ΔP)= 8.0 MPa for Winklhofer nozzle [31] (Max VVF - maximum vapour volume fraction).

F_{vap} has been varied from 50 to 150 and the effects on vapour volume fraction are shown in Fig.4.7. The change in tuning parameter might not always ensure better prediction and extensive testing is required to assure reliable prediction for a wide range of conditions. Promising results have been obtained while adopting Eulerian-Eulerian multiphase approach with Multiphase Coupled algorithm specially for Zwart-Gerber-Belamri model. Further details and sample results from Eulerian-Eulerian approach are provided in Appendix A.

Eulerian-Eulerian vapour contours obtained with Zwart-Gerber-Belamri and Schnerr-Sauer cavitation models are compared with that of the present cavitation model for ΔP = 8 MPa and are presented in Fig.4.8. Schnerr Eulerian performs better compared to the case when coupled with mixture multiphase approach. Only in the present cavitation model some vapour has been predicted at the core of the flow near the nozzle exit which is also seen in the experimental figure for same pressure difference [31].

Recently researchers at CONVERGE CFD software developed their Homogeneous Relaxation Model (HRM) coupled with volume of fluid (VOF) approach and validated their simulations with Winklhofer et al. [31]. For the case of pressure difference of 8 MPa predicitons of their and the present cavitation models are presented in Fig.4.9. For the sake of

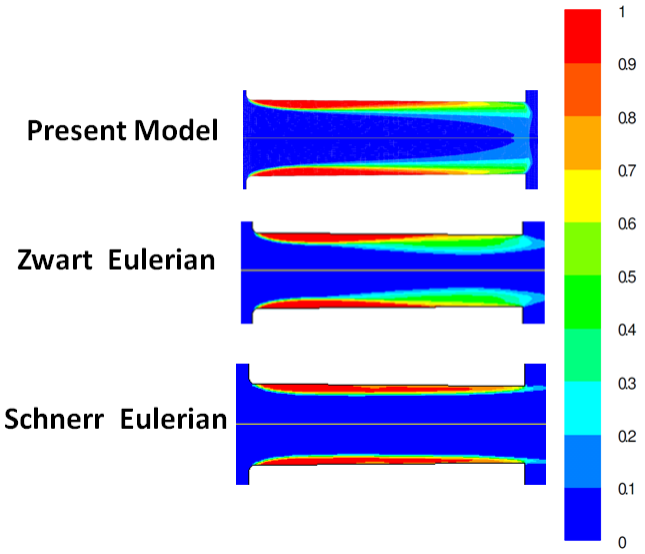

Figure 4.8: Comparison of vapour volume fraction contours obtained with Zwart-Gerber-Belamri and Schnerr-Sauer cavitation models, coupled with Eulerian-Eulerian approach, with the present cavitation model result at (ΔP)= 8.0 MPa for Winklhofer nozzle [31].

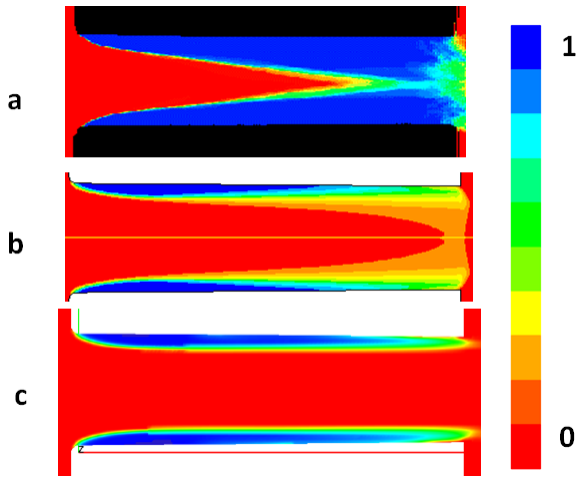

Figure 4.9: Comparison of (a) experimental image by Winklhofer et al. [31] with vapour volume fraction contours obtained from (b) the present cavitation model and (c) the VOF based HRM in CONVERGE [101], at (ΔP)= 8.0 MPa.(Blue-vapour;Red-liquid)

comparison blue denotes maximum vapour and red stands for maximum liquid. Both the models achieve supercavitation in their model predictions. Nonetheless predictions from HRM in CONVERGE do not tend to predict presence of vapour near the core at the exit which is relatively better achieved by the present cavitation model. This is probably because of adopting VOF approach as it tends to predict non-diffuse vapour region due to its interface capturing algorithm. Similar sharp and non-diffuse nature has been predicted by other VOF based cavitaiton models [149]. As a result VOF might not be a desirable multiphase approach for cavitation as we know cavitation appears as a sharp cavity and then appears a foamy mixture at the trailing edge [29].

The present model takes approximately 100,000 iterations in less than 3 hours to reach converged solution for the case of pressure difference of 8 MPa, while for the same case Zwart-Geber-Belamri model takes approximately 30,000 iterations in less than 1.5 hours and Schnerr-Sauer model takes around 5,000 iterations in 10-15 minutes or 1/6th of an hour. For Eulerian-Eulerian simulations steady state is reached in approximately 0.1 ms (time step size of 10^{-6} s) and results presented in this study are at the instant of 0.5 ms with CPU time of 9 hours for Zwart-Geber-Belamri model and around 8 hours for Schner and Sauer model for the same pressure difference. The simulations were run in a 64 bit Windows XP system, with 32 GB RAM and processor clock speed of 2.83 GHz. Serial processing was used for all the cases. The vapour contours from Eulerian-Eulerian simulations do not change significantly from 0.1 ms to 0.5 ms, but the fluctuations in the residuals subside considerably by 0.5 ms and there is no further improvement beyond 0.5 ms. The present model performed reasonably well compared to the existing models in terms of predictive capability and computational cost.

4.1.3 Quantitative Comparison

For the quantitative assessment predictions of mass flow rate and velocity are compared in this subsection. Apart from mas flow rate, velocity and volume fraction details about turbulence level at the exit are important. Hence turbulent kinetic energy information, obtained from different cavitation models, has been also provided here even though measured values were not available. Eulerian-Eulerian simulations are transient. The results from those simulations are presented here at 0.5 ms. Vapour contours typcially reach a steady state by 0.1 ms, but fluctuation of residuals often does not subside till 0.5 ms. No further improvement is observed in the residuals by running simulations beyond 0.5 ms.

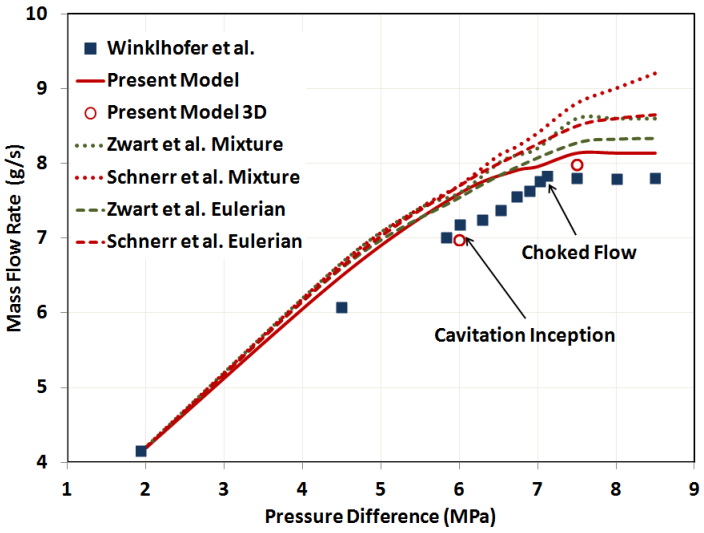

Figure 4.10: Comparison of the mass flow rate predictions from the present cavitation model, and Schnerr-Sauer and Zwart-Gerber-Belamri (mixture and Eulerian-Eulerian), with the experimental data [31] as a function of the injection pressure difference (ΔP).

Mass flow rate

The mass flow rate predicted by the present cavitation model along with those of Schnerr-Sauer and Zwart-Gerber-Belamri models (both mixture and Eulerian-Eulerian) are compared with the measured data [31] in Fig. 4.10. Typically all the models are over predicting the mass flow rates. Compared to experiment cavitation is generally under-predicted by all the models. Therefore, over-prediction of mass flow rates is expected. The predictions of mass flow rates by the present model are better than those of Zwart-Gerber-Belamri [142] and Schnerr and Sauer [132] models for high pressure differentials especially when mixture multiphase approach is adopted. Switching to Eulerian-Eulerian improves the performance of Schnerr-Sauer and Zwart-Gerber-Belamri models. Mass flow rates predicted by Zwart-Gerber-Belamri model with mixture approach does show the trend of choked flow which was obtained by Winklhofer et al. [31]. Zwart-Gerber-Belamri when coupled with Eulerian-Eulerian approach performs almost as good as the present cavitation model. However Schnerr and Sauer model with mixture approach does not show this trend and the mass flow rates increase monotonically with pressure difference. The plausible explanation would be considerable under-prediction of vapour concentrations by Schnerr and Sauer model with mixture multiphase approach under cavitating conditions. Two-phase cavitating flow often acts similar to a compressible flow [4] and thus considerable cavitation

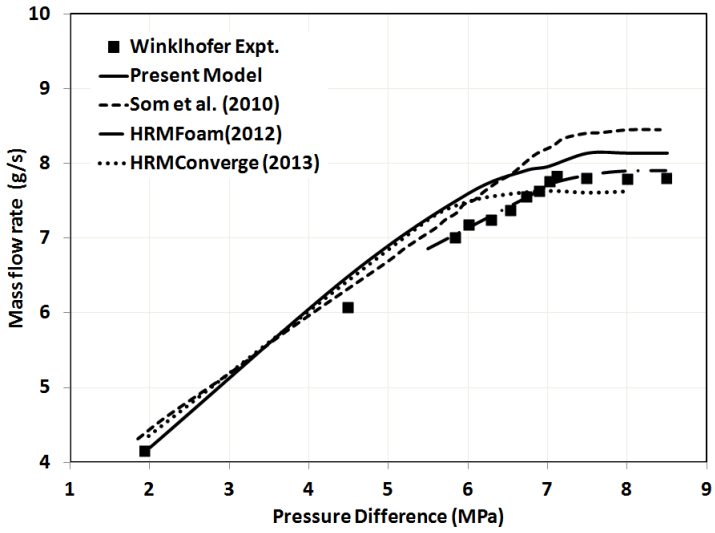

Figure 4.11: Comparison of predicted mass flow rates from the present cavitation model and different published literature results: Som et al. [70], Neroorkar et al. [98] (HRMFoam) and Zhao et al. [101] (HRMConverge), at different pressure differentials ($\Delta P = P_{in} - P_{out}$) with experimental values [31].

limits the available area for the liquid phase to pass through nozzle exit. As a result at high pressure difference choked flow can occur. Two sample cases with 3D simulations have been studied for pressure differences of 6.0 MPa and 7.5 MPa. The 3D predictions for the two cases are better. For a 3D cases flow separation and boundary layers are going occur in all 4 faces of the rectangular cross-section. This indicates 3D simulations can be promising. However 3D simulations would take few days compared to few hours for 2D simulations. The predictions from the model by Singhal et al. [127] are not shown in this figure as they are very similar to those of Som et al. [70]. The predictions of Som et al. [70] are presented in the following figure.

The mass flow rates for different pressure differentials ($\Delta P = P_{in} - P_{out}$) are also compared with the recently published predictions from different other cavitation models in Fig. 4.11. The predictions used are by Som et al. [70], Neroorkar et al. [98] and Zhao et al. [101]. Neroorkar et al. [98] implemented homogeneous relaxation model (HRM) in OpenFOAM [90] where the cavitation model is denoted as HRMFoam. Their model is based on transient mixture multiphase approach. Zhao et al. [101] implemented HRM in CONVERGE CFD software [100] using VOF approach. Zhao et al. [101] is the only study that have adopted 3D approach. Both the predictions of Neroorkar et al. [98] and Zhao et

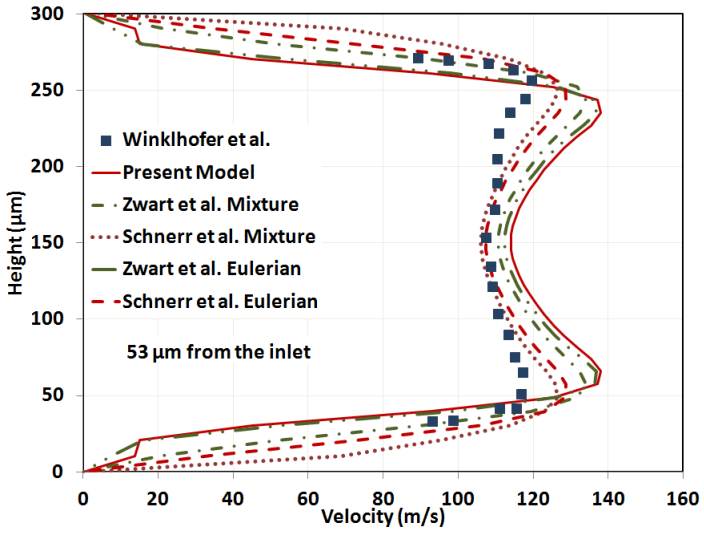

Figure 4.12: Comparison of predicted velocity profiles from the three cavitaion models using mixture and Eulerian-Eulerian multiphase approaches, at ($\Delta P = P_{in} - P_{out}$)= 6.7 MPa with experimental values measured at a location 53 μm from the nozzle inlet section [31].

al. [101] are very close to measured values. However the important point here is that both the works have used much lower liquid densities : 810 kg/m^3 (Neroorkar et al. [98]) and 730 kg/m^3 (Zhao et al. [101]). The density values are quite lower than the value used in this validation study, 835 kg/m^3. The justification of the density value used in this validation study is already provided in Material Properties section in previous chapter. Considering the property differences the mass flow rate predictions of the present cavitation model are reasonably well.

Velocity

Winklhofer et al. [31] also estimated the velocity at a distance 53 μm from the inlet section of the nozzle using fluorescence techniques. For a $\Delta P = P_{in} - P_{out} = 6.7$ MPa the model predictions are compared with measured values in Fig. 4.12. Velocity predictions using Eulerian-Eulerian multiphase approach with Zwart-Gerber-Belamri and Schnerr-Sauer models are also included here with mixture multiphase approach results using the three cavitation models. In their study Winklhofer et al. [31] stated that there were difficulties and uncertainties involved in capturing velocity data in the near wall regions. Except the near wall regions the three cavitation models manage to capture the qualitative trend

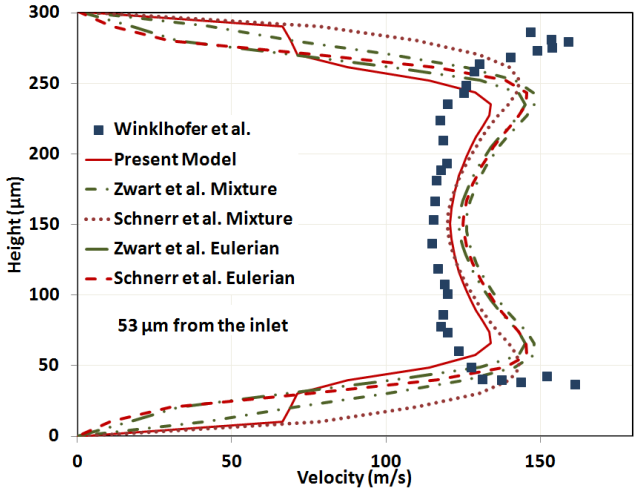

Figure 4.13: Comparison of predicted velocity profiles from the three cavitaion models using mixture and Eulerian-Eulerian multiphase approaches, at ($\Delta P = P_{in} - P_{out}$)= 8.5 MPa with experimental values measured at a location 53 μm from the nozzle inlet section [31].

properly. Schnerr and Sauer model velocity predictions are relatively better than the ones by the present cavitation and Zwart-Gerber-Belamri models. At the core of the flow maximum error is observed by the present model, +5.60% and away from the core where the velocity reaches its maximum value, both the present cavitation model and Zwart et al. Eulerian gives maximum error of around +16.24%. There is considerable difference in the velocity profiles obtained using mixture and Eulerian-Eulerian multiphase approaches for Zwart-Gerber-Belamri and Schnerr-Sauer cavitation models and the velocity predictions are not essentially getting better. Thus switching from mixture to Eulerian-Eulerian approach is not yielding better overall agreement for velocity predictions. There is a slight kink in the present cavitation model velocity profile near the wall. The present cavitation model typically predicts relatively more cavitation in the near-wall region. Zwart Eulerian also predicts more cavitation than the remaining 3 cases and it is also not smoothly going to zero. The presence of vapour and hence less drop in velocity near the wall could be the possible reasons behind the kinks.

Figure 4.13 shows the comparison of the measured and predicted velocity distribution at 53 μm from the nozzle inlet for the injection pressure differential of 8.5 MPa. It is seen that the velocity increases with increase in pressure difference. All the models predict the qualitative trend of the velocity variation for the bulk of the flow except in the near wall regions. For this case all the models have tendency to over-predict the velocity which

is expected as the mass flow rate is also over-predicted by the models as shown in Fig. 4.10. In this case Schnerr-Sauer model with mixture multiphase approach and the present cavitation model are the closer to the experimental values at the core of the flow compared to the predictions of the other models. The measured velocity in the vicinity of the wall has different trend of variation and may be due to the difficulties and uncertainties in the velocity measurements in the near wall regions. Both Schnerr-Sauer and Zwart-Gerber-Belamri models coupled with Eulerian-Eulerian approach show kinks which are not visible when coupled with mixture multiphase approach. The present model is visibly different in the near wall region compared to the other cases in the near wall region. The difference is due to the difference in the predicted concentration of vapour by the cavitation models in the near-wall regions. The kinks near the wall in both cases indicate that presence of vapour is accelerating the flow near the wall.

Present cavitation model (mixture) and Zwart-Geber-Belamri model (Eulerian-Eulerian) perform relatively well in terms of vapour volume fraction, but do not do well in terms of velocity. The reason for this discrepancy is possibly due to limitations of eddy viscosity turbulence models which were originally optimized for single-phase turbulent flows. Implementation of LES or RSM (Reynolds Stress Model) turbulence models can be attempted to investigate the reasons for such discrepancies. Therefore, relatively better performance of Schnerr and Sauer cavitation model for velocity prediction does not necessarily indicate that it should be preferred compared to the other cavitation models.

Turbulent kinetic energy

The model predictions by the present model and Zwart-Gerber-Belamri and Schnerr-Sauer have been performing relatively well. Since turbulent kinetic energy is an important variable that needs to be known from cavitation analysis. Turbulent kinetic energy (TKE) contours at $\Delta P = 8$ MPa are presented here. All the cavitation model predictions presented here are done with RNG $k-\epsilon$ turbulence model. It is observed that presenting the TKE contours using same scale is not convenient for understanding the variation of TKE in the contour results. Figure 4.14 shows how for same turbulence model the TKE varies depending on cavitation models chosen.

4.2 Comparison in an Axisymmetric Nozzle

An axisymmetric sharp-edged nozzle is considered for comparison of the models at high pressure. Here only upto 100 MPa inlet pressure is studied as it is 10 times the inlet pressure

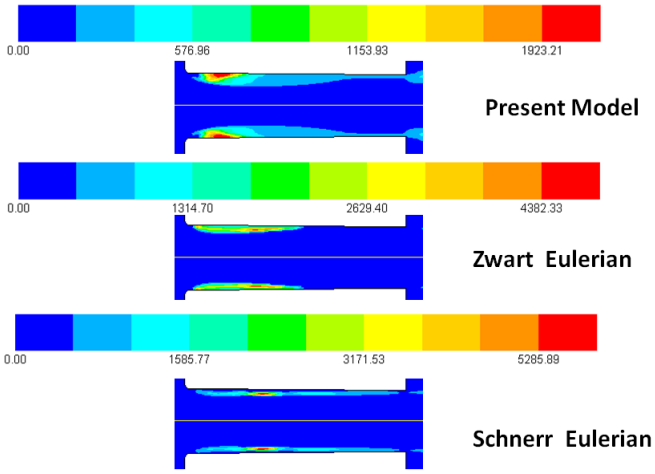

Figure 4.14: Comparison of turbulent kinetic energy (TKE) (m^2/s^2) predictions from the present model and Schnerr-Sauer and Zwart-Gerber-Belamri models (liquid) coupled with Eulerian-Eulerian approach at $\Delta P = 8$ MPa (maximum TKE values: Present model- 1923.21, Zwart Eulerian- 4382.33, Schnerr Eulerian- 5285.89).

of Winklhofer nozzle (10 MPa) [31]. Cavitation characteristics at even high pressure in the same nozzle are provided in the following chapter. The nozzle considered has the following geometric parameters: D/d = 4, L/d = 4, d = 0.15 mm. The nozzle diameter is denoted by d, length of the nozzle by L and diameters of the upstream and downstream extended domains are represented by D. A schematic representation of the domain has been already shown in Fig. 3.1. These parameters are of the same order as the characteristic dimensions of a diesel injector. The mesh used has a resolution of 24×100 in the nozzle section with 9520 cells in the entire domain. The mesh resolution assessment is provided in the following chapter involving analysis of diesel and biodiesel. The inlet pressures examined in this study are 15, 20, 25, 50 and 100 MPa with outlet pressure being fixed at 5 MPa. Figure 4.15 compares the vapour volume fraction contours obtained from the three models. The maximum concentration has been mentioned above the contours same way as in Fig. 4.6. For inlet pressure of 15 MPa Schnerr and Sauer model again considerably under-predicts the vapour concentration. In case of inlet pressure of 50 MPa all the three models achieve supercavitation. This indicates that for high pressure differentials predictions of Schnerr and Sauer model tend to be reliable. Mass flow rates for the axisymmetric nozzle predicted by the three models are almost same for all the pressure differentials examined. The values are tabulated in Table 4.2 instead of plotting because of the close proximity. Present

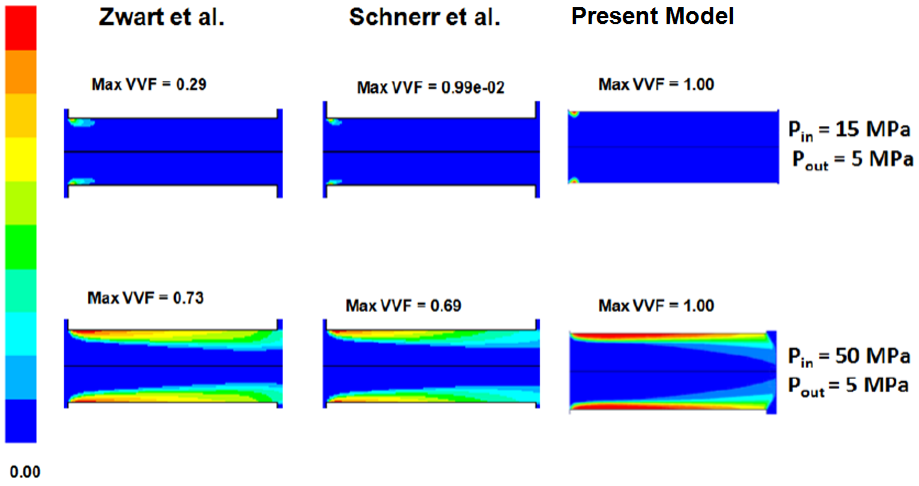

Figure 4.15: Comparison of vapour volume fraction contours at steady state for axisymmetric nozzle for the three models at inlet pressures of 15 and 50 MPa and fixed outlet pressure of 5 MPa (Maximum vapour volume fraction is abbreviated as Max VVF).

Table 4.2: Mass flow rate variation with change in pressure difference for axisymmetric nozzle with mixture approach

ΔP (MPa)	**Present Model** (g/s)	**Zwart et al.** (g/s)	**Schnerr et al.** (g/s)
10	1.73	1.72	1.73
15	2.02	2.06	2.10
20	2.26	2.30	2.39
45	3.20	3.24	3.34
95	4.55	4.56	4.65

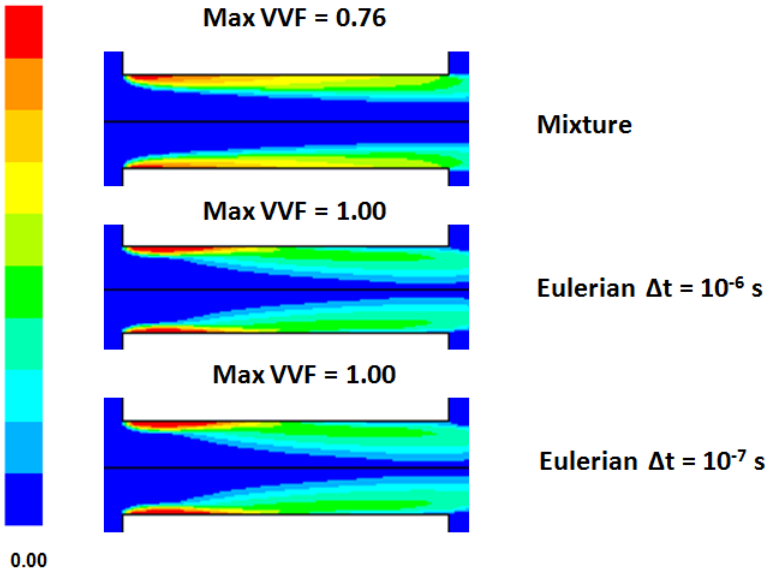

Figure 4.16: Comparison of vapour volume fraction contours for axisymmetric nozzle for Zwart-Gerber-Belamri model coupled with mixture and Eulerian multiphase approaches at inlet pressure of 100 MPa and outlet pressure of 5 MPa(Maximum vapour volume fraction is abbreviated as Max VVF. All the Eulerian-Eulerian results are at 0.5 ms.).

cavitaion model and Zwart-Gerber-Belamri [142] model predictions are very close. Schnerr and Sauer [132] mass flow rates are close to those of the other two models for low pressure differences. Nevertheless the prediction tends to deviate as the pressure difference increases. Cavitation patterns and concentrations predicted by the present model and Zwart-Gerber-Belamri are in tandem for almost all the cases. As a result there are negligible differences in the mass flow rate values. Schnerr and Sauer model does a better job for axisymmetric nozzle compared to the case of Winklhofer nozzle. This clearly indicates that assessment of the models based only on variation of discharge coefficient is not sufficient, which is often done in the literature, for example Ref. [159]. At ΔP of 95 MPa Schnerr-Sauer, coupled with Eulerian-Eulerian, predicts 4.53 g/s of mass flow rate while Zwart-Gerber-Belamri model coupled with Eulerian-Eulerian also gives mass flow rate of 4.53 g/s. The above findings have been published in a conference [158].

Figure 4.16 displays the cavitation patterns in the nozzle at inlet pressure of 100 MPa using Zwart-Gerber-Belamri model coupled with mixture and Eulerian approach (different time steps). It is seen that a time step size of 10^{-6} is sufficiently small to capture the cavitation characteristics. There are differences in prediction using the mixture and

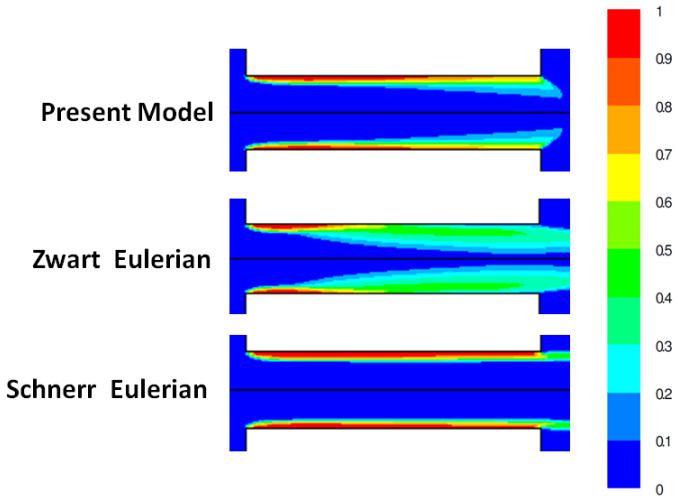

Figure 4.17: Comparison of vapour volume fraction contours for axisymmetric nozzle for Zwart-Gerber-Belamri and Schnerr-Sauer models coupled with Eulerian-Eulerian multiphase approaches and the present cavitation model at inlet pressure of 100 MPa and outlet pressure of 5 MPa.

Eulerian-Eulerian approaches. Multiphase Coupled algorithm and Per Phase Turbulence approach have been adopted for the Eulerian-Eulerian simulations as they have been proved to be desirable. Per Phase Turbulence model takes into account the turbulence transfer between the two phases. The success of this approach indicates that turbulence exchange between the two phases in a cavitating flow could be vital.

Figure 4.17 presents the volume fraction contours at 100 MPa inlet pressure and 5 MPa outlet pressure obtained from the present cavitation model, Zwart-Gerber-Belamri and Schnerr-Sauer models coupled with Eulerian-Eulerian multiphase approaches. All three predictions indicate supercavitation. At high pressure all three cavitation models provide comparable performances. However it is still interesting to see how much the prediction of two-phase flow composition changes with change in cavitation models or multiphase approaches.

Figure 4.18 presents the TKE contours at 100 MPa inlet pressure and 5 MPa outlet pressure obtained from the present cavitation model, Zwart-Gerber-Belamri and Schnerr-Sauer models coupled with Eulerian-Eulerian multiphase approaches. For the later two cases liquid phase turbulent kinetic energy information has been presented. From close observation at the contours it would be clear that the at the nozzle exit the TKE is of the order of few thousands, which is in agreement with literature findings. Schnerr-Sauer

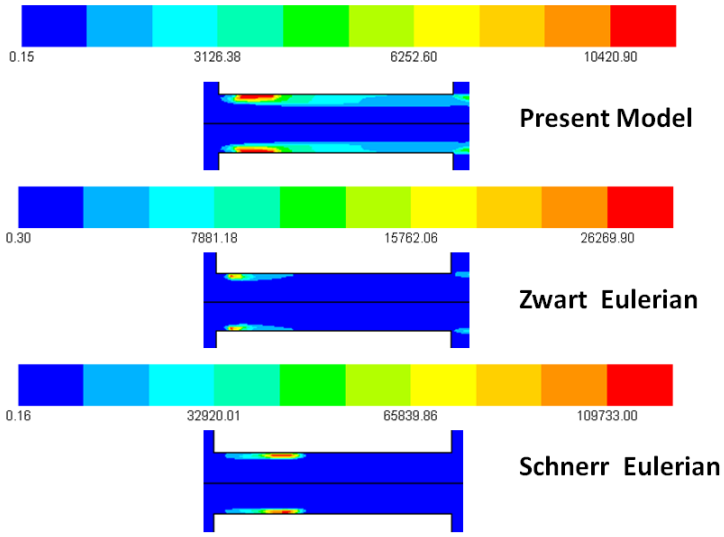

Figure 4.18: Comparison of turbulent kinetic energy (TKE) (m^2/s^2) contours for axisymmetric nozzle for Zwart-Gerber-Belamri and Schnerr-Sauer models (liquid) coupled with Eulerian-Eulerian multiphase approaches and the present cavitation model at inlet pressure of 100 MPa and outlet pressure of 5 MPa.

model predicts unusually high TKE in the cavitating region. Zwart-Gerber-Belamri and the present cavitation model values are more reasonable.

4.3 Parametric Studies

In this section role of non-condensable gases, stress effects, turbulent pressure fluctuations and bubble number density are investigated. The above-mentioned parameters are integral part of the present cavitation model. It is important to assess the significance of these factors in terms of cavitation in diesel injectors.

4.3.1 Non-condensable Gases

Non-condensable gases play an important part in the present cavitation model as well as the model by Singhal et al. [127]. In reality all liquid used in engineering applications are expected to contain trace amounts of non-condensable gases ($\approx$ ppm) [4]. In the literature

generally concentration of gas is expressed in terms of ppm. This is only correct for water as the liquid water density is 1000 kg/m^3. Typically a mass fraction of 1.5e-05 of non-condensable gas is considered to be present in fuels. It is kind of practically impossible to perfectly de-aerate a liquid used in engineering devices. These gases can exist as very small bubbles and can potentially act as nucleation sites. In the present cavitation model if there are no gas and no initial vapour then source term in Eq. B.9 will always be zero and theoretically speaking cavitation can never ever occur no matter how much pressure difference the flowing liquid is subjected to. Therefore, non-condensable gases are also mathematically important. The models which do not consider presence of non-condensable gases generally have either some adjustments in their model to have non-zero source term, e.g. Zwart-Gerber-Belamri model in case of no initial vapour [142] or some kind of internal numerical adjustments to ensure that initial liquid concentration is not exactly equal to 100 % e.g. HRM [98,101]. In Schnerr-Sauer model [132] in absence of initial vapour and no gas there is still prediction of occurrence of cavitation even though mathematically their source term goes to zero in such case. This indicates that for Schnerr-Sauer model some internal adjustments must have been made in ANSYS Fluent platform to ensure cavitation inception under favourable operating condition in case of 100 % liquid. As a result in this study for the present cavitation model a case with 0 mass fraction of non-condensable gases for operating condition of $\Delta P = 8$ MPa has been tried. Figure 4.19 shows the evidence of the role of non-condensable gases for the present cavitation model. Varying the concentrations other than zero did not yield any noticeable difference.

4.3.2 Stress

Parametric study has been done for the present cavitation model with and without stress term for a pressure difference of $\Delta P = 7.5$ MPa. Noticeable difference has not been observed. Figure 4.20 presents the effect of ignoring stress term where turbulent pressure fluctuation is still included. Som et al. [70] only indicated that including strain rate in the cavitation model can increase the probability of cavitation, but did not show to what extent it can actually affect the volume fraction predictions. In the cavitation modelling literature for high pressure diesel injectors strain rate is generally not considered. The stress effect highlighted by D. D. Joseph was mainly for creeping shear flows [130] where viscous effects are dominating over the inertia effects. D. D. Joseph only showed the regions that are more prone to cavitation due to stress. Flow in diesel injector nozzles have typically high Reynolds number indicating that inertia effects are more than viscous effects. Recently Lattice Boltzmann simulations on bubble dynamics have been carried out where bubbles are subjected to high density ratio (similar to the case of cavitation in fuel injectors) [160].

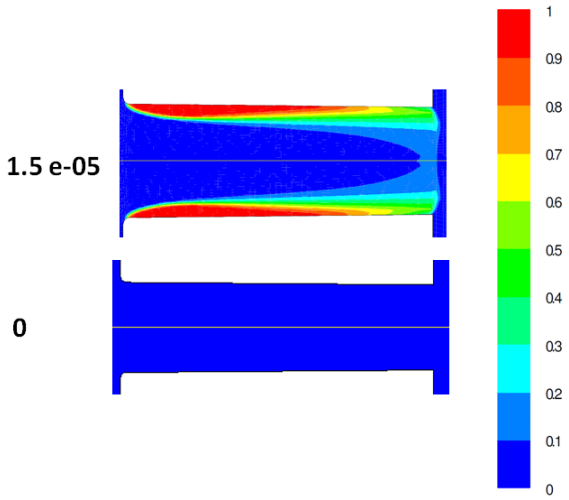

Figure 4.19: Comparison of vapour volume fraction contours with and without non-condensable gases, at (ΔP)= 8.0 MPa for Winklhofer nozzle [31].

Chen et al. [160] pointed out that shear can only distort the shape of the bubble but cannot considerably affect the change in effective bubble radius. Noticeable difference ignoring the stress term at cavitation incpetion scenario i.e. low pressure difference cases is not observed. As a result stress effects can be ignored for cavitation analysis for diesel injector applications.

4.3.3 Turbulent Pressure Fluctuation

Turbulent pressure fluctuations are not included in most cavitation models. The pressure fluctuation term containing Egler coefficient C_E is often used to estimate turbulent pressure flucutation and it includes liquid phase density [57, 117]. However, as specified before the source of C_E is not clear. Additionally turbulent fluctuation term is generally subtracted from the mean pressure. While fluctuation can be both positive or negative. Subtraction of flucutation term from mean static pressure can cause a bias to predict more cavitation. Battistoni et al. [150] discovered that considering fluctuation term ($\frac{2}{3}C_E\rho_l k_l$) can cause more cavitation than expected and got better agreement by ignoring fluctuation term. In the present study the fluctuation term is $0.47\rho k$ where mixture density is used. Singhal et al. [127] also used mixture density for estimation of flucutation terms. Both the expressions for fluctuation term in the present model and Singhal et al. model are obtained from the Ref. [120] where the correlations were proposed for single phase flow and isotropic

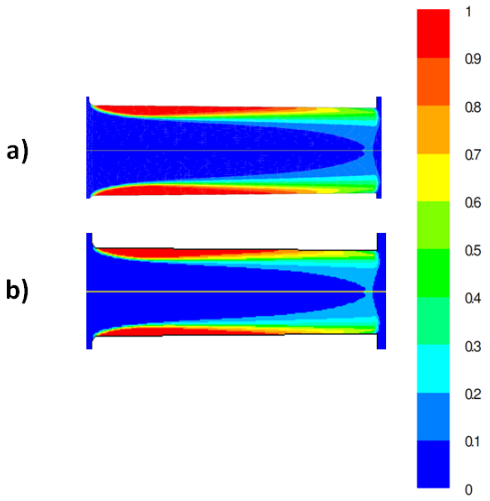

Figure 4.20: Comparison of vapour volume fraction contours for the cases a) considering saturation pressure, turbulent fluctuation and stress and b) considering saturation pressure and turbulent fluctuation at (ΔP)= 7.5 MPa for Winklhofer nozzle [31].

turbulence. Appropriate correlation for two-phase cavitating flow does not exist in the literature. In the present study sample results are shown where both pressure fluctuation and stress terms are included and in the other case both are ignored. Stress effects have been already proved to have negligible effects. Figure 4.21 shows a sample result for the case of $\Delta P = 7.5$ MPa for Winklhofer nozzle [31]. Figure 4.22 presents the effect of considering only saturation pressure compared to the case where both turbulent fluctuation and stress effects are considered with saturation pressure.

In both the figures it is seen that taking only saturation pressure into account, substantial cavitation is predicted. The fluctuation term used in the present model involves mixture density, which means the contribution of the fluctuation term will drop with increment in vapour volume fraction. As a result strong bias to enhance cavitation does not occur with the present cavitation model when turbulent fluctuation is taken into account. These results indicate that fluctuation term in the present model does not play a major role. Therefore, it means when there is high pressure difference, pressure drop around the inlet can be large enough to cause cavitation without the aid of fluctuation and stress terms. As a result consideration of only the saturation pressure could be reasonable for cavitation in fuel injector.

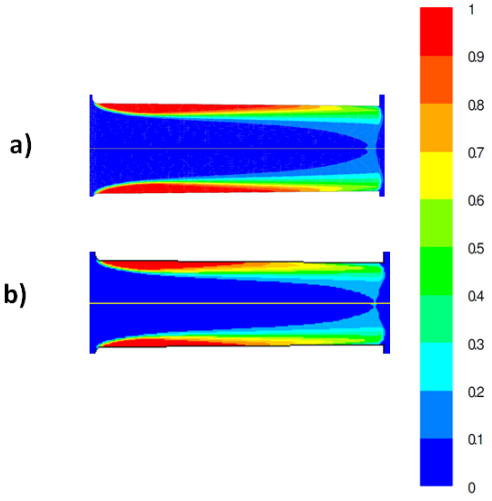

Figure 4.21: Comparison of vapour volume fraction contours for cases a) considering saturation pressure, turbulent fluctuation and stress and b) considering only saturation pressure, at (ΔP)= 7.5 MPa for Winklhofer nozzle [31].

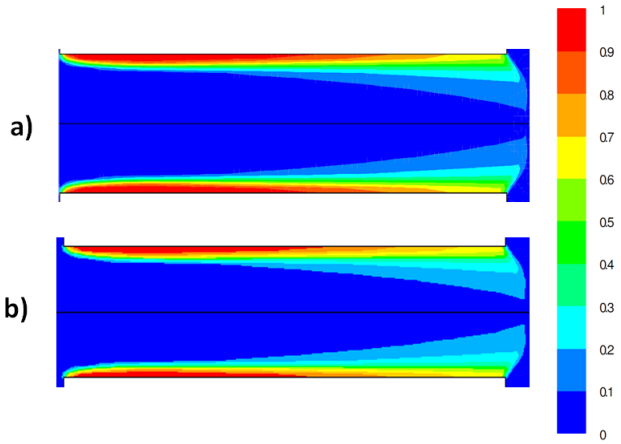

Figure 4.22: Comparison of vapour volume fraction contours for cases a) considering saturation pressure, turbulent fluctuation and stress and b) considering only saturation pressure, at (ΔP)= 45 MPa for axisymmetric nozzle.

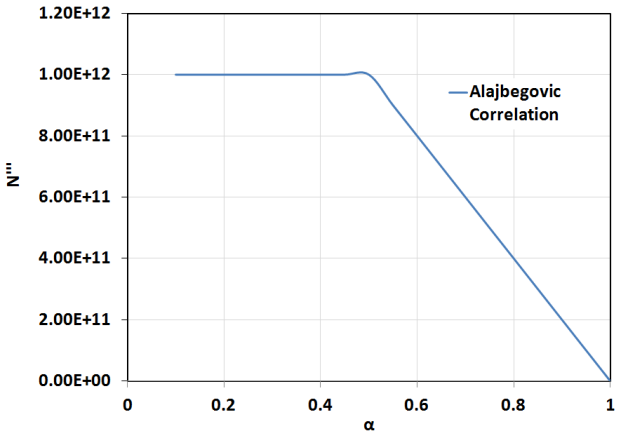

Figure 4.23: Heuristic correlation for bubble number density (N''') variation with change in vapour volume fraction (α) proposed by Alajbegovic et al. [115].

4.3.4 Bubble Number Density

It is known that there are different processes involved for evolution of bubbles causing change in bubble population over time. Assuming a constant N''' definitely misses out on those aspects in the present cavitation model. Solving for an additional governing equation for conservation of bubble population is not going to be trivial. As a way out Alajbegovic et al. in their works [112, 113, 115] proposed a heuristic methodology for variation of N''' with vapour volume fraction. Their approach was also adopted by Battistoni et al. [117] in their cavitation model implemented in AVL Fire [119]. The correlations is expressed as

$$N''' = \begin{cases} N_0''' & \alpha_v \leq 0.5 \\ 2(N_0''' - 1)(1 - \alpha_v) + 1 & \alpha_v > 0.5 \end{cases} \tag{4.1}$$

where N_0 was assumed to be 10^{12} [115, 117]. The above correlation when actually plotted will show that there is a drastic drop of N''' to unity when α approaches unity as shown in Fig. 4.23. Implementation of this correlation in the present model caused stability issues in the simulations. As a result an alternate way has been implemented to investigate the extent to which predictions can be affected due to variation in N'''.

$$N''' = \begin{cases} 10^{12} & \alpha \leq 0.5 \\ 10^{11} & \alpha > 0.5 \end{cases} \tag{4.2}$$

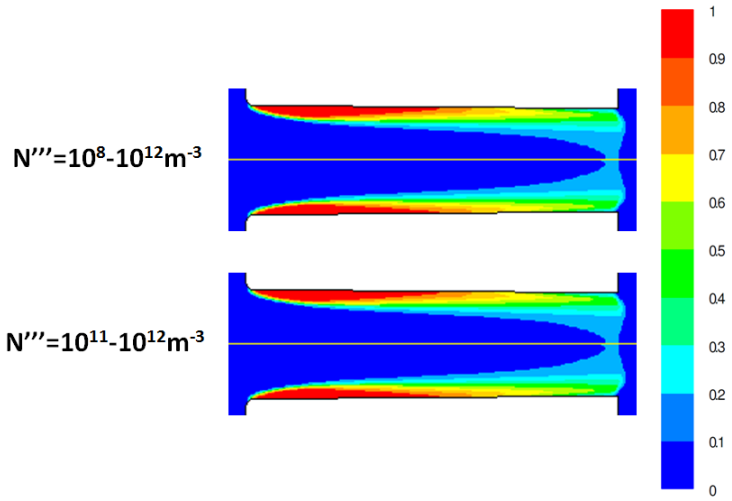

Figure 4.24: Comparison of vapour volume fraction contours at $\Delta P = 8$ MPa using Eqs. 4.2 and 4.3 for varying "N'''".

and

$$N''' = \begin{cases} 10^{12} & \alpha \leq 0.5 \\ 10^{8} & \alpha > 0.5 \end{cases} \tag{4.3}$$

The reasons behind such variations are: a) N''' mostly varies from $10^{11} - 10^{12}$ in the Alajbegovic correlation and b) Chen et al. [108] had N''' variation in the range $10^{8} - 10^{12}$. Both the variations, Eqs. 4.2 and 4.3, were attempted for the case of $\Delta P = 8$ MPa. Figure 4.24 depicts the assessment of variation of N'''. This result clearly indicates that cube root dependency of bubble radius with N''' is responsible for unperturbed behaviour of cavitation model with respect to variation of N'''. Additionally N''' decreases where α is relatively high and hence reduction in growth rate is not affecting the final result. Adding the aspect of variable N''' makes the present cavitation model physically more reasonable than the other models tested here. Consequently $N''' = 10^{12}\ m^{-3}$ has been adopted for all the remaining results. It should be noted that constant N''' cannot work for Eulerian-Lagrangian approach, as that would result in direct violation of the physics of the flow as there will be actual bubbles, with different length-scales and time-scales, involved in Lagrangian framework.

4.4 Assessment of Linear Rayleigh Equation

Most of the modelling studies use Linear Rayleigh equation for estimating the rate of bubble radius change. It is really interesting that so many intricate multi-dimensional analyses are dependant on an analytical expression. In the literature generally justification behind using such analytical expression is not given. Only work that attempted to try different methodology is by Battistoni et al. [117]. They used Non-Linear Rayleigh approach available in AVL FIRE [119]. In that approach inertia terms were considered and at each time step $\dot{R}$ was estimated in an implicit iterative manner with the help of $\ddot{R}$. $\ddot{R}$ is estimated based on the $\dot{R}$ of previous and current time step. Therefore, in that model the accuracy of the results are heavily dependant on the time-step size. Bubbles of cavities present in cavitating flow have different time-scales depending on their location in the flow-field. As a result accurate representation is not possible even in cavitaion models adopting Eulerian-Lagrangian approach because all the bubbles are assumed to be spherical in shape.

In this section some discussion has been presented on effectiveness and limitations of Linear Rayleigh by briefly analysing a single bubble growth and collapse in an environment similar to a cavitating field. Potential of Linear Rayleigh estimate in both cases have been assessed.

4.4.1 Bubble Growth

Under conditions favourable to cavitation near the inlet of the nozzle static pressure can become negative as seen by modelling studies of single phase incompressible flow in injector [9]. The concept of negative static pressure for cavitating conditions exist in the literature for quite some time [161–163]. When liquid is subjected to negative pressure i.e. tension liquid cannot exist in equilibrium and get converted to vapour and region filled with vapour have static pressure equal to the corresponding saturation pressure. This means very small gas bubbles, present in fuel, grow in those areas and liquid will also transform to vapour resulting in a rapid growth of voids.

Figure 4.25 presents an example of a negative static pressure case which a numerical result for incompressible flow would get if cavitation model is disabled. Here the growth rate of a micro-bubble is estimated under a typical situation in a fuel injector. Analytical, using Eqns. 3.11 (full Rayleigh) and 3.12 (Linear Rayleigh) as well as numerical, using Runge-Kutta method, were adopted. As shown before Linear Rayleigh originates from Eq. 3.11 which is derived from Eq. 3.10. The Full Rayleigh equation is shown here once again for convenience.

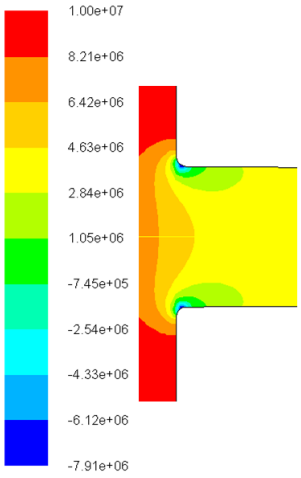

Figure 4.25: Static pressure contour for only liquid phase flow (cavitation disabled) in Winklhofer nozzle [31] for the case of $\Delta P = 8$ MPa.

$$(\dot{R})^2 = \underbrace{\frac{2(p_{\text{sat}} - p_\infty)}{3\rho_L}\left[1 - \frac{R_0^3}{R^3}\right]}_{\text{Pressure}} + \underbrace{2\frac{p_{G0}}{\rho_L}\frac{R_0^3}{R^3} ln\left(\frac{R}{R_0}\right)}_{\text{Non-condensable Gas}} - \underbrace{\frac{2\sigma_L}{\rho_L R}\left[1 - \frac{R_0^2}{R^2}\right]}_{\text{Surface Tension}}$$

Attempt has been made to assess the contribution of each term in the above equation. The first one on the R.H.S. of the above equation is denoted as Pressure, second as Gas and third as Surface Tension terms. The initial gas pressure has been calculated based on Young-Laplace equation. Initial radius is considered to be around 1.5 micron based on non-condensable gas concentration of 1.5e-05 mass fraction and bubble number density N''' of 10^{12}. It is assumed that the subjected condition is $p_{\text{sat}} - p_\infty$ is 10^6 Pa. For different bubble radii the estimation using Linear Rayleigh and Full Rayleigh as well as contribution of different terms in $\dot{R}^2$ are presented in Figs. 4.26 and 4.27. These figures indicate that Linear Rayleigh estimates for bubble growth are underestimating growth rate for very small bubbles. However for relatively larger bubbles the estimates become reasonable as the contributions of the terms due to surface tension and non-condensable gases are negligible compared to the pressure difference term.

Nonetheless in the Full Rayleigh equation viscosity term is absent. Actual Runge-Kutta estimate of bubble growth would be more convincing. Schmidt et al. [9] pointed out in his review article that residence time of a bubble in a nozzle can be in the order of microseconds. As a result a sample case has been studied where a bubble is growing from radius of 1.5 micron to approximately radius of 30 micron in 1 microsecond, subjected to

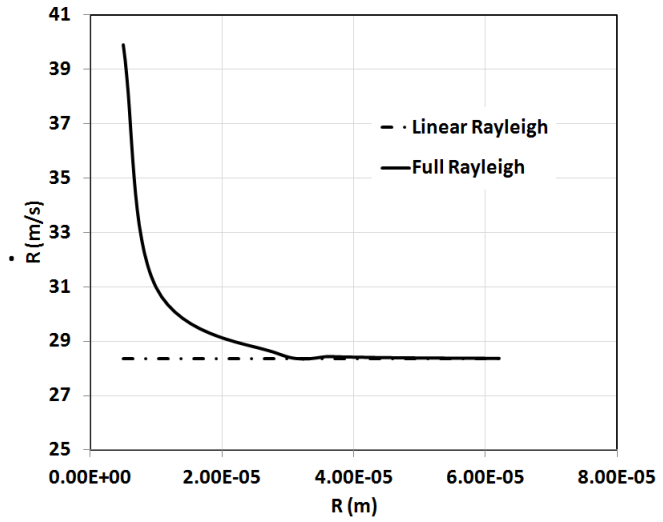

Figure 4.26: Comparison of Full Rayleigh and Linear Rayleigh estimates of bubble growth rate for different bubble radii when subjected to a typical cavitating condition in a diesel injector.

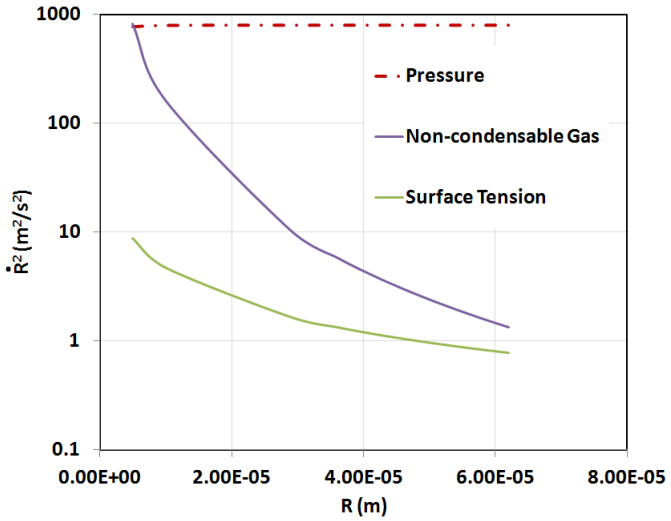

Figure 4.27: Comparison of order of magnitudes of different terms in the Full Rayleigh equation for different bubble radii when subjected to a typical cavitating condition in a diesel injector.

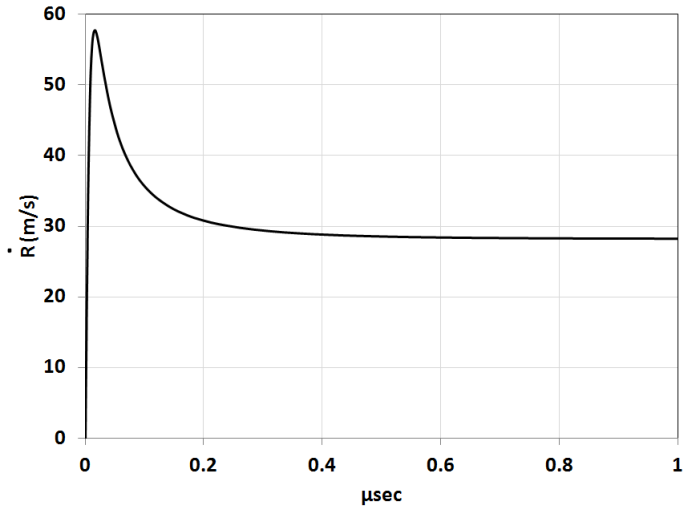

Figure 4.28: Variation of rate of change of bubble radius ($\dot{R}$) with time for a micron (initial radius) sized bubble when subjected to a typical cavitating condition in a diesel injector.

a condition of $p_{\text{sat}} - p_{\infty}$ =10^6 Pa using a Matlab code using ode45 function, a 4^{th} and 5^{th} order Runge-Kutta integration method. Sample code has been attached in Appendix D. The growth rate evolution is displayed in Fig. 4.28. After an initial surge the growth rate comes down and remain constant at a value close to the one predicted by Linear Rayleigh ($\approx$ 28.36 m/s). To further validate the utility of Linear Rayleigh for bubble growth full Rayleigh equation was implemented for growth in the cavitation UDF with collapse rate still being estimated with Linear Rayleigh. A sample result for a case of ΔP = 8 MPa for Winklhofer nozzle is presented in Fig.4.29. The vapour concentration near the wall increases to some extent, however the overall cavitation pattern is same and appreciable change in mass flow rate is not observed. Similar study has been also carried out for ΔP = 6 MPa (cavitation inception). There was no change in prediction for the low pressure case. Thus Linear Rayleigh estimate seems reasonable, so far occurrence of cavitation or bubble growth is concerned.

4.4.2 Bubble Collapse

Bubble collapse is much more complex than growth and no existing bubble dynamics equation can truly represent the behaviour of a cavitation bubble in diesel injector. Rayleigh Plesset bubble dynamics equation is based on incompressible and inviscid liquid as sur-

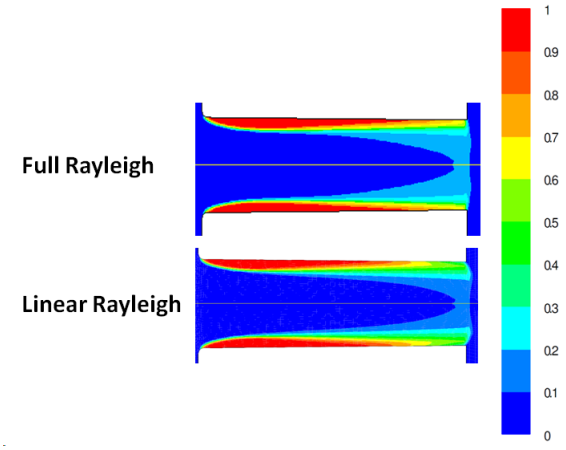

Figure 4.29: Comparison of vapour contours with Full Rayleigh and Linear Rayleigh equations for growth for a case of $\Delta P = 8.0$ MPa for Winklhofer nozzle with Linear Rayleigh still being used for collapse.

rounding medium. At bubble collapses, it is known in the literature that bubble radius drops catastrophically and adjacent liquid momentarily becomes compressible [4]. Additionally considering incompressible liquid, surrounding a bubble, sudden collapse would cause high pressure and high temperature inside a bubble which is not realistic. The bubble dynamics equations considering compressible liquid (Gilmore and Herring-Trilling equations) are more complex in nature and do not consider presence of non-condensable gases and relative velocity at bubble surface. To provide an impression of intensity of bubble collapse a numerical study for a single bubble with the Matlab code has been carried out. The bubble which grew to approximately 30 micron in 1 microsecond was subjected to high pressure with $p_{\text{sat}} - p_{\infty}$ =-10^6 Pa. Figure 4.30 displays the rapid collapse of a bubble where rate of change of bubble radius is decreasing relatively slowly and then instantaneously goes to an infinite negative value, despite the presence of non-condensable gases. Catastrophic collapse happens sooner in absence of non-condensable gases. Naturally using Linear Rayleigh equation one cannot capture this essence of collapse. More importantly it will be extremely difficult to implement the Runge-Kutta scheme in an UDF in ANSYS Fluent platform. The sudden collapse happens in the order of a nano-second which will make the cavitation simulation very unstable.

Nevertheless it should be noted that this collapse is again based on an infinite liquid medium surrounding the bubble. In typical diesel fuel injectors a bubble will be surrounded by other bubbles and probably will remain in the vicinity of nozzle wall for few microsec-

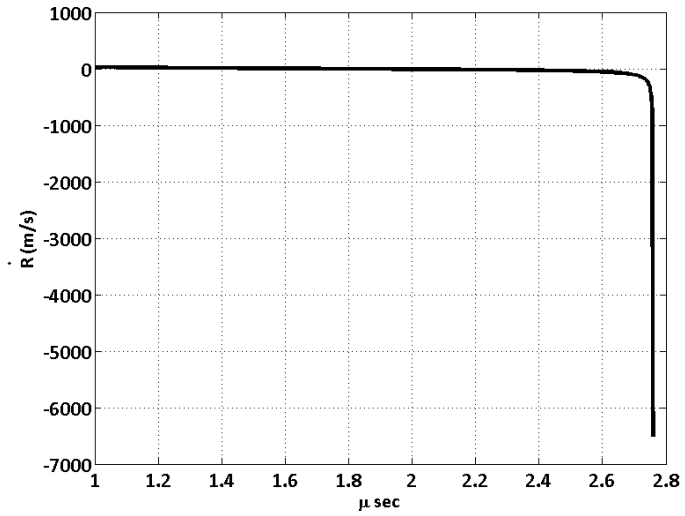

Figure 4.30: Variation of rate of change of bubble radius ($\dot{R}$) with time for 32 micron sized bubble when subjected to high pressure regions in a diesel injector.

onds. So the collapse scenario completely changes. As mentioned in the Literature Review that luminescence due to cavitation bubble collapse generally occurs after the fuel issues out of the nozzle as a jet. Probably avalanche collapse does not take place inside the injector. Literature search indicates there is an approximate time scale for bubble collapse in the vicinity of a wall. Plesset and Chapman [164] estimated the time scale for an initially spherical vapour bubble collapse near the wall which is

$$\tau \approx R_o \sqrt{\left(\frac{\rho}{\Delta p}\right)}$$

where R_o is the bubble radius before start of collapse and ρ is liquid density. As a result an approximate estimate of average bubble collapse rate near a wall would be $\frac{\Delta p}{\rho}$ which is similar to Linear Rayleigh estimate. In recent times there are many published numerical studies on bubble collapse near a wall. Nevertheless a simple expression to provide an approximate idea of the collapse rate is required. Other modelling approaches such as Eulerian-Lagrangian based Discrete Bubble Model (DBM) requires estimates of R to provide input in solving their governing equations. Even if $\dot{R}$ becomes infinite R can still be a finite small value. Consequently all the models that are based on VOF, Eulerian-Euelrian and mixture multiphase approaches cannot afford to resort to implementation of detailed bubble dynamics for estimating the source term in each computational cell.

4.5 Summary

This chapter provides insight about performance of different cavitation models as well as the multiphase approaches, pressure-velocity coupling and some important parameters affecting cavitation. The present cavitation model performed reasonably well considering its performance with respect to experimental data and other cavitation models and computational time. The performance of the present model is similar to Singhal et al. model. However the *adhoc* approximations, which were part of Singhal et al. model, have not been considered in the present cavitation model. Schnerr and Sauer, and Zwart-Gerber-Belamri cavitation models tend to perform better when switched to Eulerian-Eulerian multiphase approach specifically with Multiphase Coupled algorithm and Per Phase Turbulence Modelling approaches.

Non-condensable gases play a vital role in the present cavitation model by providing a non-zero source term when the computational domain does not have any vapour at the initial stage. Variation of bubble number density does not make noticable difference in cavitation prediction, however, inclusion of variation of number density makes the present cavitation model more consistent with the physics of the flow. Stress effects are known to be important for cavitation in creeping flows. For cavitation in high speed flows in diesel injectors stress effects are not significant. Proper expressions to estimate two-phase anisotropic turbulent flows are not available in the literature. Exclusion of turbulent pressure fluctuation does not cause significant difference and thus worth ignoring in cavitation simulations. Linear Rayleigh estimate appears to be reasonable for bubble growth and collapse considering the present state of modelling and understanding of bubble dynamics.

Chapter 5

Diesel and Biodiesel Cavitation

The model developed in this study has been used to analyse the cavitation characteristics of diesel and biodiesel in an axisymmetric nozzle of dimensions comparable to those of actual fuel injectors under injection pressures ranging from 10 MPa to 200 MPa. The axisymmetric sharp-edged nozzle, considered for the parametric study is schematically presented in Figure 3.1. The nozzle considered for the parametric study has the following geometric parameters: D/d = 4, L/d = 4, d = 0.15 mm. The nozzle diameter is denoted by d, length of the nozzle by L and diameters of the upstream and downstream extended domains are represented by D. This Chapter has been organized in the following way : a) grid independency , b) effect of pressure difference c) effect of physical properties, d) effect of turbulence models, e) effect of liquid phase compressibility, f) effect of wall roughness, g) effect of nozzle length, h) initial amplitude parameter and i) effect of pressure fluctuation. Tetradecane and methyl oleate has been used as surrogates for diesel and biodiesel respectively. Physical properties are relevant for comparative analysis and have been reported previously in Table 3.2.

5.1 Grid Independency

Three different meshes have been examined with mesh resolutions of 12×50 in Mesh I (2060 cells), 24×100 in Mesh II (9520 cells) and 48×200 in Mesh III (38080 cells) in the nozzle block (Mesh II- 24 along the diameter and 100 along the length of the nozzle). For Mesh I it is observed that the second order upwind discretization schemes were leading to divergence because the mesh is coarse. For Mesh II and Mesh III the second order discretization schemes are successfully implemented. For an inlet pressure of 100 MPa and

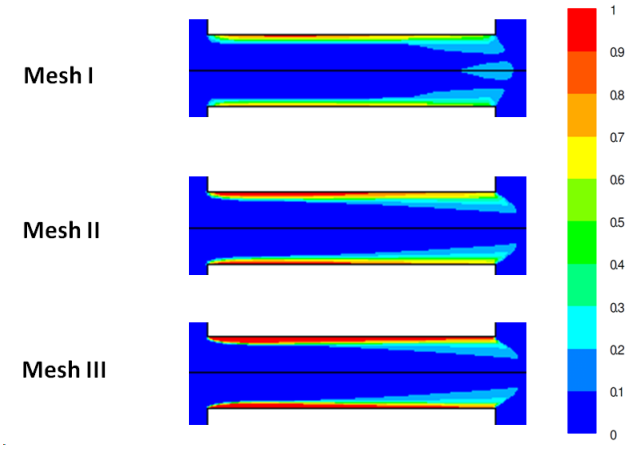

Figure 5.1: Vapour volume fraction contours obtained from the three meshes for the case of diesel with 100 MPa inlet pressure and 5 MPa outlet pressure.

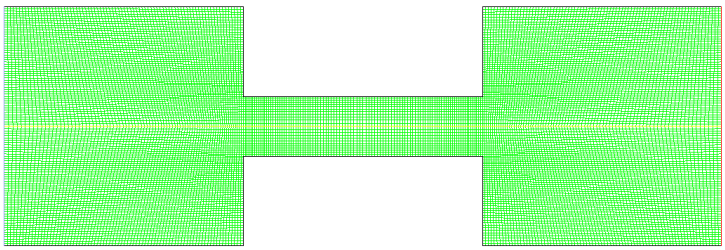

Figure 5.2: Mesh used for cavitation analysis in axisymmetric nozzle.

outlet pressure of 5 MPa, the predicted mass flow rates from Mesh II (4.55 g/s) and III (4.5 g/s) are much closer compared to the one predicted from Mesh I (4.7 g/s). Both Mesh II and Mesh III predicted supercavitation in the 100 MPa inlet pressure. The vapour volume fraction contours obtained from 3 meshes are displayed in Fig. 5.1. For the case of 200 MPa inlet pressure and 5 MPa outlet pressure the mass flow rates predicted with Mesh II and Mesh III are 6.5 g/s and 6.38 g/s respectively. There is no considerable difference in the vapour volume fraction contours predicted with the two meshes.

Based on the above-mentioned observation Mesh II has been selected as a suitable mesh for analysing cavitation in the nozzle for high injection pressures and has been shown in Fig. 5.2.

Table 5.1: Cavitation Characteristics at P_{out} = 5 MPa

Injection Pressure (MPa)	**Diesel**	**Biodiesel**
10	No Cavitation	No Cavitation
15	Cavitation Inception	No Cavitation
20	Cavitation	Cavitation Inception
25	Cavitation	Cavitation
50	Supercavitation	Supercavitation
100	Supercavitation	Supercavitation
150	Supercavitation	Supercavitation
200	Supercavitation	Supercavitation

5.2 Effect of Pressure Difference

The injection pressures examined in this study are 10, 15, 20, 25, 50, 100, 150 and 200 MPa with outlet pressure being fixed at 5 MPa for both diesel and biodiesel. A summary of cavitation characteristics observed through simulations for diesel and bio-diesel, subjected to different injection pressures with fixed outlet pressure are presented in Table 5.1. Cavitation inception occurs at an injection pressure of 15 MPa for diesel, while it is observed at an injection pressure of 20 MPa for biodiesel. For 50 MPa and higher inlet pressures both diesel and biodiesel tend to supercavitate.

Cavitation inception for diesel occurred at an injection pressure of 15 MPa while onset of cavitation was observed at an injection pressure of 20 MPa for biodiesel. Figure 5.3 shows the onset of cavitation for diesel and biodiesel. For the case of 50 MPa injection pressure both diesel and biodiesel show supercavitation in the nozzle considered in this study with the outlet pressure fixed at 5 MPa. The vapour contours for both diesel and biodiesel are presented in Fig. 5.4. In both cases supercavitation occurs. The important observation is that for very high pressure differences between the inlet and outlet sufficiently low pressure regions can develop leading to considerable cavitation of biodiesel. The reason behind the difference in cavitation characteristics at low and high pressure differences for diesel and biodiesel will be discussed in the section "Effect of Physical Properties".

The variation of mass flow rate with pressure difference has been shown in Fig 5.5. For low pressure difference the mass flow rate of diesel is little bit more than that of biodiesel, while for high pressure difference the trend is reversed. When both diesel and biodiesel

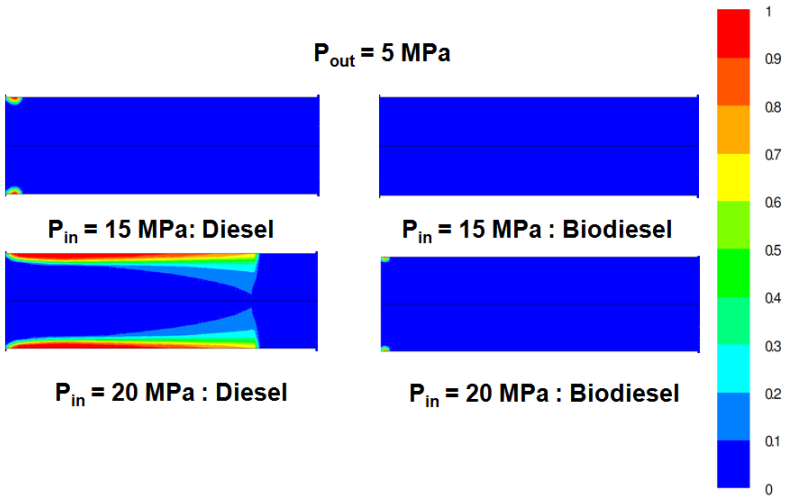

Figure 5.3: Comparison of vapour volume fraction contours at cavitation inception of diesel and biodiesel

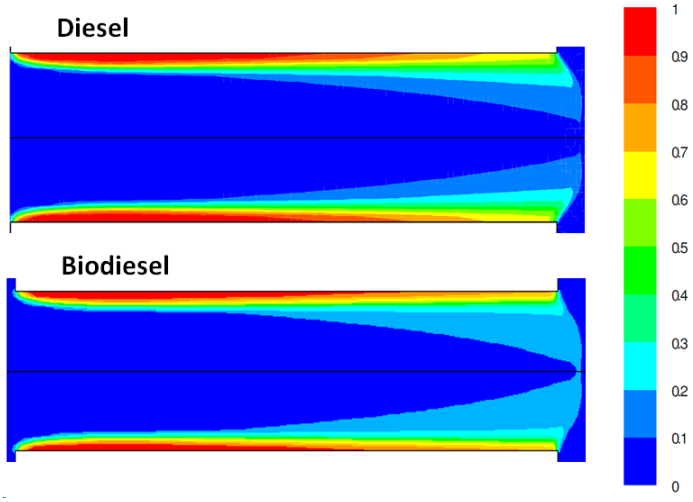

Figure 5.4: Comparison of vapour volume fraction contours of supercavitation of diesel and biodiesel at an injection pressure of 50 MPa and outlet pressure of 5 MPa

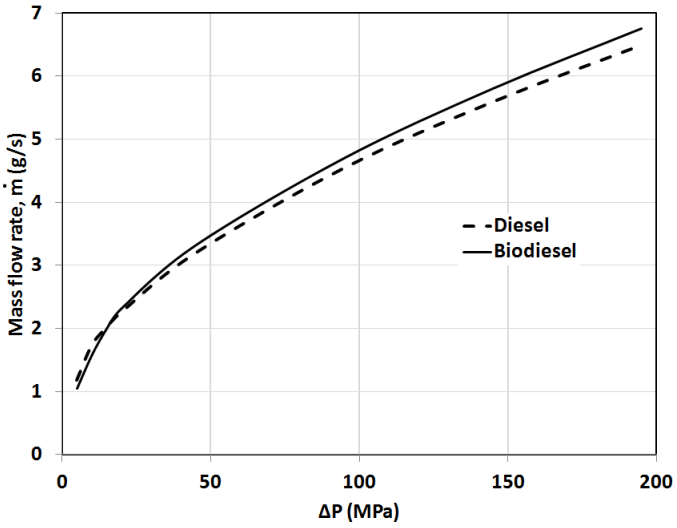

Figure 5.5: Comparison of mass flow rates of diesel and biodiesel for different pressure differentials (between inlet and outlet,ΔP) with outlet pressure being 5 MPa.

undergo considerable cavitation or supercavitation the liquid phase is not in complete contact with the nozzle wall and as a result the resistance to the bulk flow due to viscous effects is not prominent as the vapour phase viscosities are very low. Similar trends have been observed in experimental study of diesel and biodiesel cavitation at low injection pressures by Suh et al. [35]. Therefore, the extent of cavitation is the determining factor for the mass flow rate of diesel and biodiesel. The above result has been published in a conference [165].

The two important non-dimensional parameters that helps to characterize the diesel and biodiesel cavitating flow are discharge coefficient (C_D) and Reynolds number (Re) as mentioned before in the Introduction chapter. Figure 5.6 displays the change of discharge coefficient (C_D) and Reynolds number (Re) with the injection pressure difference (ΔP) between the inlet and outlet. The actual mass flow rate values are obtained from the simulation results. For higher pressure differences the values of C_D for both diesel and biodiesel come very close to 0.61 which is the characteristic value of C_c for very high pressure differences [9]. C_D values for diesel are higher than that of biodiesel for low pressure differences, however for high pressure differences the trend is reversed. At low pressure differences biodiesel being more viscous will have lower flow efficiency. On the other hand when supercavitation takes place biodiesel flow will not be affected by viscosity as it is shrouded with vapour film. Diesel being lighter than biodiesel will have lower flow

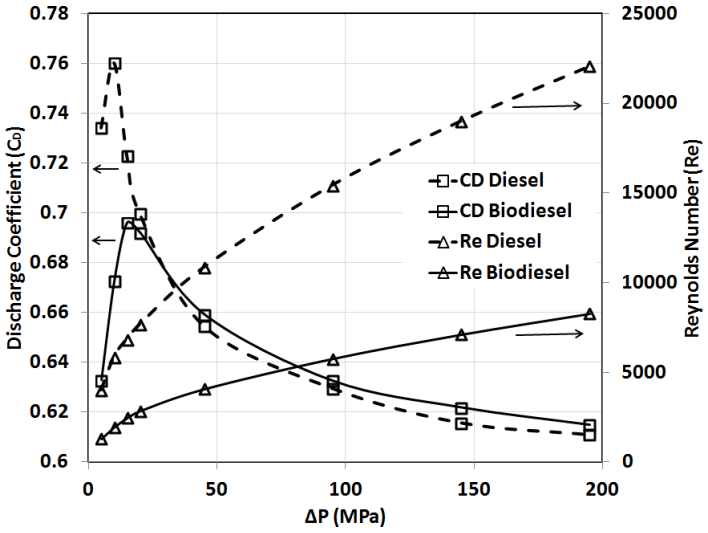

Figure 5.6: Comparison of discharge coefficient (C_D) and Reynolds number (Re) for diesel and biodiesel for different cavitating conditions at different injection pressure differences (between the inlet and outlet, ΔP) with outlet pressure being 5 MPa.

efficiency with respect to biodiesel. The increase in C_D in non-cavitating region indicates with higher pressure difference viscous losses become negligible, while decrease in C_D at high pressure differences is because with more cavitation effective exit area of the flow is reducing. For the Reynolds number a large difference is seen between diesel and biodiesel at any given pressure difference. The average velocity values for a given pressure difference at the nozzle exit are close for diesel and biodiesel. Viscosity of biodiesel, used in this study, is approximately 2.5 times higher than that of diesel. Therefore, at any given pressure difference, the numerator in Re for diesel can be close to that of biodiesel, while the denominator of Re of biodiesel is always 2.5 times higher than that of diesel. As a result transition to turbulence is much quicker in case of diesel compared to biodiesel. Similar variation of the Reynolds number of diesel and biodiesel was also observed by Suh et al. [35] in their experimental study. The above result has been published in a journal article [157].

5.3 Effect of Physical Properties

From Table 3.2 it is clear that the two key physical properties that have considerable difference between the two fuels are liquid phase viscosity (Diesel-0.0025 Pa.s; Biodiesel-0.00694 Pa.s) and saturation pressure (Diesel-1000 Pa; Biodiesel-1 Pa). Liquid phase densities are different but not by order of magnitude (Diesel-822.7 kg/m^3;Biodiesel-877.2 kg/m^3). Vapour phase properties are not only different, but they are order of magnitude lower compared to those of liquid phase. Surface tension is not considered in the present model. Battistoni et al. [117] in their cavitation analysis of diesel and biodiesel observed that in cases where the flow is not fully cavitating, liquid phase viscosity affects the discharge coefficient. They observed that saturation pressure and density do not play a major role in determining the nature of cavitating flow even though there are considerable differences for the two fuels.

Hence a similar numerical experiment has been carried out by considering hypothetical fluids with property values swapping between diesel and biodiesel. For inlet pressures 50 MPa and above both diesel and biodiesel supercavitate. However for 25 MPa inlet pressure diesel supercavitate and biodiesel does not. As a result the numerical experiment has been done for the given geometry of the nozzle for an inlet pressure of 25 MPa and outlet pressure of 5 MPa and four different cases have been compared : a) diesel, b) diesel with saturation pressure of biodiesel, c) diesel with viscosity of biodiesel and d) biodiesel. Figure 5.7 presents the vapour contours for four different cases. The extent of the cavitating region drastically reduces when diesel viscosity is replaced by that of biodiesel and the cavitation pattern looks almost the same as that of biodiesel. For this given pressure difference biodiesel has lower velocities around the inlet edge, thus lower dynamic pressures due to higher viscosity. Therefore, the difference between the saturation pressures of 1000 Pa for diesel and 1 Pa for biodiesel is negligibly small compared to the dynamic pressures associated with velocities of hundreds of m/s. Consequently biodiesel cavitates less compared to diesel in this case. Thus it is inferred that liquid viscosity plays a more important role compared to the saturation pressure when the pressure difference across the nozzle is not high enough to cause extensive cavitation. The above findings have been published in a journal article [157]. It has also been observed that turbulent viscosity near the inlet, in the cavitating regions, turbulent viscosity is in the order of 10^{-4} to 10^{-5} kg/(m.s) where liquid phase molecular viscosity is considerably higher for example 0.0025 kg/(m.s) for diesel. When fuel enters the nozzle hole the molecular viscosity dominates over turbulent viscosity in the cavitating regions. In the non-cavitating regions turbulent viscosity is in the order of molecular viscosity or even higher upto the order of 10^{-1} kg/(m.s). The molecular viscosity is playing an important role for the low pressure difference cases, where Reynolds number

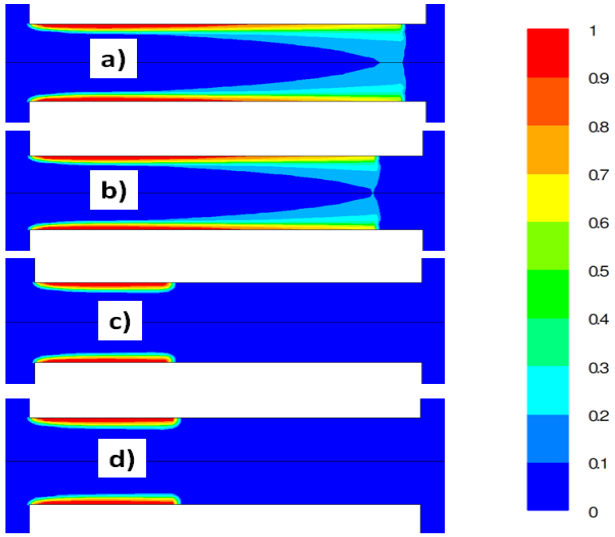

Figure 5.7: Comparison of vapour volume fraction contours of diesel and biodiesel for the inlet pressure of 25 MPa and outlet pressure of 5 MPa: a) diesel, b) diesel with biodiesel saturation pressure, c) diesel with biodiesel viscosity and d) biodiesel.

is relatively low and the flow is probably in the transitional regime. At high Reynolds number, however turbulent viscosity is dominant and molecular viscosity is not going to play a determining role. Therefore for high pressure differential cases i.e. cases with high Reynolds number, both diesel and biodiesel undergo considerable cavitation. In actual fuel injectors when the needle is open, injection pressure is very high (≈200 MPa or higher) and turbulent viscosity will be dominating over molecular viscosity in those scenarios.

5.4 Effect of Turbulence Models

Three turbulence models, realizable and renormalization group or RNG $k-\epsilon$ models and Shear-Stress Transport or SST $k-\omega$ model are tested to analyse the effects of turbulence models in cavitation analysis. All these three models are known to have certain advantages over standard $k-\epsilon$ and $k-\omega$ models. RNG $k-\epsilon$ model is supposed to be better than standard $k-\epsilon$ model as it is developed to give good results for high as well as low Reynolds numbers [67]. While realizable $k-\epsilon$ model gives better performance for flows involving rotation, boundary layers under strong adverse pressure gradients, separation and recirculation [67]. SST $k-\omega$ model is expected to be more reliable than the standard one because

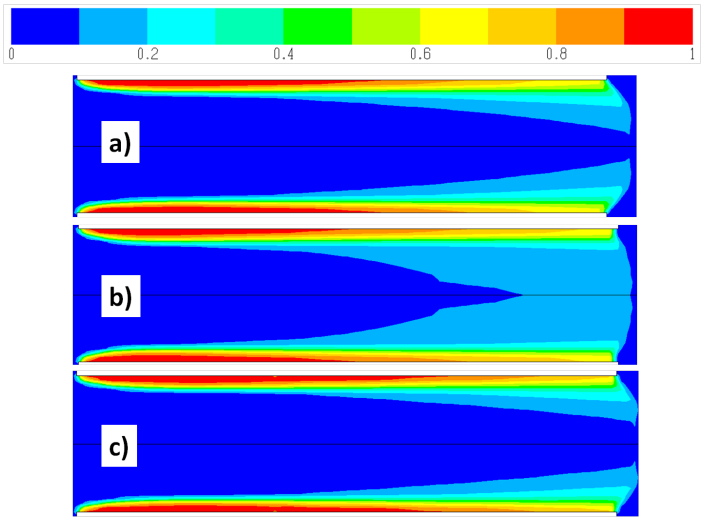

Figure 5.8: Comparison of vapour volume fraction contours for diesel obtained from different turbulence models: a) RNG $k-\epsilon$, b) realizable $k-\epsilon$ and c) SST $k-\omega$ model, with the inlet pressure of 50 MPa and outlet pressure of 5 MPa.

in this model characteristics of both $k-\epsilon$ and $k-\omega$ models are incorporated with the help of a blending function [67]. Hence this model is expected to work well in near wall regions as well as away from the wall and gives good performance for a wide range of flows. For SST $k-\omega$ turbulence model low Reynolds number correction has not been used as it can capture the essence of viscous sublayer without this correction [67]. It is also generally recommended to avoid this correction if accurate information about laminar to turbulent transition is not available [67].

For an inlet pressure of 50 MPa and outlet pressure of 5 MPa results from three different turbulence models are presented in Fig. 5.8. This result has been published in a journal article [157]. The vapour contour for realizable $k-\epsilon$ model is visibly different from other two models. The reason behind noticeable difference is that $C_{\mu t}$ is not constant as it is in the other two models used in comparison. SST $k-\omega$ model predicts a relatively longer high concentration region near the wall, but away from the wall the vapour distribution is similar to RNG $k-\epsilon$ model. This is because away from the wall SST $k-\omega$ model behaves similar to a typical $k-\epsilon$ model. Figure 5.9 shows the turbulent kinetic energy distribution in the nozzle area for the 3 models used. Realizable $k-\epsilon$ model generates order of magnitude higher value compared to RNG $k-\epsilon$ and SST $k-\omega$ models.

Figure 5.10 presents the variation in vapour contour for an inlet pressure of 50 MPa

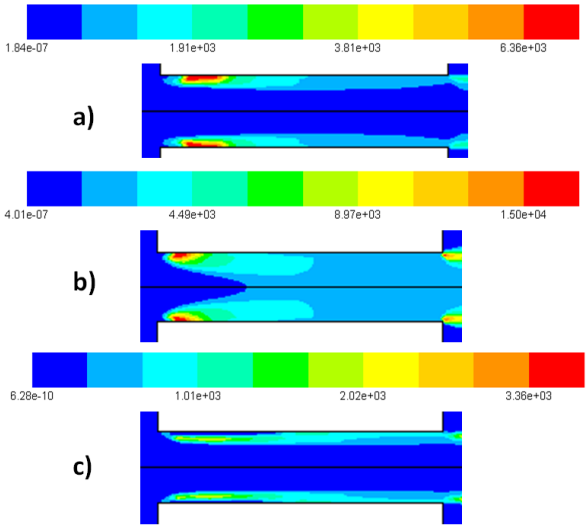

Figure 5.9: Comparison of turbulent kinetic energy contours for diesel obtained from different turbulence models: a) RNG $k-\epsilon$, b) realizable $k-\epsilon$ and c) SST $k-\omega$ model, with the inlet pressure of 50 MPa and outlet pressure of 5 MPa.

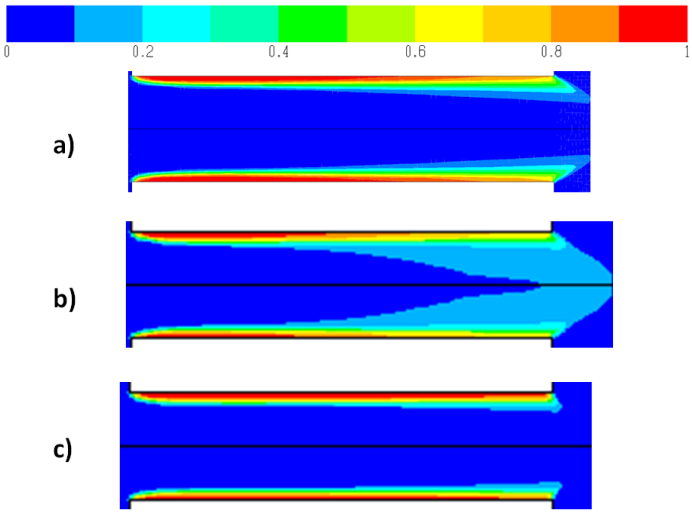

Figure 5.10: Comparison of vapour volume fraction contours for diesel obtained from different turbulence models: a) RNG $k-\epsilon$, b) realizable $k-\epsilon$ and c) SST $k-\omega$ model, with the inlet pressure of 150 MPa and outlet pressure of 5 MPa.

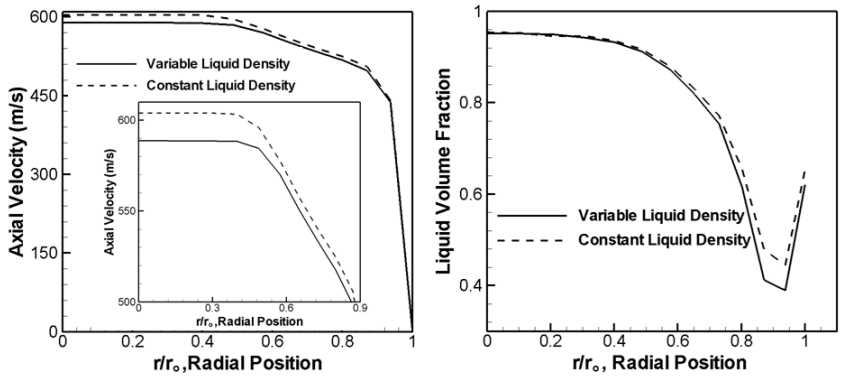

Figure 5.11: Comparison of velocity and liquid volume fraction profiles for diesel at the exit of the nozzle section for inlet pressure at 150 MPa and outlet pressure at 5 MPa.

and outlet pressure of 5 MPa results from three different turbulence models. For SST $k-\omega$ model first order schemes had to be used except for pressure and vapour for stability reasons. Compressibility could not be implemented for SST $k-\omega$ due to stability issues. The mass flow rates were found to be very close to each other for these three models. The RNG $k-\epsilon$ model was found to be relatively more stable compared to the other two models especially for higher pressure differences. Realizable $k-\epsilon$ model takes considerably more time to converge specially for biodiesel. SST $k-\omega$ model does not provide stable results for all cases. As a result RNG $k-\epsilon$ model is considered to be a reliable turbulence model for cavitation analysis in diesel injectors.

5.5 Effect of Liquid Compressibility

Compressibility of the liquid phase has been accounted for in this study. The vapour phase has been always considered to be compressible by using ideal gas law for density variation. Since the outlet pressure was fixed at 5 MPa the change in the liquid phase density becomes prominent only at very high injection pressure. Noticeable difference due to compressibility in velocity field is not observed for inlet pressure up to 100 MPa. For an injection pressure of 150 MPa liquid phase density is kept constant and also varied for both diesel and biodiesel to understand the effect of liquid density variation. The velocity and the liquid volume fraction profiles at the exit of the nozzle section are plotted in Fig. 5.11 for diesel fuel. Apparently, there is not much difference in the velocity profiles in the two cases: variable liquid density and constant liquid density. For the variable liquid

Table 5.2: Effect of liquid density variation in case of diesel fuel

Flow Parameters	**Variable Liquid Density**	**Constant Liquid Density**
Mass flow rate (g/s)	5.6	5.5
Maximum velocity magnitude (m/s)	592	607
Maximum liquid phase density (kg/m^3)	914	822.7

Table 5.3: Effect of liquid density variation in case of biodiesel fuel

Flow Parameters	**Variable Liquid Density**	**Constant Liquid Density**
Mass flow rate (g/s)	5.8	5.7
Maximum velocity magnitude (m/s)	573	586
Maximum liquid phase density (kg/m^3)	961	877.2

density, the velocity seems to be slightly lower compared to the constant liquid density case. However, if the core region is magnified, it can be seen that there is around 15-20 m/s of difference due to compressibility. There is some difference in liquid volume fraction towards the wall. It is also seen that with liquid density variation the liquid mass fraction is lower than that of constant liquid density. When the liquid phase is compressible, liquid density adjacent to the cavitating regions is low as the local pressure will be quite low. Hence the vapour bubbles can push the liquid phase more compared to the case where the liquid phase density is constant. Near the wall the liquid volume fraction abruptly rises and that is because the profile is at the exit of the nozzle section and at that axial location, near the wall the cavitating region has almost ended. The above findings have been published in a journal article [157].

Tables 5.2 and 5.2 presents the mass flow rate, maximum liquid phase density and maximum liquid phase velocity for the two cases for diesel and biodiesel fuel respectively. There is around 10% deviation in liquid phase density from the constant value. The liquid density variation thus affects the velocity field. Figure 5.12 shows the liquid phase Mach number and volume fraction contours for a case of 150 MPa injection pressure and outlet pressure fixed at 5 MPa. From the liquid Mach number contour it is seen that the liquid phase Mach number can go as high as 0.44. Mach number contour is presented with the

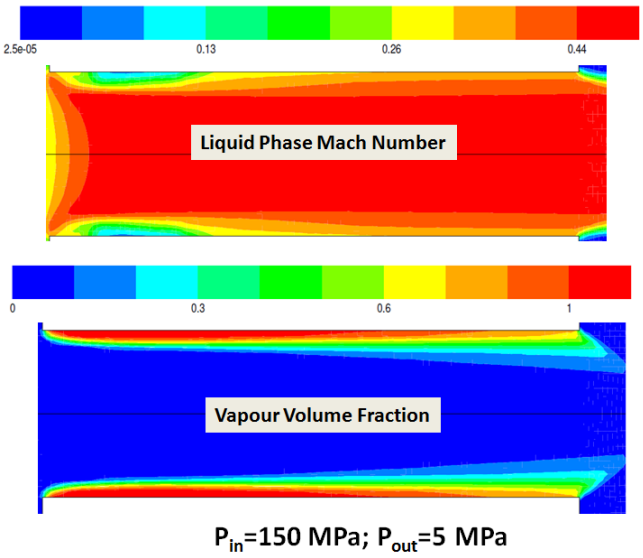

Figure 5.12: Liquid phase Mach number and vapour volume fraction contours for diesel fuel in the nozzle section for injection pressure of 150 MPa and outlet pressure of 5 MPa.

vapour contour to emphasize how the Mach number varies in the liquid phase dominant region as that is the region of interest for analysing the relevance of liquid compressibility formulation. It is seen from Fig. 5.13 that the liquid phase Mach number for biodiesel can go as high as 0.41, and there is no significant change in mass flow rate values by considering liquid phase biodiesel as compressible. Figure 5.14 compares the liquid phase Mach numbers for diesel and biodiesel at 200 MPa inlet pressure and 5 MPa outlet pressure depicting further increase of compressibility at higher pressures. Schmidt and Corradini in their review article [9] indicated that liquid phase Mach number can exceed 0.4. It should be also noted that inside a fuel injector there are needle movements and injection pressure fluctuations causing temporal variations in the flow field. There are pressure waves propagating back and forth inside the injector. Therefore, liquid phase compressibility is definitely an important factor to be considered for the cavitating flow.

5.6 Effect of Wall Roughness

Wall roughness has also been addressed in this study. Echouchene et al. [148] carried out the numerical study of wall effects on cavitation for a large nozzle of diameter of 8 mm with wall roughness height going upto 100 microns. In case of fuel injector the diameter of

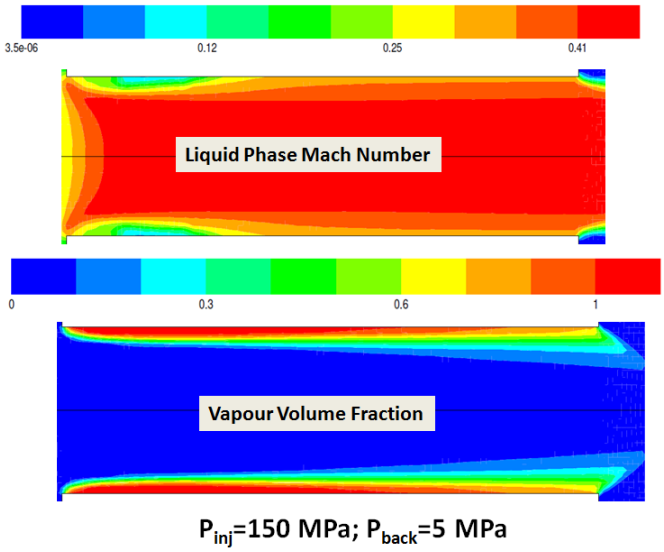

Figure 5.13: Liquid phase Mach number and vapour volume fraction contours for biodiesel fuel in the nozzle section for injection pressure of 150 MPa and outlet pressure of 5 MPa.

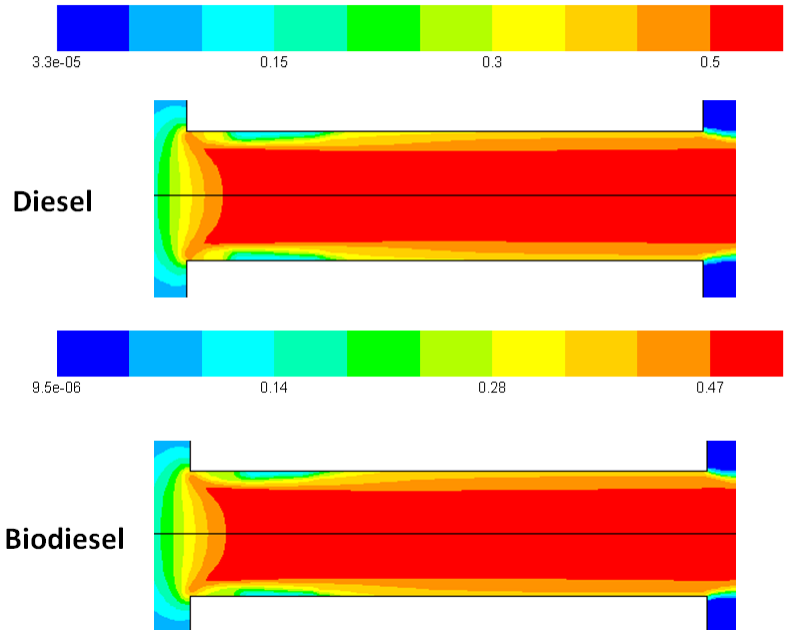

Figure 5.14: Comparison of liquid phase Mach number contours for diesel and biodiesel in the nozzle section for injection pressure of 200 MPa and outlet pressure of 5 MPa.

Figure 5.15: Vapour volume fraction contours for a) smooth wall and b) wall roughness height of 5 microns for diesel at inlet pressure of 15 MPa and outlet pressure of 5 MPa

Figure 5.16: Vapour volume fraction contours for a) smooth wall and b) wall roughness height of 5 microns for biodiesel at inlet pressure of 20 MPa and outlet pressure of 5 MPa

the holes are in the range of 150−200 microns. In actual fuel injectors the roughness height is in the range of 400−500 nm [166]. From the work by Echouchene et al [148] it is known that wall roughness is not important for high pressure differences as there is considerable cavitation for high pressure difference and the liquid phase is not fully in contact with the wall. Hence the wall roughness does not affect the flow under those conditions. Therefore, wall roughness height has been suggested to be important only for cases of cavitation inceptions.

For diesel the injection pressure required is 15 MPa and for biodiesel it is 20 MPa with an outlet pressure of 5 MPa. There is an upper limit of wall roughness height that can be used in the modelling study. The wall roughness height cannot be more than the dimension of the cell adjacent to the wall in the direction perpendicular to it [67]. Based on the resolution of Mesh II chosen for this study 5 microns is calculated to be the limiting height for surface roughness. Vapour contours for the cases of smooth wall and a wall with roughness height of 5 microns are compared in Figs. 5.15 and 5.16 for diesel and biodiesel respectively. Noticeable differences are not observed in the vapour contours for both diesel and biodiesel which means in actual fuel injectors where surface roughness is at sub-micron level the wall roughness is not going to be a matter of concern for cavitation in fuel injectors. The above findings have been published in a journal article [157].

5.7 Effect of Nozzle Length

Previous studies indicate that converging nozzles tend to cavitate less as the flow separation is suppressed. Moreover, nozzles with rounded inlet experience less cavitation compared to nozzles with sharp-edged inlet, because flow separation is enhanced for nozzles with sharp-edged inlets. Effect of nozzle length is relatively less explored. To understand the effect of nozzle length, cavitation simulations have been done with three L/d ratios, 2, 4 and 6. Previous studies have shown that with change in nozzle length the discharge coefficient of diesel fuel is not affected significantly [69]. The mass flow rates with change in L/d ratio for an inlet pressure of 25 MPa remained almost constant. Generally discharge coefficient does not change significantly with change in length, which suggests clearly that the mass flow rate values should not be changing considerably. However, it is noted that there is a decreasing tendency of mass flow rate with increase in L/d ratio. This is because with increment in nozzle length there is more contact area between the liquid phase and the solid wall which enhances the resistance to the flow. Figure 5.17 shows the cavitation patterns of diesel in three different nozzles for three different L/d ratios (2, 4 and 6) for d = 150 μm with inlet pressure of 25 MPa and outlet pressure of 5 MPa. For the shortest

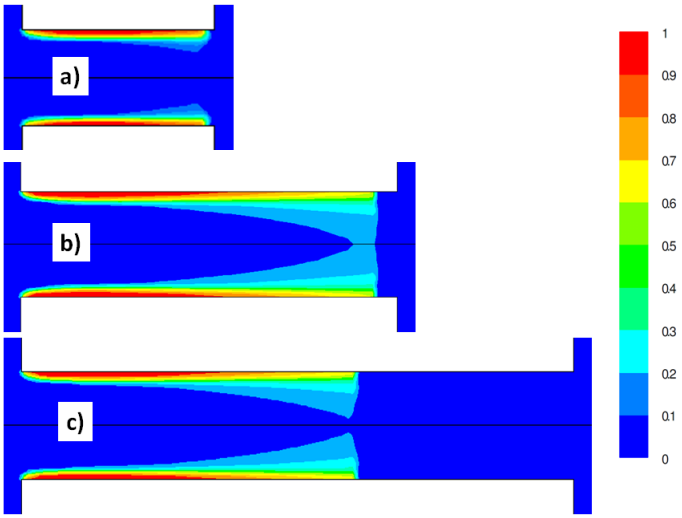

Figure 5.17: Comparison of vapour volume fraction contours with different L/d ratios for diesel for an inlet pressure of 25 MPa and outlet pressure of 5 MPa.

nozzle supercavitation occurs, while for L/d = 4 and 6 cavitation region do not reach the exit of the nozzle especially in case of L/d = 6. The range of cavitation region for L/d = 6 is very close to that in case of L/d = 4. Thus it is seen that length of the nozzle can govern the composition of the two-phase flow in the nozzle for a given pressure difference.

5.8 Model Prediction For Initial Amplitude Parameter

Initial amplitude parameter is often used to characterize the flow at the exit of the fuel injector. It is generally denoted as amp_0. The concept of amp_0 originates from Taylor Analogy Breakup (TAB) model [167] and amp_0 is mathematically defined as

$$amp_0 = \frac{1}{C_b r_0 \omega_0} \cdot \sqrt{\frac{2}{3} k_0} \tag{5.1}$$

where ω_0 is the initial droplet oscillation frequency and is expressed as

$$\omega_0 = \sqrt{C_k \frac{\sigma}{\rho_l r_0^3} - \left(\frac{C_d \mu_l}{2\rho_l r_0^2}\right)^2} \tag{5.2}$$

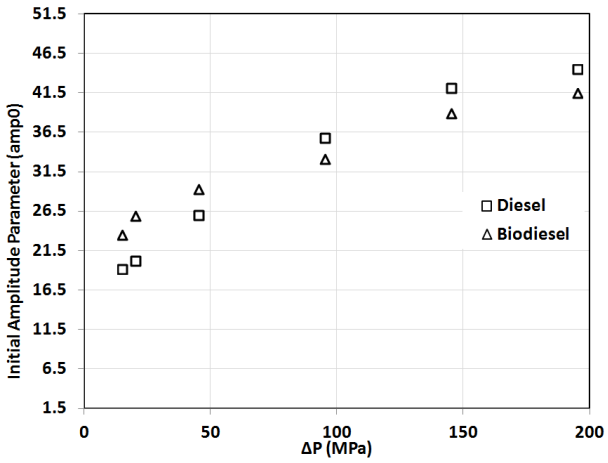

Figure 5.18: Variation of initial amplitude parameter for diesel and biodiesel for axisymmetric nozzle with change in pressure difference.

and k_0 is the average turbulent kinetic energy at nozzle exit, r_0 is the nozzle exit radius as well as the hypothesized initial droplet radius after the liquid fuel jet leaves the nozzle, with $C_b = 0.5$, $C_k = 8$ and $C_d = 5$. The values of the constants have been obtained from Refs. [167, 168]. The values of area-averaged turbulent kinetic energy are obtained from the numerical simulations. The parameter amp_0 provides an estimate about the influence of the turbulent intensity at the nozzle exit on the initial droplet breakup [167].

Figure 5.18 depicts the evolution of amp_0 with change in pressure differences. Higher amp_0 indicates larger spray angle and smaller droplets [167]. Larger droplets are less prone to deviate radially as axial inertia will be higher. This means at higher pressure differences diesel is going to have wider spray angles and smaller droplets and at lower pressure differences biodiesel will have wider spray angle as well as smaller droplets. At lower pressure differences biodiesel will have lower axial momentum due to higher viscosity and hence will be relatively affected more by the radial disturbances at the exit. While at higher pressure differences diesel will have less axial momentum as due to extensive cavitation both liquid diesel and biodiesel will have less contact with the wall and density of biodiesel being higher, biodiesel will have higher inertia.

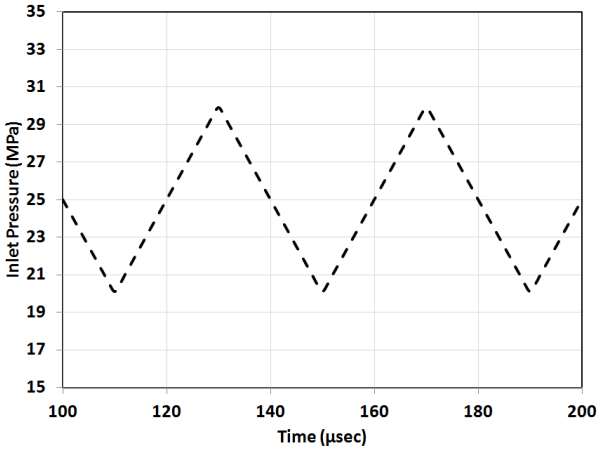

Figure 5.19: Sample inlet pressure fluctuation while mean inlet pressure is 25 MPa.

5.9 Effect of Pressure Fluctuation

In an actual fuel injector the injection pressure does not remain constant even if the needle is fully open. There are typically oscillations in the needle as well as fluctuations in the injection pressure. There can be more than one reason behind such vacillations. The common rail maintaining the fuel at very high pressure can make the liquid fuel compressible and promote transmission of pressure waves back and forth. Additionally when the needle closes and then again opens, the impact with the needle seat also causes perturbations. Examples of intense pressure fluctuations ($\approx$ 10 - 20 %) are available in the literature [101, 169]. While modelling the pressure fluctuations for a fixed needle opening a triangle wave [169] is often used to approximately represent pressure fluctuations at the inlet. Effect of pressure fluctuation has been only studied for diesel. In this study pressure fluctuation effects are investigated for both diesel and biodiesel using the present cavitation model. Amplitude of 20 % of mean inlet pressure has been implemented and a sample pressure variation with time is shown in Fig. 5.19.

Figures 5.20 and 5.21 show the variation of vapour contours during the time duration 100 - 130 μs for both diesel and biodiesel at mean inlet pressure of 25 MPa and outlet pressure of 5 MPa. It is interesting to note that with drop in inlet pressure the vapour region expands in the core region and contracts when the inlet pressure goes up. This is because with drop in inlet pressure vapour region pushes the liquid phase, and when inlet pressure rises increased liquid inertia pushes the vapour region. In other words sharp increment in pressure is causing the vapour bubbles to collapse. Similar observations were made by

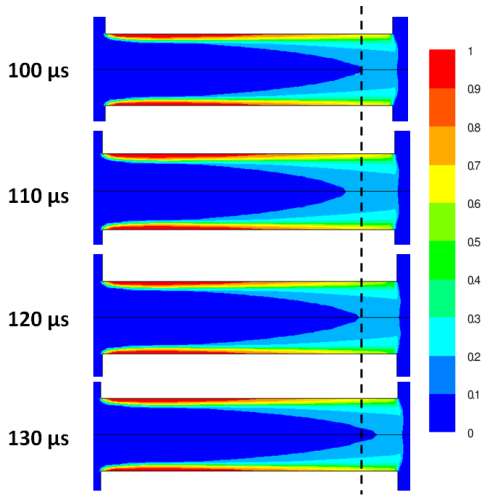

Figure 5.20: Effect of pressure variation for short time span on vapour volume fraction for diesel at mean inlet pressure of 25 MPa and outlet pressure of 5 MPa.

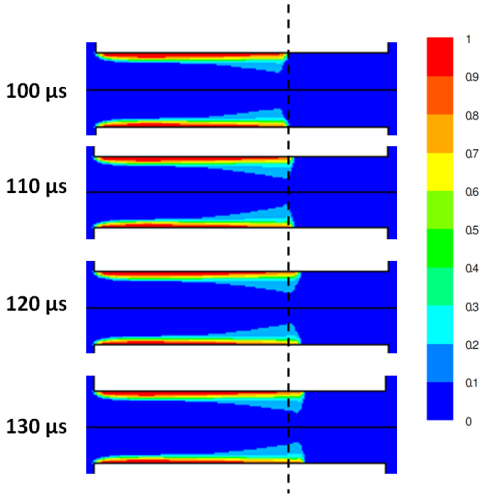

Figure 5.21: Effect of pressure variation for short time span on vapour volume fraction for biodiesel at mean inlet pressure of 25 MPa and outlet pressure of 5 MPa.

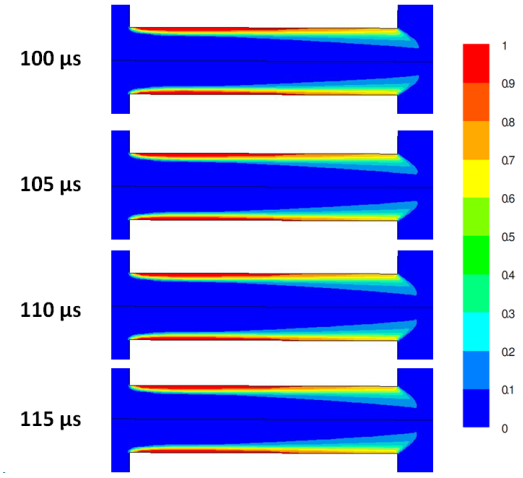

Figure 5.22: Effect of pressure variation for short time span on vapour volume fraction for biodiesel at mean inlet pressure of 100 MPa and outlet pressure of 5 MPa.

Wang et al. [169]. For short time duration diesel fluctuations are more apparent compared to biodiesel. However in longer time-span it has been observed pressure fluctuation can considerably enhance biodiesel cavitation. For two-phase problem, friction from fluid flow is known to be the source of damping for pressure fluctuations [170]. Viscosity plays a key role for generating fluid friction. Biodiesel viscosity being higher than that of diesel could be providing more damping and affecting the response of biodiesel to pressure fluctuations. Similar observations have been made in a pressure fluctuation study with Singhal et al. cavitation model for a nozzle with different dimensions for mean inlet pressures of 33 MPa and 55 MPa [171].

For a higher mean inlet pressure of 100 MPa the variations are not very apparent in terms of vapour volume fraction contours which is evident from Fig. 5.22. The vapour volume fraction pattern only changes to a small extent at the tip of the cavitation region, protruding away from nozzle exit. Therefore the differences due to pressure fluctuations, for high mean inlet pressure, are not significant in terms of vapour concentration at the exit.

5.10 Summary

Diesel and biodiesel cavitation have been investigated in this chapter. Both diesel and biodiesel cavitate considerably when there is enough pressure difference to overcome effects

of viscous resistance. Liquid phase viscosity plays a key role compared to other physical properties such as liquid phase density or saturation pressure. RNG $k-\epsilon$ turbulence model is reasonable for cavitation modelling in fuel injectors. Liquid phase compressibility causes appreciable change at very high (≈ 150 MPa) inlet pressures. Wall roughness does not have an effect on cavitation especially considering level of surface smoothness ensured inside a fuel injector. Nozzle length affects the two-phase flow compositions, but does not cause significant change in mass flow rates. For highly cavitating conditions diesel tends to have higher initial amplitude parameter compared to biodiesel indicating smaller droplets and wider spray angles. Pressure fluctuation effects on vapour contours are more apparent at lower inlet pressures specifically for diesel. Higher viscosity seems to dampen the response of biodiesel when subjected to pressure fluctuations.

Chapter 6

Needle Movement Effects on Cavitation

In this chapter effects of needle movements and inlet pressure fluctuations on cavitation are investigated. Dynamic meshing has been employed in ANSYS Fluent platform to capture the essence of needle motion with time. Both diesel and biodiesel cavitation has been analysed under the influence of needle movements. The needle movement is difficult to be captured in numerical simulations. First order time-implicit has been used for discretization over time domain as it is the only option available in ANSYS Fluent platform for dynamic meshing. First order discretization schemes had to be used for ensuring stability of the transient problem. For the needle motion study, liquid phase compressibility could not be investigated for stability reasons. Nevertheless the fluctuations in injection pressure and needle positions can be caused by the compressibility of the liquid fuel. Therefore effect of liquid compressibility is indirectly manifested in the fluctuations.

6.1 Injector Details

A six-hole mini-sac fuel injector has been considered. The injector has the following dimensions: d = 169 μm, L/d = 4.7, conicity (K) = 0, inlet rounding radius (r/R) = 0. Figure 6.1 shows the schematic of a typical mini-sac fuel injector. The injector, considered here, is similar to the one used by Som et al. [70,128] (L/d = 4.2), but with longer holes (L/d = 4.7). Som et al. [128] performed steady state simulations with inlet pressure 130 MPa and outlet pressure of 3 MPa with a similar injector. In this study transient simulations have

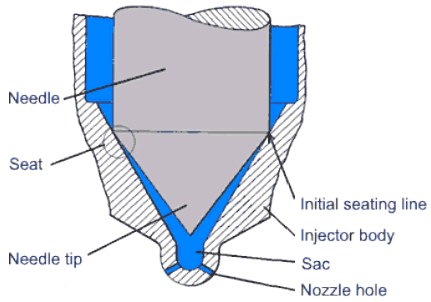

Figure 6.1: Typical mini-sac fuel injector [172].

been carried out. The operating conditions are similar to that of Som et al. for needle open conditions. The needle lift profile and the injection pressure variations are shown in Fig. 6.2. Time-span of the injection is 3 ms. The mean injection pressure, once the needle is open, is around 136 MPa. The outlet pressure remains fixed at 3 MPa. Full needle lift is at 275 μm.

6.2 Dynamic Meshing

The movement of the needle has been simulated with the help of dynamic meshing capability of ANSYS Fluent. There are mainly 3 types of options available for dynamic meshing: a) smoothing, b) dynamic layering and c) remeshing. During creation and merging/destruction of cells for simulating needle movement it is vital to ensure that no negative volume is created. For small deformations only, smoothing is recommended, while remeshing does not have such restriction. The current problem involves simultaneous expansion and collapse of cells along the boundary of the needle. Implementing dynamic layering for such a situation is more complicated. As a result remeshing is chosen for the current study. During numerical simulations the needle cannot be fully closed. Minimum one layer of cell thickness between the fixed and moving surfaces has to be maintained at the minimum needle opening position. Following steps has been implemented for simulating needle motion for cavitation analysis.

- Obtain steady state solution without enabling cavitation and maintaining the needle at minimum opening
- Provide needle movement and pressure variations with time as input files

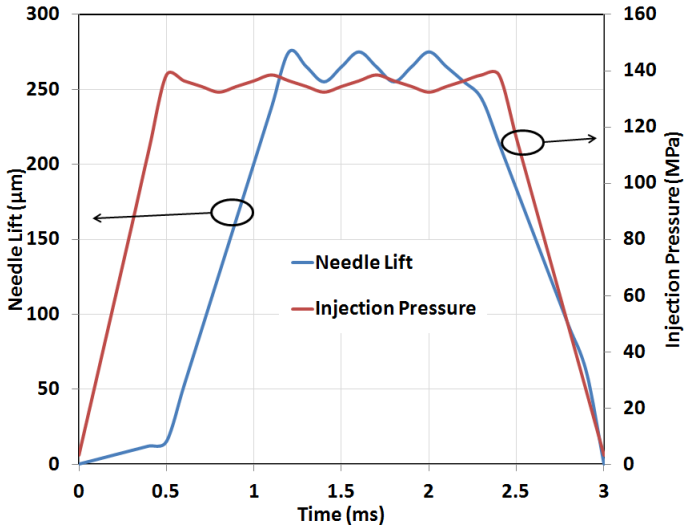

Figure 6.2: Profiles of the needle lift and the injection pressure variations for the injector considered.

- Execute needle motion only to ensure no negative volume gets created during needle motion
- Enable cavitation and perform transient simulations with needle movements and pressure variations

Once the problem is setup correctly negative volume should not be occurring during the simulations.

6.3 Mesh and Computational Domain

The mesh file has been obtained from Argonne National Laboratory. The mesh represents a 60 ° sector of the multi-hole injector. The injector hole has structured mesh while rest of the domain has tetrahedral elements. There are 32421 cells at full needle opening. Holes have grid density 12 grid points along diameter of 169 microns i.e. 14.08 microns of grid size and 48 grid points along length of 798 microns i.e. 16.63 microns. In other studies of needle movement, for example in Ref. [101] grid convergence was achieved for 10 microns as optimum grid size for nominal pressure of 150 MPa for a single hole nozzle. However 20 micron, as minimum cell size, did not yield poor performance. In the same work at 78 MPa

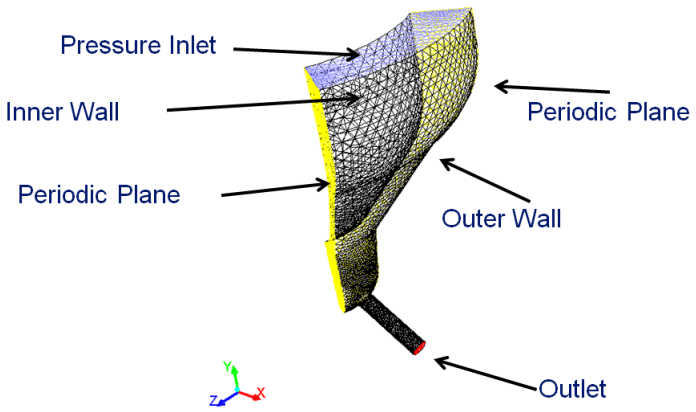

Figure 6.3: Mesh and computational domain used for needle movement in the present study.

for the case of multi-hole nozzle 12.5 microns were used as minimum cell size. The present mesh, used in current study, is coarse around the needle and needle sac, but the resolution in the hole is close to the value of typical optimum cell sizes. Performing needle motion in 3D case at higher grid resolutions will be computationally extremely demanding. A large domain beyond the exit of injector hole and considerable extension of the top portion of the domain are required to capture compressibility effects which would again require huge computational resources. As a result cavitation analysis with needle movements has been done at the current mesh resolution. The computational domain has been illustrated in Fig. 6.3.

6.4 Results and Discussion

Cavitation characteristics for both diesel and biodiesel have been studied for the needle movement simulations with the proposed cavitation model. At different time instants the results are presented and the corresponding injection pressure and needle lift positions are mentioned. The contour plots correspond to mid-plane in the 60 ° sector. The vapour contours of diesel and biodiesel at the opening part of the needle at 0.5 ms, at needle lift of 15 μm and P_{inj} of 138.6 MPa are shown in Fig. 6.4. Figure 6.5 presents vapour volume fraction contours of diesel and biodiesel at 2 ms, at needle lift of 275 μm and P_{inj} of 132.5 MPa. At 2.4 ms diesel cavitation reaches outlet while biodiesel cavitation ends very close to the outlet. For 2.4 ms at needle lift of 213.89 μm and P_{inj} of 138.6 MPa volume fraction

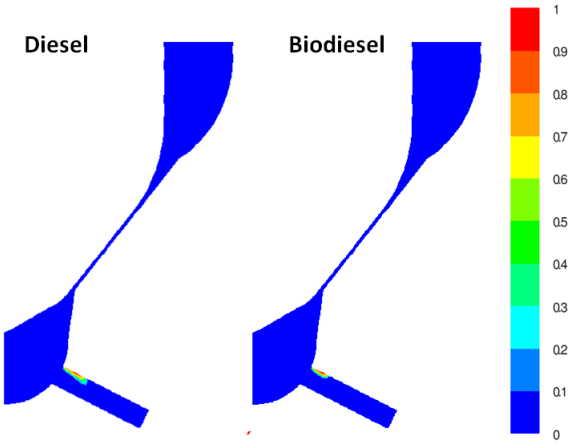

Figure 6.4: Comparison of diesel and biodiesel vapour volume fraction contours at mid-plane at 0.5 ms, at needle lift of 15 μm and P_{inj} of 138.6 MPa

contours are shown in Fig. 6.6. Overall it is seen biodiesel is cavitating less compared to diesel initially, but finally both diesel and biodiesel are having considerable cavitation. The difference in cavitation behaviour could be again attributed to difference in viscosity. As time progresses pressure difference eventually overcomes the viscous resistance resulting in substantial cavitation for both the fuels.

Comparison can be made with results of Som et al. [128] since the injector and operating conditions are similar. For 130 MPa steady inlet pressure Som et al. got supercavitation for diesel and much less cavitation for biodiesel. In the present study the mean inlet pressure (136 MPa), at needle open position, is higher than 130 MPa and it is going up to 138.6 MPa. As a result considerable cavitation of biodiesel is expected. The velocity magnitude of diesel and biodiesel at 2 ms are in the order of 500 m/s and are shown in Fig. 6.7. Som et al. [128] got velocity magnitudes in the order of 500 m/s for diesel and biodiesel. The mass flow rates of diesel and biodiesel through the outlet at 2 ms are close. Diesel mass flow rate is 7.06 g/s and biodiesel has higher mass flow rate of 7.38 g/s. Since biodiesel is having considerable cavitation, viscosity is not providing much resistance to the biodiesel flow. At high pressure turbulent viscosity is expected to dominate over molecular viscosity. The mass flow rate predictions by Som et al. [128] was also around 7 g/s.

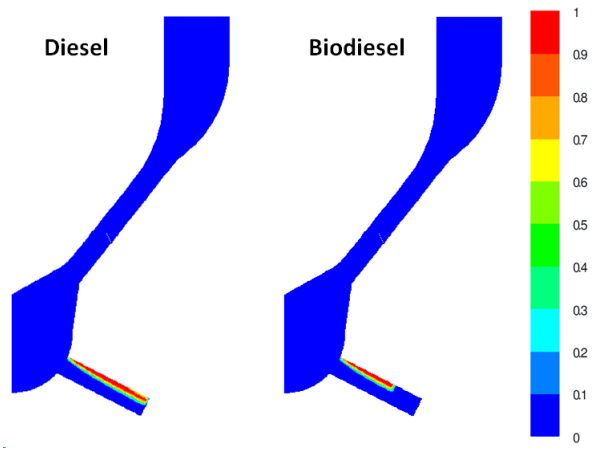

Figure 6.5: Comparison of diesel and biodiesel vapour volume fraction contours at mid-plane at 2 ms, at needle lift of 275 μm and P_{inj} of 132.5 MPa

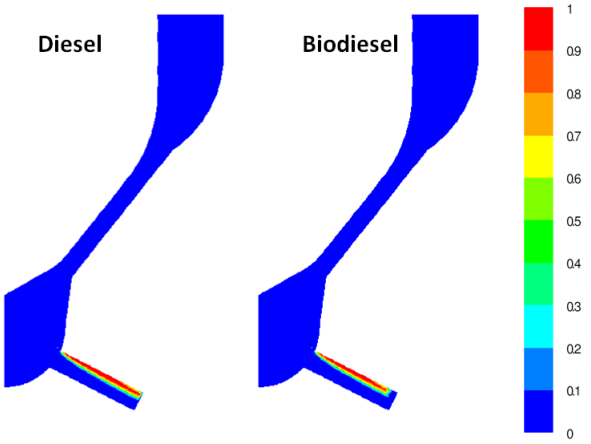

Figure 6.6: Comparison of diesel and biodiesel vapour volume fraction contours at mid-plane at 2.4 ms, at needle lift of 213.89 μm and P_{inj} of 138.6 MPa

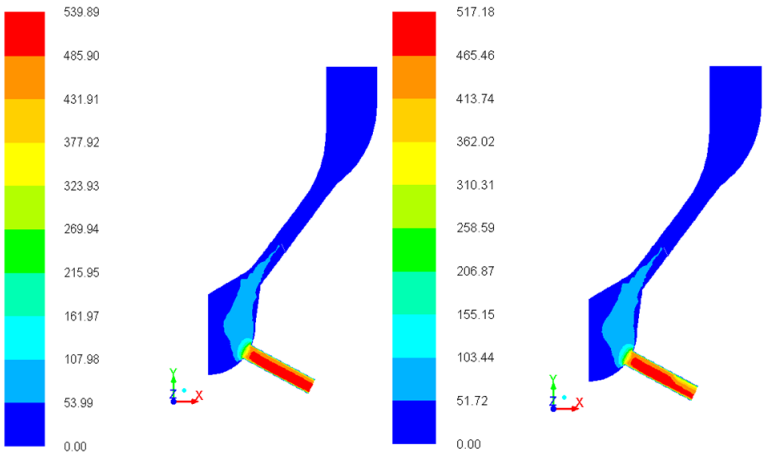

Figure 6.7: Comparison of diesel and biodiesel velocity magnitude contours at 2 ms, at needle lift of 275 μm and P_{inj} of 132.5 MPa

6.5 Summary

The present cavitation model has been successfully implemented in a complex geometry with needle movements and inlet pressure fluctuations. Cavitation patterns at different time instants with different needle positions and injection pressures are reported. Diesel cavitation has been observed to be relatively more compared to that of biodiesel at the initial stage. However due to higher mean inlet pressure and pressure fluctuations biodiesel cavitation is finally comparable to that of diesel which results in increase mass flow rate as the biodiesel density is higher than that of diesel. Overall velocity magnitude of diesel is more than that of biodiesel because of lower viscosity of diesel with respect to biodiesel. The findings of the needle movement cavitation studies are in accordance with the results of Som et al. [128] indicating that the predictions from the present cavitation model are reasonable.

Chapter 7

Summary and Future Work

In this study a cavitation model coupled with mixture multiphase approach has been developed. The model has been assessed by comparing with experimental data as well as some of the existing cavitation models. The present cavitation model provides reasonable prediction of cavitation at low and high pressure differences with relatively low computational time. The present study also investigated the effects of key parameters that can affect cavitation such as stress in fluid flow, turbulent pressure fluctuations, variation in bubble number density, physical properties, liquid phase compressibility, wall roughness, turbulence models, inlet pressure fluctuations, and needle movements in an actual fuel injector. Summary of the findings from the present study and recommendations for future work for cavitation in fuel injectors are provided in this chapter.

7.1 Summary of Present Study

It is important to ensure that assumptions and approximations made while formulating a model are consistent with the physics of the flow. Most of the existing cavitation models involve questionable assumptions without providing any justifications. The cavitation model by Singhal et al. had issues with abrupt and unjustified approximations. In their model We number was introduced, even though they assume zero relative velocity between the two phases for deriving their model. Singhal et al. model had tuning parameters which are not in the order of unity. Proper model formulation should yield tuning parameters in the order of unity. Schnerr-Sauer cavitation model defined bubble number density in terms of total liquid volume instead of total mixture volume, which should only be reasonable for dilute mixtures. For cavitating flows considerable vapour by volume is formed resulting in

non-dilute mixtures. They did not consider presence of non-condensable gases which are vital for cavitation initiation. Zwart-Gerber-Belamri cavitation model assumes constant bubble radius in their model which is physically not correct since the average bubble radius should vary with change in vapour volume fraction. However with the use of tuning parameters their model provides reasonable performance. Their tuning parameters are also not in the order of unity. Their model also did not consider non-condensable gases, but made adjustments in the cavitation model to ensure non-zero source term when there is no vapour initially in the domain. The present model refrained from making adhoc approximations adopted by the above mentioned cavitation models. Therefore the formulation of the present model is more consistent and reasonable in terms of model assumptions.

At the current stage the present model has been only coupled with mixture approach. To investigate the utility of Eulerian-Eulerian approach, two cavitation models, Schnerr-Sauer and Zwart-Gerber-Belamri have been tested with both the multiphase approaches. Eulerian-Eulerian approach appeared to be more effective, with increase in the computational time. The relative velocity between the two phases cannot always be neglected. Therefore better performance of cavitation models coupled with Eulerian-Eulerian approach is justified. Methodology adopted for pressure velocity coupling also affects the model prediction. For Eulerian-Eulerian simulations Multiphase Coupled algorithm provided better numerical stability. Per phase turbulence modelling approach yielded better performance as it takes into account the turbulence interaction between the liquid and vapour phases. At higher pressures performance of all the cavitation models are comparable which indicate Schnerr-Sauer and Zwart-Gerber-Belamri cavitation models are typically tuned for high pressure conditions. In actual fuel injectors, during the injection period, the pressure difference varies from low to high values. Therefore it is necessary that cavitation models provide appreciable prediction at both low and high pressure differences.

Variation of bubble number density did not yield noticeable difference in cavitation predictions for fuel injectors. Nevertheless variation of bubble number density in cavitation model is generally physically more reasonable and for cavitation in other applications such as marine science, pumps etc. variable bubble number density can be important. Stress effects are not significant for high Reynolds number cavitating flow in diesel injectors. The stress-induced cavitation has mostly been studied for creeping flows. The concept behind effect of turbulent fluctuations is not well understood yet. The source of most commonly used turbulent fluctuation correlation involving Egler coefficient (C_E) is not clear. Other correlations available in the literature, have been obtained for single-phase isotropic flow. Ignoring turbulent fluctuations does not provide considerable difference with the present cavitation model. Linear Rayleigh estimate appears to be reasonable for cavitation analysis. Pursuing detailed bubble dynamics with mixture, VOF or Eulerian-

Eulerian multiphase approaches will not only require huge computational time, but also will cause stability issues especially for bubble collapse conditions.

Diesel and biodiesel comparative study for cavitation has been done. Liquid phase viscosity appears to be the most determining factor. Difference in viscosity causes difference in pressure drop around the inlet for diesel and biodiesel resulting in different cavitation characteristics at low pressure differences. Order of magnitude difference in saturation pressure does not play a major role in cavitation. At high pressure differences both diesel and biodiesel have substantial cavitation. Liquid phase compressibility is important at high pressure differences (inlet pressure of $\approx$ 150 MPa) resulting in liquid phase Mach numbers greater than 0.4. Pressure fluctuations affect vapour volume fraction distribution specially for diesel over a short-time span. Biodiesel cavitation is also affected if the pressure fluctuation is maintained for longer time-span. The proposed cavitation model has also been implemented in complex geometry of a fuel injector with needle movements and inlet pressure fluctuations. Needle movement effects on cavitation of diesel and biodiesel have been examined and the results are comparable with literature result. Finer mesh and inclusion of liquid phase compressibility will require substantial computational resource.

Some key points can be highlighted as a summary of the present study,

- A cavitation model, providing "accurate" predictions (engineering perspective) at reasonable computational cost and consistent assumptions has been developed and implemented in two and three dimensional cases.
- Eulerian-Eulerian multiphase approach provides better performance compared to mixture multiphase approach specifically with Multiphase Coupled algorithm and per phase turbulence modelling approach.
- Liquid phase compressibility becomes important for very high injection pressures ($\approx$ 150 MPa).
- Pressure fluctuations is vital for prediction of cavitation patterns at lower injection pressures for both short and long time span.
- Liquid phase viscosity plays a key role in cavitation inception or low Reynolds number cases in terms of physical properties. At high Reynolds number turbulent viscosity is dominant.
- Linear Rayleigh estimate is reasonable at the current stage of model development for cavitation analysis.
- Non-condensable gases should be considered.

7.2 Recommendations for Future Work

Cavitation has been studied for last few decades using experimental and numerical methods. However there is still ample scope of improvement. More rigorous experimental studies at high pressure, are necessary with good quality images and quantitative analysis along with proper uncertainty analysis. More works are needed for turbulence modelling in cavitating flows. Liquid phase compressibility has not been implemented in case of actual fuel injector for most of the modelling studies. No cavitation model exists for blended diesel-biodiesel cavitation while substantial works are taking place to utilise blended fuels in internal combustion engines. Typically isothermal conditions are assumed for cavitation modelling. Recent findings at Engine Combustion Network (ECN) indicate that temperature difference of 25-30 K can occur for modern diesel injectors. Further model developments may be required for non-isothermal studies of cavitation. Biodiesel at higher temperature can undergo thermal cracking causing formation of small solid particles. Modelling such a complex phenomena will be very challenging.

Following recommendations for future work can be made based on the findings of this study and recent developments in the scientific community.

- Studies should be undertaken for obtaining high quality reliable experimental data.
- Efforts are needed to implement the present cavitation model with Eulerian-Eulerian approach.
- Extensive numerical study of needle movements with compressibility effects should be undertaken by accessing super-computing facilities.
- The present model should be tested with ECN nozzles in future.
- More studies are needed to understand turbulent fluctuation effects.
- LES or RSM turbulence models should be tested to investigate further about the role of turbulence models in cavitation.
- A blended cavitation model for diesel and biodiesel mixtures should be formulated to keep up with the recent trends in the industry.
- Attempts should be made to understand effect of thermal gradients on cavitation in fuel injectors.
- Thermal cracking phenomenon should be explored for use of biodiesel at high temperatures.

APPENDICES

Appendix A

Two-fluid Eulerian-Eulerian Cavitation Models

A.1 Governing Equations

The Eulerian-Eulerian multiphase model, involves solving two sets of the standard Reynolds averaged Navier-Stokes equations and using any standard turbulence model, if required. For the two-fluid or Eulerian-Eulerian multiphase model mass and momentum conservation equations are solved for both liquid and vapour phases. Since Schnerr and Sauer and Zwart-Gerber-Belamri models are implemented with Eulerian-Eulerian approach, the fluid consists of only liquid and vapour and no gas for the Eulerian-Eulerian approach. The pressure p is shared by both phases. The mass and momentum conservation equations for each phase are as follows:

$$\frac{\partial(\alpha_q \rho_q)}{\partial t} + \frac{\partial(\alpha_q u_{j,q} \rho_q)}{\partial x_j} = R_P \tag{A.1}$$

$$\begin{aligned} \frac{\partial(\alpha_q \rho_q u_{i,q})}{\partial t} + \frac{\partial(\alpha_q \rho_q u_{i,q} u_{j,q})}{\partial x_j} &= -\alpha_q \frac{\partial p}{\partial x_i} + \frac{\partial \tau_{ij,q}}{\partial x_j} \\ &\quad + M_{qp} + u_{i,q} R_P \end{aligned} \tag{A.2}$$

where

$$\tau_{ij,q} = \left[\alpha_q \mu_{\text{eff,q}} \left(\frac{\partial u_{i,q}}{\partial x_j} + \frac{\partial u_{j,q}}{\partial x_i} - \frac{2}{3} \frac{\partial u_{i,q}}{\partial x_i} \right) \right]$$

q stands for phase index and M_{qp} represents the momentum exchange between the two phases. The closure equation becomes

$$\sum_{q=1}^{2} \alpha_q = 1 \tag{A.3}$$

The momentum exchange term is estimated in terms of interphase momentum exchange coefficient K_{qp} [67].

$$M_{qp} = K_{qp}(u_{i,q} - u_{i,p})$$

where $K_{qp} = \frac{\alpha_p \alpha_q \rho_q f}{\tau_q}$, f is the drag function dependent on the drag coefficient C_d and τ_q is the relaxation time-scale. Schiller Naumann correlation [67] has been used to calculate the drag coefficients. Schiller Naumann correlation is based on relative Reynolds number (based on relative velocity of two phases), as shown below,

$$C_d \begin{cases} = 24\left(1 + 0.15 Re_{\text{rel}}^{0.687}\right)/Re_{\text{rel}} & Re_{\text{rel}} \leq 1000 \\ = 0.44 \quad Re_{\text{rel}} > 1000 \end{cases}$$

A.2 Turbulence Modelling Approach

For Eulerian-Eulerian multiphase model two types of $k-\epsilon$ turbulence modelling approaches are investigated, a) mixture turbulence modelling approach and b) per phase turbulence modelling approach. Mixture turbulence modelling approach uses only one set of turbulence model equations while two sets of governing equations are solved for mass and momentum. Per Phase Turbulence Modelling approach is more effective as it involves two sets of turbulence model equations. Details about the performance of the two approaches will be provided in the Chapter "Model Assessment". In the per phase turbulence modelling approach turbulent kinetic energy exchange is taken care by the following expression

$$T_{qp} = K_{qp}(C_{qp}k_q - C_{pq}k_p) \tag{A.4}$$

Additionally there is also turbulence drag term which considers turbulent momentum transfer between the two phases. The turbulence diffusivities are directly computed from the transport equations. It is computationally more intensive than other approaches such as Mixture Turbulence Model and Dispersed Turbulence Model available in ANSYS Fluent platform, but more accurate for cases where turbulence exchange between the two phases are significant.

Table A.1: Details about the parametric cases with mixture and Eulerian-Eulerian approaches (PC SIMPLE-segregated; Multiphase Coupled- coupled)

Case	**Approach**	**Time-step** s	**P-V Coupling**	**Turbulence Model**
I	Mixture	N/A	SIMPLEC	Mixture
II	Eul.-Eul.	10^{-5}	Phase Coupled SIMPLE	Mixture
III	Eul.-Eul.	10^{-6}	Phase Coupled SIMPLE	Mixture
IV	Eul.-Eul.	10^{-7}	Phase Coupled SIMPLE	Mixture
V	Eul.-Eul.	10^{-6}	Multiphase Coupled	Mixture
VI	Eul.-Eul.	10^{-6}	Multiphase Coupled	Per Phase

A.3 Numerical Experiments

Both Schnerr and Sauer model and Zwart-Gerber-Belamri have been tested with cell based Green Gauss and Least Squares gradient calculation methods. There is no difference in the numerical prediction by switching these methods. Zwart-Gerber-Belamri model has been tested here when coupled with Eulerian-Eulerian multiphase approach for Winklhofer nozzle [31]. Parametric studies have been carried out for $\Delta P = P_{in} - P_{out} = 8.0$ MPa with different time step sizes, pressure-velocity coupling algorithms and multiphase turbulence modelling approaches. This study has been carried out to ensure best possible output from Eulerian-Eulerian multiphase approach. The pertinent details of the six cases are shown in Table A.1.

Vapour volume fraction contours for six different cases are shown in Fig. A.1. The above result has been published in a conference [158]. The conventional colour scheme has been used for vapour volume fraction contours and will be followed for the remaining part of this thesis. Time step size of 10^{-6} s has been selected for other Eulerian-Eulerian cases. Though the vapour contours look same for all the three time step sizes with all other parameters remaining same, time step size of 10^{-6} provides better stability. Phase Coupled SIMPLE (PC-SIMPLE) and Multiphase Coupled solution methods have been only attempted and Full Multiphase Coupled method has not been examined. Full Multiphase Coupled couples the phase velocity, shared pressure and volume fractions corrections simultaneously and

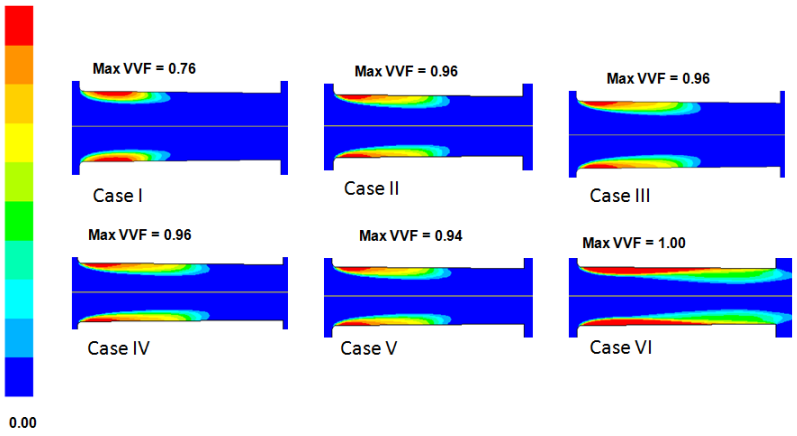

Figure A.1: Comparison of vapour volume fraction contours using mixture and Eulerian-Eulerian multiphase approaches for Zwart-Gerber-Belamri model, at (ΔP)= 8.0 MPa (Maximum vapour volume fraction is abbreviated as Max VVF. All the Eulerian-Eulerian results are at 0.5 ms.).

seems to be most efficient method from theoretical perspective. Nonetheless there are some practical constraints that lead to problems in robustness and excessive CPU usage. The continuity constraint and range of variation of volume fraction (from 0 to 1) provide physical limits which deter the implementation of this method [67]. Additionally this method becomes useful only for dilute cases. PC-SIMPLE is a special type of SIMPLE method meant for multiphase problems and is numerically robust. The pressure correction coefficients are based on the overall continuity. On the other hand Multiphase Coupled method solves phase velocity and pressure corrections simultaneously [67]. It also involves implicit inclusion of the lift forces and the mass transfer rates in the general matrix [67]. As a result PC-SIMPLE and Multiphase Coupled methods are the only viable options for cavitation simulations. It is observed that the convergence characteristics are better for Multiphase Coupled compared to PC-SIMPLE. Phase Coupled SIMPLE is a special type of SIMPLE method or segregated algorithm used in Eulerian-Eulerian simulations. Multiphase Coupled is a type of coupled algorithm meant for Eulerian-Eulerian simulations. In Eulerian-Eulerian approach the mass and momentum conservation equations are solved for each phase. It will make sense to have separate turbulence conservation equations for the two phases. Using a mixture turbulence model in Eulerian-Eulerian approach will most likely lead to wrong prediction for missing out essential characteristics of the two-phase interacting flow. It seems for this reason "supercavitation" is predicted in Case VI as observed in the experiment [31]. The residuals for Cases III and V are presented in

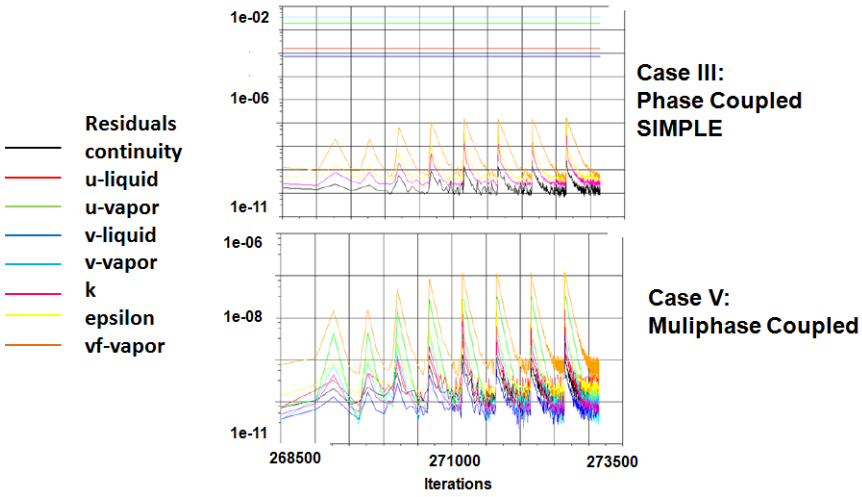

Figure A.2: Comparison of residuals for PC-SIMPLE and Multiphase Coupled solution methods when used with Eulerian-Eulerian multiphase approach coupled with Zwart-Gerber-Belamri model, at (ΔP)= 8.0 MPa for Winklhofer nozzle [31].

Fig.A.2. All the residuals are converging well for Multiphase Coupled and hence it should be preferred for Eulerian-Eulerian simulations.

Appendix B

Models For Mass Source Term

B.1 Present Model

For convenience the derivation has been shown considering the flow to be one-dimensional and consists of liquid and vapour.

The mixture density can be expressed as

$$\rho = \alpha_v \rho_v + (1 - \alpha_v)\, \rho_l \tag{B.1}$$

The overall continuity can be written as

$$\frac{\partial}{\partial t}\rho + \frac{\partial}{\partial x}(\rho u) = 0 \tag{B.2}$$

From B.2,

$$\frac{D\rho}{Dt} = -\rho \frac{\partial}{\partial x} u \tag{B.3}$$

The vapour phase mass conservation equation is,

$$\frac{\partial}{\partial t}(\alpha_v \rho_v) + \frac{\partial}{\partial x}(\alpha_v \rho_v u) = \dot{m}_v \tag{B.4}$$

and the liquid phase mass conservation equation is,

$$\frac{\partial}{\partial t}\left[(1 - \alpha_v)\, \rho_l\right] + \frac{\partial}{\partial x}\left[(1 - \alpha_v)\, \rho_l u\right] = -\dot{m}_v \tag{B.5}$$

Combining B.4 and B.5 we can get,

$$\frac{\partial}{\partial t}\left(\alpha_v \rho_v\right) + \frac{\partial}{\partial x}\left(\alpha_v \rho_v u\right) = -\frac{\partial}{\partial t}\left[\left(1-\alpha_v\right)\rho_l\right] - \frac{\partial}{\partial x}\left[\left(1-\alpha_v\right)\rho_l u\right] \tag{B.6}$$

$$\Rightarrow \frac{D\alpha_v}{Dt}\left(\rho_l - \rho_v\right) = \rho\frac{\partial u}{\partial x}$$

The material derivative of volume fraction of vapour phase can be expressed in terms of bubble number density, volume fraction of vapour phase and average bubble surface velocity.

$$\alpha_v = N^{'''}\frac{4}{3}\pi R^3$$

and

$$\frac{D\alpha_v}{Dt} = \left(N^{'''}4\pi\right)^{1/3}\left(3\alpha_v\right)^{2/3}\frac{DR}{Dt} \tag{B.7}$$

Using B.6 in B.4 we get,

$$\dot{m}_v = \rho_v\frac{D\alpha_v}{Dt} + \frac{\rho_v}{\rho}\alpha_v\rho\frac{\partial u}{\partial x}$$

$\Rightarrow \dot{m}_v = \rho_v\frac{D\alpha_v}{Dt} + \frac{\rho_v}{\rho}\alpha_v\left(\rho_l - \rho_v\right)\frac{D\alpha_v}{Dt}$ [B-6]

$$\dot{m}_v = \frac{\rho_v\rho_l}{\rho}\frac{D\alpha_v}{Dt} \tag{B.8}$$

Substituting $\frac{D\alpha_v}{Dt}$ from B.7 and using $R_P = \dot{m}_v$ we get,

$$R_P = \frac{3\alpha_v}{R}\,\frac{\rho_v\rho_l}{\rho}\frac{DR}{Dt} \tag{B.9}$$

Further details are already provided before in Mass Source Term subsection in chapter 3.

B.2 Singhal et al. model

The underlying assumption of Singhal approach is Equal Velocity Equal Temperature (EVET) that is the two phases share the same velocity and temperature at the interface. In the present study of cavitation in injector nozzles temperature effects are not important

as the bubble dynamics will fall in to inertia-controlled regime. The important assumption is no relative velocity between the two phases. The argument provided by Singhal et al. [127] behind this assumption was that the relative velocity of the high speed flow will be very small compared to the mean velocity of the fuel injector nozzle. Singhal et al. [127] formulated their model for the phase change rate expressions from the source term ($\dot{m}_v = \frac{\rho_v \rho_l}{\rho} \frac{D\alpha_v}{Dt}$) in Eq.2.16. Using $\alpha_v = N''' \frac{4}{3}\pi R^3$ Singhal et al. got

$$\frac{D\alpha_v}{Dt} = \left(N''' 4\pi\right)^{1/3} (3\alpha_v)^{2/3} \frac{DR}{Dt}$$

Singhal et al. expressed R as

$$R = \frac{0.061 We \sigma}{2\rho_l V_{rel}^2}$$

where Weber number is a non-dimensional number that is based on relative velocity of a bubble. They also assumed that phase change rates are proportional to relative velocity and not to the square of it, using Eq. B.9 ($R_P = \frac{3\alpha_v}{R} \frac{\rho_v \rho_l}{\rho} \frac{DR}{Dt}$) Singhal et al. got,

$$R_P = \frac{6\alpha_v V_{rel}}{0.061 \sigma We} \frac{\rho_v \rho_l \rho_l}{\rho} \frac{DR}{Dt} \tag{B.10}$$

or

$$R_e = \frac{6\alpha_l V_{rel}}{0.061 \sigma We} \frac{\rho_v \rho_l \rho_l}{\rho} \frac{DR}{Dt} \tag{B.11}$$

where R_P is replaced by R_e for liquid to vapour phase change.

It should be noted at this stage that the assumption of linear dependence on the relative velocity was not justified in the work by Singhal et al. [127]. This was followed by two more approximations without sufficient justifications:

1. The relative velocity can be considered to be of the same order of magnitude as the characteristic turbulent velocity which can be further approximated as square root of turbulent kinetic energy, $\sqrt{k}$.

2. The phase change rate expression should be proportional to the concentration of donor phase i.e. liquid phase volume fraction α_l in case of R_e instead of vapour volume fraction α_v.

Singhal et al. then introduced dimensionless tuning parameter C_e such that, $R_e = C_e \frac{\sqrt{k}}{\sigma} \frac{\rho_v \rho_l \rho_l}{\rho} \alpha_l \frac{DR}{Dt}$ where $C_e = \frac{6}{0.061 We}$. Additionally the volume fractions were converted to mass fractions,

$$\alpha_v = f_v \frac{\rho}{\rho_v} \quad , \quad \alpha_l = f_l \frac{\rho}{\rho_l}$$

Finally for cavitation i.e. $p<p_v$ they arrived at

$$R_e = C_e \frac{\sqrt{k}}{\sigma} \rho_l \rho_v \sqrt{\frac{2(p_v - p)}{3\rho_l}} (1 - f_v) \tag{B.12}$$

and for condensation i.e. $p>p_v$,

$$R_c = C_c \frac{\sqrt{k}}{\sigma} \rho_l \rho_l \sqrt{\frac{2(p - p_v)}{3\rho_l}} f_v \tag{B.13}$$

In the above expressions the bubble surface velocity was estimated using the Linear Rayleigh Equation. The values of C_e and C_c have been tuned and was found out to be equal to 0.02 and 0.01 respectively. This also brings to a point where it is seen that above equations are not dimensionally consistent. Moreover, the value of tuning parameters should ideally be of the order of unity, not order of magnitude lower or higher. If proper approximations have been done the dimensions of the parameters on the two sides of the equation should be in the same order and therefore, it is likely that value of tuning parameters will be in the order of unity.

Singhal et al. [127] used standard $k-\varepsilon$ model for his analysis. They considered the effect of turbulence in cavitation by adding an estimate of turbulent pressure fluctuation to the saturation pressure for calculating the threshold pressure of the phase change. They argued that saturation pressure of the fluid can be elevated by fluctuations which is not correct from thermodynamics point of view. The estimate of turbulent pressure fluctuations were obtained assuming that turbulence is isotropic [120]. In reality turbulence is not isotropic. However, they assumed isotropic behaviour for the modelling work.

$$p'_{turb} = 0.39\rho k$$

$$p_v = p_{sat} + p'_{turb}/2 \tag{B.14}$$

Singhal et al. [127] used constant density for both liquid and vapour phases.

There are quite a few areas in Singhal et al. model formulation where the assumptions and approximations are either not justified. In the derivation of phase change rates Singhal et al. had to get an estimate of average bubble radius and they introduced Weber number to accomplish their task. Singhal et al. defined Weber number in terms of relative velocity between the two phases. One of the key assumptions of single-fluid approach is that there is no relative velocity between the two phases. Zero relative velocity is also one of the underlying assumptions of Rayleigh-Plesset equation. Hence by using Weber number Singhal

et al. contradicted his own assumption. Many more *adhoc* assumptions and approximations were made by Singhal et al. in his formulation without proper justifications. This necessitates the formulation of phase change rate expressions without any contradictory assumptions or unjustified approximations.

Before going to the details of formulation of present cavitation model it is important to mention about contributions of Som et al. briefly. They proposed a modified criterion for cavitation inception based on the works by D.D. Joseph [129, 130]. Instead of the classical criterion of p<p_v the criterion used was,

The maximum tension criterion,

$$-p - 2\mu D_{11} + p_v > 0$$

and the minimum tension criterion,

$$-p + 2\mu D_{11} + p_v > 0$$

where,

$$D_{11} = \sqrt{\left(\frac{\partial u}{\partial x}\right)^2 + 0.25\left(\frac{\partial u}{\partial y} + \frac{\partial v}{\partial x}\right)^2}$$

B.3 Schnerr and Sauer Model

Schnerr and Sauer [132] derived the exact expression for the net mass transfer from liquid to vapour from the Eq. B.9 ($R_P = \frac{3\alpha_v}{R}\frac{\rho_v\rho_l}{\rho}\frac{DR}{Dt}$). As mentioned before their model only consists of vapour and liquid. They expressed α as

$$\alpha = \frac{\frac{4}{3}\pi R^3 N'''}{1+\frac{4}{3}\pi R^3 \eta}$$

The bubble number density N''' was considered to be constant ($=10^{13}\frac{1}{m^{-3}}$) and was defined in terms of per unit volume of liquid. The time derivative of α was used to express source term in terms of $\frac{DR}{Dt}$. Finally using Linear Rayleigh equation the source term was derived as

$$R_P = \frac{3\alpha(1-\alpha)}{R}\frac{\rho_v\rho_l}{\rho}(-1)^j\sqrt{\frac{2\left(|p-p_{\text{sat}}|\right)}{3\rho_l}} \tag{B.15}$$

where

$$p - p_{\text{sat}} \begin{cases} > 0 & j = 1 \quad \text{for vapour condensation} \\ < 0 & j = 2 \quad \text{for vapour formation} \end{cases}$$

Therefore, the key difference between the present cavitation model and Schnerr and Sauer model is $(1-\alpha)$ in the source term R_P. As a result for all other parameters remaining the same estimate of source term from Schnerr and Sauer is going to be $(1-\alpha)$ times of that of the present cavitation model. Moreover Schnerr and Sauer did not consider turbulent pressure fluctuations and stress effects on the local mean effective pressure. It should be noted that Schnerr-Sauer and their group has defined bubble number density in terms of per unit volume of liquid phase in contrary to the common practice of defining the bubble number density in terms of per unit control volume. For dilute mixtures i.e. with low vapour concentrations this difference will not cause appreciable difference, but will not be correct to use for mixtures with considerable vapour concentrations.

B.4 Zwart-Gerber-Belamri Model

Zwart, Gerber and Belamri [142] made the assumption of a constant bubble size to calculate the total interphase mass transfer rate per unit volume, R_P. They did not consider existence of non-condensable gases. They derived their source term from the derivative of total mass of vapour present in the mixture and then made adjustments to obtain non-zero source term for cavitation inception (when initial vapour content is zero in the domain) and finally ended up introducing two tuning parameters. Using $R_P = N'''\left(4\pi R^2 \rho_v \frac{DR}{Dt}\right)$ and $\alpha = N'''\left(\frac{4}{3}\pi R^3\right)$ they got

$$R_P = \frac{3\alpha\rho_v}{R}\sqrt{\frac{2\left(p - p_{\text{sat}}\right)}{3\rho_l}} \tag{B.16}$$

For $p < p_{\text{sat}}$ (vapour formation),

$$R_P = F_{vap}\frac{3\alpha_{nuc}\left(1-\alpha\right)\rho_v}{R}\sqrt{\frac{2\left(|p - p_{\text{sat}}|\right)}{3\rho_l}} \tag{B.17}$$

and $p > p_{\text{sat}}$ (liquid formation),

$$R_P = F_{cond}\frac{3\alpha\rho_v}{R}\sqrt{\frac{2\left(|p - p_{\text{sat}}|\right)}{3\rho_l}} \tag{B.18}$$

where the parameters used in this model are $\alpha = \alpha_v$, $F_{vap} = 50; F_{cond} = 0.01$, $R = 10^{-6}m$ is the bubble radius, $\alpha_{nuc} = 5 \times 10^{-4}$ is the nucleation site volume fraction. The vapour

formation equation was made different from the liquid formation one. Therefore there are two different equations to ensure non-zero source term for cavitating conditions. They also assumed bubble radius to be a constant value which is not justified. With change in volume fraction average bubble radius should change. In the present cavitation model even when N''' is constant bubble radius still changes with variation in volume fraction. Thus this important aspect of bubble size evolution is missing in their model. The order of magnitude difference in the tuning parameters is probably the effect of the approximation mentioned before. Moreover the tuning parameters in this model also are order of magnitude different from unity. In spite of these limitations their model has achieved success because the parameters F_{vap} and F_{cond} were rigorously tuned to obtain desirable results [142].

Appendix C

UDFs implemented

C.1 Singhal Cavitation Model

The following UDF is not required when implemented in ANSYS Fluent 12 platform.

```
#include "udf.h"
#define c_evap 0.02
#define c_con 0.01
DEFINE_CAVITATION_RATE(user_cav_rate, c, t, p, rhoV, rhoL, mafV, p_v,cigma, f_gas,
m_dot)

double p_vapour = *p_v;
double dp, dp0, source;
double fgas = *f_gas;
double sigma = *cigma;
p_vapour + = 0.195*C_R(c,t)*C_K(c,t);
dp = p_vapour - ABS_P(p[c], op_pres);
source = sqrt((2.0/3.0)*rhoL[c]*ABS(dp));


    if(dp > 0.0)
*m_dot = c_evap*rhoV[c]*source*sqrt(C_K(c,t))*(1.0/sigma)*(1-mafV[c]-fgas);
else
*m_dot = -c_con*rhoV[c]*source*sqrt(C_K(c,t))*(1.0/sigma)*mafV[c];
```

C.2 Present Cavitation Model

The following UDF has been used for implementing the present cavitation model in ANSYS Fluent platform.

```
    #include “udf.h”
#define c_evap 1.00
#define c_con 1.00

DEFINE_CAVITATION_RATE(user_cav_rate, c, t, p, rhoV, rhoL, mafV, p_v,cigma, f_gas,
m_dot)
{
double p_vapour = *p_v;
double dp0, Rdotv,alpha,lambda,nB,Rb;
double fgas = *f_gas;
double sigma = *cigma;
lambda= (C_DUDX(c,t)+C_DVDY(c,t)+sqrt((C_DUDX(c,t)-C_DVDY(c,t))*(C_DUDX(c,t)-
C_DVDY(c,t))+(C_DUDY(c,t)+C_DVDX(c,t))*(C_DUDY(c,t)+C_DVDX(c,t)));
alpha = 1-(C_R(c,t)/rhoL[c])*(1-fgas-mafV[c]);
nB = 1E+12;
Rb = pow(((3*alpha)/(4*3.14*nB)),(1/3));
p_vapour += 0.47*C_R(c,t)*C_K(c,t);
dp0 = p_vapour + C_MU_EFF(c,t)*lambda - ABS_P(p[c], op_pres);
Rdotv = sqrt((2.0/3.0)*ABS(dp0)*(1.0/rhoL[c]));/*Neglecting surface tension and non-
condensable gases*/

    if(dp0 > 0.0)

*m_dot = c_evap*rhoV[c]*rhoL[c]*(1/C_R(c,t))*Rdotv*3*(alpha/Rb);

    else

*m_dot = -c_con*rhoV[c]*rhoL[c]*(1/C_R(c,t))*Rdotv*3*(alpha/Rb);
}
```

C.3 Density Variation

The following UDF has been used for implementing the liquid density variation in ANSYS Fluent platform. # include “udf.h”
#define BMODULUS 1.5e9
#define rho_ref 822.7
#define p_ref 100000

```
    DEFINE_PROPERTY(superfluid_density, c, t)
{
double rho;
double p, dp;
double p_operating;

p_operating = RP_Get_Real ("operating-pressure");
p = C_P(c,t) + p_operating;
dp = p-p_ref;
rho = rho_ref/(1.0-dp/BMODULUS);
return rho;
}
DEFINE_PROPERTY(sound_speed, c,t)
{
double a;
double p, dp,p_operating;
p_operating = RP_Get_Real (“operating-pressure”);
p = C_P(c,t) + p_operating;
dp = p-p_ref;
a = (1.-dp/BMODULUS)*sqrt(BMODULUS/rho_ref);
return a;
}
```

C.4 Inlet Pressure Fluctuation

The following UDF has been used for implementing the inlet pressure fluctuations in ANSYS Fluent platform.

(Sample code for 100 MPa mean inlet pressure)

```
#include "udf.h"
#include "math.h"
DEFINE_PROFILE(pressure_profile,t,i)
{
face_t f;
double current_time;
current_time = RP_Get_Real("flow-time");

begin_f_loop(f,t)
{
F_PROFILE(f, t, i) = (1e6)*(100.+0.2*100.*(8./(3.14159*3.14159))*((sin(157079.*current_time))-
(1/9.)*(sin(3*157079.*current_time))+(1/25.)*(sin(5.*157079.*current_time))
-(1/49.)*(sin(7.*157079.*current_time))+(1/81.)*(sin(9.*157079.*current_time))
-(1/121.)*(sin(11.*157079.*current_time))+(1/169.)*(sin(13.*157079.*current_time))
-(1/225.)*(sin(15.*157079.*current_time))+(1/289)*(sin(17.*157079.*current_time))
-(1/361.)*(sin(19.*157079.*current_time))));
}
end_f_loop(f,t)
}
```

Appendix D

ODE45

D.1 Bubble Growth

Matlab main program and subroutine for solving isolated single bubble growth

ti=0;
tf=0.000001;
[t,y]=ode45(@f,[ti,tf],[(1.53*(1e-6)),0]);y=R(Radius at time t)
s=[t,y];

Function "f"
function formulae = f(t,y)
a=1e6;pressure difference psat-pinf
b=835;liquid density- kg/m^3
c=0.0025;liquid viscosity
d=0.02;surface tension
e=10025140.81;Gas pressure
formulae=[y(2);(a/(b*y(1)))+(e*(1.53*(1e-6)/y(1)^3)/(b*y(1))-(4*c*y(2)/(b*(y(1)^2)))-(2*d/(b*(y(1)^2)))
-(3*(y(2)^2)/(2*y(1)))];

D.2 Bubble Collapse

Matlab main program and subroutine for solving isolated single bubble collapse

```
    tbc=0.000001;
tfc=0.0000027584;
[t,y]=ode45(@fc,[tbc,tfc],[(32.11*(1e-06)),28.26]);y=R(Radius at time t)
s=[t,y];
```

Function "fc"

```
function formulaec = f(t,y)
a=-1e6;pressure difference psat-pinf
b=835;liquid density- kg/m^3
c=0.0025;liquid viscosity
d=0.02;surface tension
e=10025140.81;Gas pressure
formulaec=[y(2);(a/(b*y(1)))+(e*(1.53*(1e-6)/y(1)^3)/(b*y(1))-(4*c*y(2)/(b*(y(1)^2)))-(2*d/(b*(y(1)^2)))
-(3*(y(2)^2)/(2*y(1)))];
```

References

[1] Statistical review of world energy full report. Technical report, British Petroluem, 2009.

[2] Richard Basshuysen. *Gasoline Engine with Direct Injection: Processes, Systems, Development, Potential*. Springer Verlag, 2009.

[3] Wolfgang Berg. Legislation for the reduction of exhaust gas emissions. In *The Handbook of Environmental Chemistry*, volume 3. Springer-Verlag Berlin Heidelberg, 2003.

[4] C. E. Brennen. *Cavitation and Bubble Dynamics*. Oxford University Press, 1995.

[5] J-P Franc and J-M. Michel. *Fundamentals of Cavitation*. Kluwer Academic Publishers, 2005.

[6] R. T. Knapp. *Cavitation*. McGraw-Hill, 1970.

[7] Francis Strickland. *The dynamics of change: insights into organisational transition from the natural world*. Routledge, 1998.

[8] Kerson Huang. *Introduction to statistical physics*. Taylor and Francis, 1998.

[9] D.P. Schmidt and M.L. Corradini. The internal flow of diesel fuel injector nozzles: a review. *International Journal of Engine Research*, 2:1–22, 2001.

[10] C. Crua. *Combustion Processes in a Diesel Engine*. PhD thesis, School of Engineering, University of Brighton, Brighton, UK, December 2002.

[11] Carsten Baumgarten. *Mixture Formation Internal Combustion Engines*. Springer, 2005.

[12] P. K. Wu and G. M. Faeth. Onset and end of drop formation along the surface of turbulent liquid jets in still gases. *Physics of Fluids*, 7(11):2915–2917, 1995.

[13] M. Arai, M. Shimizu, and H. Hiroyasu. Similarity between the breakup lengths of a high speed liquid jet in atmospheric and pressurized conditions. Technical report, Los Alamos National Laboratory, 1991.

[14] H. Hiroyasu, M. Shimizu, and M. Arai. Breakup length of a liquid jet and internal flow in a nozzle. ICLASS, 1991.

[15] J. Bode. *Zum Kavitationseinfluß auf den Zerfall von Flüssigkeitsstrahlen.* PhD thesis, Max-Planck-Institut für Strömungsforschung, Göttingen, Germany, 1991.

[16] C. Soteriou, R. Andrews, and M. Smith. Direct injection diesel sprays and the effect of cavitation and hydraulic flip on atomization. Number SAE Paper 950080. Society of Automotive Engineers World Congress, 1995.

[17] N. Tamaki, M. Shimizu, and H. Hiroyasu. Enhanced atomization of a liquid jet by cavitation in a nozzle hole. Pasadena, CA, USA, 2000. 8^{th} Int. Conf. on Liquid Atomization and Spray Systems.

[18] S. N. Soid and Z. A. Zainal. Spray and combustion characterization for internal combustion engines using optical measuring techniques - a review. *Energy*, 36:724–741, 2011.

[19] O. Reynolds. The causes of the racing of the engines of screw steamers investigated theoretically and by experiment. *Institution of Naval Architects, Trans*, 14:56–67, 1873.

[20] C.A. Parsons. *The steam turbine on land and at sea.* Lecture to the Royal Institution, London, 1906.

[21] W. E. Ranz. Some experiments on orifice sprays. *Canadian Journal of Chemical Engineering*, page 175, 1958.

[22] Volkswagen. Diesel direct injection. http://www.vw.ca/en/tools/navigation/footer/help/technical_glossary/diesel_direct_injection.html, 2014.

[23] W. Bergwerk. Flow pattern in diesel nozzle spray holes. *Proceedings of Institution of Mechanical Engineers*, 173:655, 1959.

[24] R.A. Furness and S.P. Hutton. Experimental and theoretical studies of two-dimensional fixed-type cavities. *ASME Journal of Fluids Engineering*, 97:515–522, 1975.

[25] W.H. Nurick. Orifice cavitation and its effect on spray mixing. *ASME Journal of Fluids Engineering*, 98:681–687, 1976.

[26] H. Chaves, M. Knapp, A. Kubitzek, F. Obermeier, and T. Schneider. Experimental study of cavitation in the nozzle hole of diesel injectors using transparent nozzles. Number SAE Paper 950290. Society of Automotive Engineers World Congress, 1995.

[27] C. Badock, R. Wirth, A. Fath, and A. Leipertz. Investigation of cavitation in real size diesel injection nozzles. *International Journal of Heat and Fluid Flow*, 20:538–544, 1999.

[28] O. Genge and P. Roosen. Optische untersuchung kavitierender stroemungen innerhalb verschiedener planarer, nicht achsensymmetrischen duesen. Annual Scientific Conference on Gesellschaft für angewandte Mathematik and Mechanik, Göttingen, 2000.

[29] C. Arcoumanis, H. Flora, M. Gavaises, and M. Badami. Cavitation in real-size multi-hole diesel injector nozzles. Number SAE Paper 2000-01-1249. Society of Automotive Engineers World Congress, 2000.

[30] C. Arcoumanis, M. Gavaises, H. Flora, and H. Roth. Visualisation of cavitation in diesel engine injectors. *Mécanique and Industries*, 2:375–381, 2001.

[31] E. Winklhofer, E. Kull, E. Kelz, and A. Morozov. Comprehensive hydraulic and flow field documentation in model throttle experiments under cavitation conditions. ILASS Europe, 2001.

[32] H. Roth and M. Gavaises. Cavitation initiation, its development and link with flow turbulence in diesel injector nozzles. Number SAE 2002-01-0214. SAE International, Society of Automotive Engineers World Congress, 2002.

[33] H. Li and S. H. Collicott. Visualization of cavitation in high-pressure diesel injector orifices. *Atomization and Sprays*, 16:875–886, 2006.

[34] H. K. Suh and C. S. Lee. Effect of cavitation in nozzle orifice on the diesel fuel atomization characteristics. *International Journal of Heat and Fluid Flow*, 29:1001–1009, 2008.

[35] H. K. Suh, S. H. Park, and C. S. Lee. Experimental inevestigation of nozzle cavitating flow characteristics for diesel and biodiesel fuels. *International Journal of Automotive Technology*, 9:217–224, 2008.

[36] Z. He, W. Zhong, Q. Wang, Z. Jiang, and Y. Fu. An investigation of transient nature of the cavitating flow in injector nozzles. *Applied Thermal Engineering*, 54:56–64, 2013.

[37] R. D. Lockett, L. Liverani, D. Thaker, and C. Arcoumanis. The characterisation of diesel cavitating flow using time-resolved light scattering. In *IMechE Conference on Injection Systems for IC Engines*, London,U.K., May 2009.

[38] Sergey Martynov. *Numerical Simulation of the Cavitation Process in Diesel Fuel Injectors*. PhD thesis, The University of Brighton, 2005.

[39] O. Asi. Failure of a diesel engine injector nozzle by cavitation damage. *Engineering Failure Analysis*, 13:1126–1133, 2006.

[40] M. Gavaises. Flow in valve covered orifice nozzles with cylindrical and tapered holes and link to cavitation erosion and engine exhaust emissions. *International Journal of Engine Research*, 9:435–447, 2008.

[41] K. Im, S. Cheong, C. F. Powell, M. D. Lai, and J. Wang. Unraveling the geometry dependence of in-nozzle cavitation in high-pressure injectors. Technical report, Scientific Reports, Nature, June 2013.

[42] C. Soteriou, R. Andrews, and M. Smith. Further studies of cavitation and atomization in diesel injection. Number SAE Paper 1999-01-1486. Society of Automotive Engineers World Congress, 1999.

[43] A. G. Gelalles. Coefficients of discharge of fuel injection nozzles for compression-ignition engines. Technical Memo 373, NACA, 1931.

[44] R. D. Reitz. *Atomization and other breakup regimes of a liquid jet.* PhD thesis, Princeton University, Princeton, New Jersey,, 1978.

[45] A. Knox-Kelecy. *Turbulent flow in a scale model of diesel fuel injector nozzle hole.* PhD thesis, University of Wisconsin, 1992.

[46] T. R. Ohrn, D. W. Senser, and A. H. Lefebvre. Geometric effects on spray cone angle for plain-orifice atomizers. *Atomization and Sprays*, 1:253–268, 1991.

[47] J. M. Desantes, R. Payri, F. J. Salvador, and J. Gimeno. Measurements of spray momentum for the study of cavitation in diesel injection nozzles. Number SAE 2003-01-0703. SAE International, Society of Automotive Engineers World Congress, 2003.

[48] J. Benajes, J. V. Pastor, R. Payri, and A. H. Plazas. Analysis of the influence of diesel nozzle geometry in the injection rate characteristic. *ASME Journal of Fluids Engineering*, 126:63–71, January 2004.

[49] F. Payri, V. Bermúdez, R. Payri, and F. J. Salvador. The influence of cavitation on the internal flow and the spray characteristics in diesel injection nozzles. *Fuel*, 83:419–431, 2004.

[50] J. M. Desantes, J. Arrègle, J. J. López, and S. Hermens. Experimental characterization of outlet flow for different diesel nozzle geometries. Number SAE Paper 2005-01-2120. Society of Automotive Engineers World Congress, 2005.

[51] F. Payri, J. Arrègle, J. J. López, and S. Hermens. Effect of cavitation on the nozzle outlet flow, spray and flame formation in a diesel engine. Number SAE Paper 2006-01-1391. Society of Automotive Engineers World Congress, 2006.

[52] B. Bicer, A. Tanaka, T. Fukuda, and A. Sou. Numerical simulation of cavitation phenomena in diesel injector nozzles. ILASS Asia, 2012.

[53] L. N. Randall. Rocket applications of the cavitating venturi. *Journal of the American Rocket Society*, 22(1):28–38, January 1952.

[54] R. Payri, X. Margot, and F. Salvador. A numerical study of the influence of diesel nozzle geometry on the inner cavitating flow. Number SAE Paper 2002-01-0215. Society of Automotive Engineers World Congress, 2002.

[55] D. Bauer. *Planung und Durchführung von Experimenten zur Validierung eines CFD-Codes für Kavitationsströmungen*. PhD thesis, Technische Universität Bergakademie Freiberg, Germany, 2005.

[56] H. Roth. *Experimental and computational investigation of cavitation in diesel injector nozzles*. PhD thesis, Imperial College, University of London, London, UK, 2004.

[57] E. Giannadakis, M. Gavaises, and C. Arcoumanis. Modelling of cavitation in diesel injector nozzles. *Journal of Fluid Mechanics*, 616:153–193, 2008.

[58] D. Bauer, H. Chaves, and C. Arcoumanis. Measurements of void fraction distribution in cavitating pipe flow using X-Ray CT. *Measurement Science and Technology*, 23:10pp, 2012.

[59] K. Jiao and X. Li. Water transport in polymer electrolyte membrane fuel cells: Review. *Progress in Energy and Combustion Science*, 37:221–291, 2011.

[60] M. Kureta, T. Hibiki, K. Mishima, and H. Akimoto. Study on point of net vapor generation by neutron radiography in subcooled boiling flow along narrow rectangular channels with short heated length. *International Journal of Heat and Mass Transfer*, 46:1171–1181, 2003.

[61] N. N. Takenaka, T. T. Kadowaki, Y. Y. Kawabata, I. C. Lim, and C.M. Sim. Visualization of cavitation phenomena in a diesel engine fuel injection nozzle by neutron radiography. *Nuclear Instruments and Methods in Physics Research A*, 542:129–133, 2005.

[62] Neutron radiography. http://mnrc.ucdavis.edu/radiography.html.

[63] J. Park, X. Li, D. Tran, T. Abdel-Baset, D.S. Hussey, D. L. Jacobson, and M. Arif. Neutron imaging investigation of liquid water distribution in and the performance of a PEM fuel cell. *International Journal of Hydrogen Energy*, 33:3373–3384, 2008.

[64] P. Petersson and M. Aldén. Laser-based velocity measurement techniques (ldv and piv). http://www.forbrf.lth.se/english/research/measurement_methods/laser_based_velocity_measurement_techniques_ldv_and_piv/, 2012.

[65] E. Giannadakis, D. Papoulias, M. Gavaises, C. Arcoumanis, C. Soteriou, and W. Tang. Evaluation of the predictive capability of diesel nozzle cavitation models. Number SAE Paper 2007-01-0245. Society of Automotive Engineers World Congress, 2007.

[66] P. G. Aleiferis, Y. Hardalupas, D. Kolokotronis, A. M. K. P. Taylor, and T. Kimura. Investigation of the internal flow field of a diesel model injector using particle image velocimetry and cfd. Number SAE Paper 2007-01-1897. Society of Automotive Engineers World Congress, 2007.

[67] ANSYS FLUENT. *ANSYS Fluent 12 Documentation*.

[68] David P. Schmdit. *Cavitation in Diesel Fuel Injector Nozzles*. PhD thesis, University of Wisconsin - Madison, 1997.

[69] D.P. Schmidt, C. J. Rutland, and M. L. Corradini. A fully compressible two-dimensional model of high speed cavitating nozzles. *Atomization and Sprays*, 9:255–276, 1999.

[70] S. Som, S. K. Aggarwal, E.M. El-Hannouny, and D.E. Longman. Investigation of nozzle flow and cavitation characteristics in a diesel injector. *ASME Journal of Engineering for Gas Turbine and Power*, 132:1–12, 2010.

[71] J. Weisbach. *Mechanics of engineering: Theoretical mechanics, with an introduction to the calculus*. Van Nostrand Book Co. New York, 1875.

[72] M. Böhle, D. Etling, U. Müller, K. R. S. Sreenivasan, U. Riedel, and J. Warnatz. *Prandtls Essentials of Fluid Mechanics*, volume 158 of *Applied Mathematical Sciences*. Springer, second edition, 2004.

[73] D. P. Schmidt and M. L. Corradini. Analytical prediction of the exit flow of cavitating orifices. *Atomization and Sprays*, 7(6):603–616, 1997.

[74] L. Rayleigh. On the pressure developed in a liquid during the collapse of a spherical cavity. *Philosophical Magazine*, 34:94–98, 1917.

[75] M.S. Plesset. The dynamics of cavitation bubbles. *ASME Journal of Applied Mechanics*, 16:228–231, 1949.

[76] F.R. Gilmore. The growth and collapse of a spherical bubble in a viscous compressible liquid. Technical report, Hydrodynamic Laboratory, California Institute of Technology. Pasadena : Office of Naval Research, 1952.

[77] C. Herring. Theory of the pulsations of the gas bubble produced by an underwater explosion. Technical report, O.S.R.D., 1941.

[78] L. Trilling. The collapse and rebound of a gas bubble. *Journal of Applied Physics*, 23:14–17, 1952.

[79] J.G. Kirkwood and H.A. Bethe. The pressure wave produced by an underwater explosion. Technical report, O.S.R.D., 1942.

[80] A. N. Kolmogorov. The local structure of turbulence in incompressible viscous fluids at very large reynolds numbers. *Dokl. Akad. Nauk. SSSR*, 30:299–303, 1941.

[81] A. N. Kolmogorov. On the degeneration of isotropic turbulence in an incompressible viscous fluids. *Dokl. Akad. Nauk. SSSR*, 31:538–541, 1941.

[82] Y. Delannoy and J.L. Kueny. Two phase flow approach in unsteady cavitation modelling. *ASME Journal Fluids Engineering Division (FED)*, 98:153–158, 1990.

[83] O. Coutier-Delgosha, R. Fortes-Patella, and J. L. Reboud. Evaluation of the turbulence model influence on the numerical simulations of unsteady cavitation. *ASME Journal of Fluids Engineering*, 125:38–45, January 2003.

[84] R. K. Avva, A. Singhal, and D. H. Gibson. An enthalpy based model of cavitation. *Cavitation and Multiphase Forum, ASME Journal Fluids Engineering Division (FED)*, 1995.

[85] D. P. Schmdit, C. J. Rutland, and M. L. Corradini. A numerical study of cavitating flow through various nozzle shapes. Number SAE Paper 971597. Society of Automotive Engineers World Congress, 1997.

[86] G.B. Wallis. *One-dimensional two-phase flow*. McGraw-Hill, 1969.

[87] C. D. Ohl, A. Philipp, and W. Lauterborn. Cavitation bubble collapse studied at 20 million frames per second. *Annalen der Physik*, 507(1):26–34, 1995.

[88] N. Dumont, O. Simonin, and C. Habchi. Numerical simulation of cavitating flows in diesel injectors by a homogeneous equilibrium modeling approach. CAV2001, Fourth International Symposium Cavitation, 2001.

[89] C. Habchi, N. Dumont, and O. Simonin. Multidimensional simulation of cavitating flows in diesel injectors by a homogeneous mixture modeling approach. *Atomization and Sprays*, 18:129–162, 2008.

[90] OpenCFD Ltd. *OpenFOAM ® Documentation*, 2014.

[91] F. J. Salvador, J. V. Romero, Roselló, and J. Martínez-López. Validation of a code for modeling cavitation phenomena in diesel injector nozzles. *Mathematical and Computer Modelling*, 52(7–8):1123–1132, October 2010.

[92] F.J. Salvador, S. Hoyas, R. Novella, and J. Martínez-López. Numerical simulation and extended validation of two-phase compressible flow in diesel injector nozzles. *Proceedings of the Institution of Mechanical Engineers, Part D:Journal of Automobile Engineering*, 225:545–563, 2011.

[93] Los Alamos National Laboratory. *KIVA-3V Manual*, 1999.

[94] W. Ning, R. D. Reitz, R. Diwakar, and A. M. Lippert. A numerical investigation of nozzle geometry and injection condition effects on diesel fuel injector flow physics. Number SAE Paper 2008-01-0936. Society of Automotive Engineers World Congress, 2008.

[95] Y. Wang, W. G. Lee, R. Reitz, and R. Diwakar. Numerical simulation of diesel sprays using an eulerian-lagrangian spray and atomization (elsa) model coupled with nozzle flow. Number SAE Paper 2011-01-0386. Society of Automotive Engineers World Congress, 2011.

[96] D. P. Schmidt, S. Gopalakrishnan, and H. Jasak. Multi-dimensional simulation of thermal non-equilibrium channel flow. *International Journal of Multiphase Flow*, 36:284–292, 2010.

[97] K. Neroorkar and D. Schmidt. A computational investigation of flash-boiling multi-hole injectors with gasoline-ethanol blends. Number SAE Paper No. 2011-01-0384. Society of Automotive Engineers World Congress, 2011.

[98] K. Neroorkar, B. Shields, R. O. Grover, A. P. Torres, and D. Schmidt. Application of the homogeneous relaxation model to simulating cavitating flow of a diesel fuel. Number SAE Paper No. 2012-01-1269. Society of Automotive Engineers World Congress, 2012.

[99] Z. Bilicki and J. Kestin. Physical aspects of the relaxation model in two-phase flow. *Proceedings of the Royal Society of London: Series A*, 428:379–397, 1990.

[100] CONVERGENT SCIENCE. *CONVERGE™ 2.1.0 User Guide & Reference*.

[101] H. Zhao, S. Quan, M. Dai, E. Pomraning, P. K. Senecal, Q. Xue, M. Battistoni, and S. Som. Validation of a three-dimensional internal nozzle flow model including automatic mesh generation and cavitation effects. Number ICEF 2013-19167. Proceedings of the ASME 2013 Internal Combustion Engine Division Fall Technical Conference, 2013.

[102] A. Kubota, H. Kato, and H. Yamaguchi. Finite difference analysis of unsteady cavitation on a two-dimensional hydrofoil. Hiroshima, September 1989. In Proceedings of the 5^{th} International Conference on Numerical Ship Hydrodynamics.

[103] A. Kubota, H. Kato, and H. Yamaguchi. A new modelling of cavitating flows: a numerical study of unsteady cavitation on a hydrofoil section. *Journal of Fluid Mechanics*, 240:59–96, 1992.

[104] J. Smagorinsky. General circulation experiments with the primitive equations. i: The basic experiment. *Monthly Weather Review, American Meteorological Society*, 91(3):99–164, March 1963.

[105] Y. Chen and S. D. Heister. A numerical treatment for attached cavitation. *ASME Journal of Fluids Engineering*, 116:613–618, September 1994.

[106] Y. Chen and S. D. Heister. Two-phase modeling of cavitating flows. *Computers and Fluids*, 24(7):799–809, 1995.

[107] Y. Chen and S. D. Heister. Modeling hydrodynamic nonequilibrium in cavitating flows. *ASME Journal of Fluids Engineering*, 118(1):172–178, March 1996.

[108] Y. Chen and S. D. Heister. Modeling cavitating flows in diesel injectors. *Atomization and Sprays*, 6:709–726, 1996.

[109] R. A. Bunnell, S. D. Heister, C. Yen, and S. H. Collicott. Cavitating injector flows: Validation of numerical models and simulations of pressure atomizers. *Atomization and Sprays*, 9(5):1999, September-October 1999.

[110] R. A. Bunnell and S. D. Heister. Three-dimensional unsteady simulation of cavitating flows in injector passages. *ASME Journal of Fluids Engineering*, 122:791–797, December 2000.

[111] H. A. Grogger and A. Alajbegovic. Calculation of the cavitating flow in venturi geometries using two fluid model. Washington, D.C., 1998. Proceedings of FEDSM 98-1998 ASME Fluid Engineering Division Summer Meeting.

[112] H. A. Grogger and A. Alajbegovic. Three-dimensional cavitation calculations in nozzles. University of California, Santa Barbara, CA, USA, 1999. Proceedings of Second Annual Meeting, Institute of Multifluid Science and Technology.

[113] A. Alajbegovic, H. A. Grogger, and H. Philipp. Calculation of cavitation in nozzles using the two-fluid model. Halifax, NS, Canada, 1999. Proceedings of 7^{th} Annual Conference, Computational Fluid Dynamics Society.

[114] A. Alajbegovic, H. A. Grogger, and H. Philipp. Calculation of transient in nozzle using the two-fluid model. Indianapolis, IN, USA, 1999. Proceedings of 12^{th} Annual Conference on Liquid Atomization Spray Systems.

[115] A. Alajbegovic, G. Meister, D. Greif, and B. Basara. Three phase cavitating flows in high-pressure swirl injectors. *Experimental Thermal and Fluid Science*, 26:677–681, 2002.

[116] E. B. W. Edelbauer, A. Alajbegovic, R. Tatschi, and Kegl B. Ganippa L.C. Volmajer, M. Coupled simulations of nozzle flow, primary fuel jet breakup, and spray formation. *ASME Journal of Engineering for Gas Turbines and Power*, 127:1–22, 2005.

[117] M. Battistoni and C.N. Grimaldi. Analysis of transient cavitating flows in diesel injectors using diesel and biodiesel fuels. *SAE Int. J. Fuels Lubr.*, 2010.

[118] M. Battistoni, C. Grimaldi, and F. Mariani. Coupled simulation of nozzle flow and spray formation using diesel and biodiesel for ci engine applications. Society of Automotive Engineers World Congress, 2012.

[119] AVL. *Fire® Documentation*.

[120] J. O. Hinze. *Turbulence*. McGraw Hill, New York, 2^{nd} edition, 1975.

[121] K. Hanjalic, M. Popovac, and M. Hadziabdic. A robust near-wall elliptic relaxation eddy-viscosity turbulence model for cfd. *International Journal of Heat and Fluid Flow*, 25(6):1047–1051, 2004.

[122] R. F. Kunz, D. A. Boger, D. R. Stinebring, T. S. Chyczewski, and H. J. Gibeling. Multi-phase cfd analysis of natural and ventilated cavitation about submerged bodies. San Francisco, California, July 1999. Proceedings of FEDSM 99 3^{rd} ASME/JSME Joint Fluids Engineering Conference.

[123] R. F. Kunz, D. A. Boger, D. R. Stinebring, T. S. Chyczewski, J. W. Lindau, H. J. Gibeling, S. Venkateswaran, and T. R. Govindan. A preconditioned navier-stokes method for two-phase flows with application to cavitation prediction. *Computers & Fluids*, 29:849–875, 2000.

[124] J. W. Lindau, R. F. Kunz, D. A. Boger, D. R. Stinebring, and H. J. Gibeling. High reynolds number, unsteady, multiphase cfd modeling of cavitating flows. *ASME Journal of Fluids Engineering*, 124:607–616, 2002.

[125] A. J. Chorin. A numerical method for solving incompressible viscous flow problems. *Journal of Computational Physics*, 2:12–26, 1967.

[126] P. C. Hohenberg and B. I. Halperin. Theory of dynamic critical phenomena. *Reviews of Modern Physics*, 49(3):435–479, July 1977.

[127] A. K. Singhal, M. M. Athavale, H. Li, and Y. Jiang. Mathematical basis and validation of the full cavitation model. *ASME Journal of Fluids Engineering*, 124:617–624, 2002.

[128] S. Som, D.E. Longman, A.I. Ramirez, and S. K. Aggarwal. A comparison of injector flow and spray characteristics of biodiesel with petrodiesel. *Fuel*, 89:4014–4024, 2010.

[129] D. D. Jospeh. Cavitation in a flowing liquid. *Physical Review E*, 51:1649–1650, 1995.

[130] D. D. Jospeh. Cavitation and the state of stress in a flowing liquid. *Journal of Fluid Mechanics*, 366:367–378, 1998.

[131] W.O. Winer and S. Bair. The influence of ambient pressure on the apparent shear thining of liquid lubricants - an overlooked phenomenon. pages 395–398. Proceedings of the Institute of Mechanical Engineers - Tribology, 1987.

[132] G.H. Schnerr and J. Sauer. Physical and numerical modeling of unsteady cavitation dynamics. Fourth International Conference on Multiphase Flow, 2001.

[133] J. Sauer and G. H. Schnerr. Unsteady cavitating flow: a new cavitation model based on a modified front capturing method and bubble dynamics. Boston, MA, USA, 2000. FEDSM'00-2000 ASME Fluid Engineering Division Summer Meeting.

[134] W. Yuan, J. Sauer, and G. H. Schnerr. Modeling and computation of unsteady cavitation flows in injection nozzles. Paris, France, 2000. 1^{st} International Colloquium Microhydrodynamics.

[135] W. Yuan and G. H. Schnerr. Cavitation in injection nozzles: effect of injection pressure fluctuations. Paris, France, 2001. 4^{th} International Colloquium Microhydrodynamics.

[136] W. Yuan and G. H. Schnerr. Numerical simulation of two-phase flow in injection nozzles: Interaction of cavitation and external jet formation. *ASME Journal of Fluids Engineering*, 125(6):963–969, November 2003.

[137] CD-Adapco. *STAR-CD* ®.

[138] F. Payri, X. Margot, S. Patouna, F. Ravet, and M. Funk. A CFD study of the effect of the needle movement on the cavitation pattern of diesel injectors. Number SAE Paper No. 2009-24-0025. Society of Automotive Engineers World Congress, 2009.

[139] X. Margot, S. Hoyas, P. Fajardo, and S. Patouna. CFD study of needle motion influence on the spray conditions of single-hole injectors. ILASS - Europe 2010, 23^{rd} Annual Conference on Liquid Atomization and Spray Systems, 2010.

[140] X. Margot, S. Hoyas, P. Fajardo, and S. Patouna. CFD study of needle motion influence on the exit flow conditions of single-hole injectors. *Atomization and Sprays*, 21(1):31–40, 2011.

[141] S. Patouna. *A CFD study of cavitation in real size diesel injectors*. PhD thesis, Universitat Politècnica de València, Valencia, Spain, February 2012.

[142] P.J. Zwart, A.G. Gerber, and T. Belamri. A two-phase flow model for predicting cavitation dynamics. Fifth International Conference on Multiphase Flow, 2004.

[143] Dynaflow Inc. Bubble dynamics. http://www.dynaflow-inc.com/Services/Bubble-Dynamics-UNDEX.htm, 2014.

[144] Scaling effect on bubble dynamics in a tip vortex flow: Prediction of cavitation inception and noise. Technical report, Dynaflow Inc., 2000.

[145] G.L. Chahine, C. Hsiao, J. Choi, and Wu X. Bubble augmented waterjet propulsion: Two-phase model development and experimental validation. 27^{th} Symposium on Naval Hydrodynamics, 2008.

[146] G.L. Chahine. Numerical simulation of bubble flow interactions. *Journal of Hydrodynamics*, 21(3):316–332, 2009.

[147] Sandia National Laboratory. Engine combustion network (ECN). http://www.sandia.gov/ecn/workshop/ECN3.php, 2014.

[148] F. Echouchene, H. Belmabrouk, L. L. Penven, and M. Buffat. Numerical simulation of wall roughness effects in cavitating flow. *International Journal of Heat and Fluid Flow*, 32:1068–1075, 2011.

[149] W Yuan and G. H. Schnerr. Numerical simulation of two-phase flow in injection nozzles: Interaction of cavitation and external jet formation. *ASME Journal of Engineering of Fluids Engineering*, 125:963–969, 2003.

[150] M. Battistoni, S. Som, and D. Longman. Comparison of mixture and multifluid models for in-nozzle cavitation prediction. *ASME Journal of Engineering for Gas Turbines and Power*, 136:(061506)1–12, June 2014.

[151] Y. Ra, R. Reitz, J. McFarlane, and C. Daw. Effects of fuel physical properties on diesel engine combustion using diesel and bio-diesel fuels. Number SAE Paper 2008-01-1379. Society of Automotive Engineers World Congress, 2008.

[152] J. Szybist, D. Morris, and A.L. Boehman. Diesel fuel formulation effects on injection timing and emissions. volume 48. Fuel Chemistry Division, Argonne National Laboratory, 2003.

[153] M. Jia, D. Hou, J. Li, M. Xie, and H. Liu. A micro-variable circular orifice fuel injector for hcci-conventional engine combustion part i numerical simulation of cavitation. Number SAE Paper 2007-01-0249. Society of Automotive Engineers World Congress, 2007.

[154] H. Liu, S. Strank, M. Werst, R. Hebner, and J. Osara. Combustion emissions modeling and testing of neat biodiesel fuels. Number ES2010-90038. Proceedings of the ASME 2010 4th International Conference on Energy Sustainability ES 2010, 2010.

[155] Y. Li. Equations of state of water and sea water. *Journal of Geophysical Research*, 72(10):2665–2678, May 1967.

[156] J. Kotz, P. Treichel, J. Townsend, and D. Treichel. *Chemistry and Chemical Reactivity*. Cengage Learning, 2014.

[157] K. Saha, E. Abu-Ramadan, and X. Li. Modified single-fluid cavitation model for pure diesel and biodiesel fuels in direct injection fuel injectors. *ASME Journal of Engineering for Gas Turbines and Power*, 135:(062801)1–8, June 2013.

[158] K. Saha and X. Li. Assessment of different cavitation models in mixture and eulerian framework for two-phase flow in diesel injectors. Number ICEF 2013-19201, Dearborn, Michigan, USA, October 2013. ASME 2013 Internal Combustion Engine Division Fall Technical Conference.

[159] H. Li, F.J. Kelecy, and A. Egelja-Maruszewski. Advanced computational modeling of steady and unsteady cavitating flows. ASME International Mechanical Engineering Congress and Exposition, 2008.

[160] X. Chen, C. Zhong, and X. Yuan. Lattice boltzmann simulation of cavitating bubble growth with large density ratio. *Computers and Mathematics with Applications*, 61:3577–3584, 2011.

[161] E. Herbert, S. Balibar, and F. Caupin. Cavitation pressure in water. *Physical Review E.*, 74:(041603)1–22, 2006.

[162] K. B. Bader, J. L. Raymond, J. Mobley, C. C. Church, and D. F. Gaitan. Inertial cavitation threshold dependence on static pressure. Number 4pPA3. 159th Meeting Acoustical Society of America/NOISE-CON 2010, 2010.

[163] L. J. Briggs. Limiting negative pressure of water. *Journal of Applied Physics*, 21:721–722, 1950.

[164] M. S. Milton S. Plesset and R. B. Chapman. Collapse of an initially spherical vapour cavity in the neighbourhood of a solid boundary. *Journal of Fluid Mechanics*, 47(2):283–290, May 1971.

[165] K. Saha, E. Abu-Ramadan, and X. Li. Cavitaton modeling for fuel flow in injectors under high-pressure injection. University of Manitoba, Canada, June 2012. CSME 2012 Biennial Conference.

[166] E. Peiner, M. Balke, and L. Doering. Form measurement inside fuel injector nozzle spray holes. *Microelectronic Engineering*, 86:984—986, 2009.

[167] J. Jian-Rong Qin, T. Tomohisa Dan, M. Ming-Chia Lai, C. Savonen, E. Schwartz, and W. Brkyzik. Correlating the diesel spray behavior to nozzle design. Number SAE Paper 1999-01-3555. Society of Automotive Engineers World Congress, 1999.

[168] C. A. Chryssakis, D. N. Assanis, and F. X. Tanner. Atomization models. In Nasser Ashgriz, editor, *Handbook of Atomization and Sprays: Theory and Applications*. Science and Business Media, 2011.

[169] X. Wang and W. Su. Influence of injection pressure fluctuations on cavitation inside a nozzle hole at diesel engine conditions. Number SAE Paper 2008-01-0935. Society of Automotive Engineers World Congress, 2008.

[170] J. V. Madison. Isenthalpic oscillations with quadratic damping in saturated two-phase fluids. 6^{th} International Conference on Computational and Experimental Methods in Multiphase and Complex Flow, 2011.

[171] K. Saha, E. Abu-Ramadan, and X. Li. Characteristics of two-phase fuel flow in diesel injectors: diesel vs. biodiesel. University of Manitoba, Canada, May 2011. CICS 2011.

[172] DieselNet Technology. Diesel fuel injector nozzles. https://www.dieselnet.com/tech/engine_fi_nozzle.php, 2011.